Development of Next Generation 3-Dimensional *In vitro* Soft Tissues Models for Biomaterial Testing: Controlling Construct Properties with Fluid Flow

Josephine PF Wong

For the degree of Doctor of Philosophy

2016

Declaration

I, Josephine Wong, confirm that the work presented in this thesis is my own. Where information has been derived from other sources, I confirm that this has been indicated in the thesis.

Acknowledgments

I am forever grateful for the constant inspiration, guidance and support from my primary supervisor, Robert Brown; without which I would not have grown so much as a researcher. I am also grateful for the invaluable support and advice from Vivek Mudera, Umber Cheema and Rebecca Porter who have helped deepen my understanding in this field of study.

Furthermore, my thanks go to the staff and student I have had the privilege to work with; especially Noah Tan, Dominique Thomas, Claire Walsh, Katerina Stamati, Julia Jones, Prasad Sawadkar who have all made the past four years both enjoyable and enlightening.

Finally, I would like to thank the people I am lucky enough to have in my life. My friends, for their understanding. My brother, for always being there for me; and my parents, who continue to unconditionally believe in, and support me in everything I do. This thesis is dedicated to them.

Abstract

Pre-clinical biomaterial development and testing have traditionally relied on 2D *in vitro*, or complex *in vivo* assays. It is essential for the cell environment to match the natural tissue in terms of matrix density, architecture, components (including stress/strains) for tissue models to behave in a natural manner. The aim of this project is to improve existing *in vitro* models for the biomaterial testing.

Plastically compressed collagen hydrogels were used to create a simple and accessible 3D model. Improvement in hydrogel stiffness was achieved using pre-crosslinked, polymeric collagen, as a starting material. Hydrogels were formed by blending polymeric and monomeric collagens, which delayed the aggregation of collagen fibrils, and enabled cell incorporation at physiological pH.

Plastic compression of the novel hydrogel resulted in stiffer constructs; however, during compression, cells were exposed to reversible (i.e. using mobile macromolecules) increases in cell-damaging fluid shear stresses.

In the material degradation model, it was found that the release rates of PLGA degradation products were influenced by cells in the collagen matrix; and differed significantly between 2D (24 hours) and 3D (7 days) models. Imaging of cells cultured within the biomaterial also demonstrate the up-take of biomaterials within cells within the model after 10 days in culture.

Nanoparticle drug delivery via hyaluronan nanoparticle (HA-NP) was im-

proved by increasing blockage at the fluid leaving surface (FLS). The HA-NP was designed to gradually release trapped simvastatin, which was measured indirectly via BMP2 production over time. Although results were inconclusive, initial experiments demonstrated sustained BMP2 production by cells over 5-9 days.

This work has demonstrated novel ways to improve the stiffness of the model construct, and an improved understanding of particle movement within the hydrogel during plastic compression. The models for biomaterial testing have demonstrated that it was possible to track biomaterials in the construct/cells over time, enabling real-time monitoring of the biomaterial and cells at the implant site.

Contents

List of Figures

List of Tables

Chapter 1

Introduction

Tissue engineering (TE) was described by Langer and Vacanti (1993) as "an interdisciplinary field that applies the principles of engineering and life sciences toward the development of biological substitutes that restore, maintain, or improve tissue function or a whole organ". This still holds true for many TE applications, yet it is clear the field has evolved beyond this scope, to encompass biological substitutes that are aimed at replicating tissue environment and function *in vitro* (as a tissue model) for use as a tool in the study of basic cell biology and cell/tissue response to external stimuli (i.e. drugs, biomaterials, etc.).

One of the main approaches/aims in TE is to produce off-the-shelf tissue replacements that can replace impaired or lost tissue function, when wound healing is limited by the regeneration capacity in humans (i.e. leading to scar tissue which can impede tissue function). The complexity of whole organ means that current engineered constructs cannot replace the "whole unit". Instead, they are designed at the tissue level to only 'fix' parts of a damaged organ/tissue. These repairs can be performed using autologous, allogeneic or xenogenic transplants; but when there is a lack of healthy donor tissue, or concerns of donor site morbidity or large injury sites, artificial implant constructs can become an important tool in restoring lost tissue function.

The success rates in recovering tissue function varies depending on the complexity of the tissue structure and the level of cell involvement (i.e. in biointegration) in the tissue function (i.e. it is easier to create the physical scaffold for tissue such as tendons and cornea which does not have a high reliance on cells to function). However, the mechanisms underlying the cell involvement in tissue repair and biointegration of tissue implants is complex and not fully understood. An improved understanding of cell behaviour and environmental cues which trigger such responses within biological tissues is essential to achieve improved post-implant outcomes.

In order to have better control over cell behaviour, TE requires an interdisciplinary approach to the design of implant materials.

Many current TE implants are able to achieve partial restoration of tissue function, with the caveat of potential scarring at the implant site and susceptibility to material failure over time. This is particularly the case if the implant material is insufficiently integrated with the surrounding tissue.

Modern approaches to produce a functional tissue that is designed to replace tissue lost to trauma or disease, now acknowledge the need for cell involvement for long term success of the implanted construct. However, the difficulty in engineering a successful construct lies in the difficulty in understanding cell behaviour within their natural environment, and the ability to use this knowledge to control cell behaviour within an artificial construct. This means that a trial-and-error approach to the development of biomaterial formulation and structure is adopted, to create an implant which can stimulate a physiological cell response.

This is where model systems (*in vivo* and *in vitro* (supplemented with computational and mathematical models); further discussed in section 1.3) are needed to test and screen biomaterials for the efficient development of improved biomaterials, used to replace lost tissue function. Additionally, tissue

models designed to act like natural tissues can be used to help understand and predict human tissue response to stimuli (i.e. implant biomaterials, drugs, etc.). These model systems can be thought of as a stand alone screening tool, designed with selected tissue specific features/variables found in native tissues (at the right amount and location); which can be used to further develop implantable biological substitutes, and can be used to study cell interaction with its extracellular matrix (ECM), other cells and implant biomaterials. This approach has so far been useful and important in understanding cell response (i.e. growth factor secretion, gene regulation, matrix remodeling, etc.) to mechanical and chemical characteristics of biomaterials.

A particular focus of this thesis will be to develop tissue models which can help improve the efficiency and efficacy of biomaterial development, by screening and selecting for material compositions and/or physical properties that lead to improved cell response and implant outcome.

The understanding of cell interaction with its extracellular matrix, and resultant cell response are key to producing reliable tissue models. These models are especially relevant for later stages of biomaterial development, where the availability of a reliable *in vitro* screening platform for biomaterials will increase efficiency of data gathering, and minimise the use of animal models (and associated ethical, time and cost implications); especially when there is also the question of human relevance in animal models. In short, there is a need for a reliable, relevant (representative of the cell interaction within the target tissue) and accessible platform to test and develop biomaterials.

1.1 Research motivations

The main motivation for this research is for the advancement of current 3-Dimensional (3D), *in vitro* tissue modeling platforms. This is in the context of

improving *in vitro* 3D models, for the testing of biomaterials (for its possible effects on the local tissue upon implantation. Studies of particular interest are:

- Material longevity within the body

- Degradation and remodeling rates of materials in a tissue-like environment

- Cell response and behaviour within the material over time

- Effect of biomaterial on surrounding tissue/cells over time

Although, much of the tissue responses to biomaterials are traditionally tested *in vivo* (animal model), there are various limitations to the use of animal models (please see section 1.3.1).

As discussed further in section 1.2, many current biomaterials are composed of synthetic materials. Yet, a full understanding of the effects of synthetic materials on the body, particularly at the cellular level, is often lacking. Although many *in vitro* and *in vivo* models already exist to gauge the safety and efficiency of biomaterial implants, there is still a need for an *in vitro*, human relevant, tissue model that is **simple, accessible, reproducible and quick to produce**. In particular, there is a need for a species and tissue specific model which allows for:

- The simplification and isolation of test variables

- Easy monitoring and testing of the model

- The study of biomaterial effects on human tissues, especially its cells, over a extended period of time in a natural-tissue like ECM environment

With the aim to:

- Produce a replicable and reliable tissue model

- Increase model relevance to human tissue

- Improve tissue specificity (by incorporating tissue relevant cell types, or physical characteristics into the material)

- Increase productivity (i.e. higher throughput)

- Reduce time, effort and resources in biomaterial testing

The main purpose of this research is to engineer a tissue-like construct that is capable of producing and predicting native soft-tissue responses to biomaterials (which are highly dependent on resident cells). These constructs must be able to react to external stimuli in a tissue-like manner (i.e. a skin model should behave like skin (in health and in disease) in terms of gene regulation, protein composition and/or cell responses).

Since the natural tissue is often too complex to reproduce and analyse, the aim is not to create identical tissue mimics. However, most tissues can be simplified and be defined by its predominant physical and chemical features (i.e. matrix stiffness, cell/matrix density, matrix alignment, presence of other proteins and growth factors). The strategy is therefore to produce *in vitro* tissue models by incorporate these engineerable features into the basic collagen scaffold to produce "tissue specific" models.

The approach is to use the minimum number of these "building blocks" (physiochemical cues) to direct cells into behaving in a physiological manner.

1.2 Tissue engineering – biomaterials as implants or tissue models?

Although tissue implants are made to mimic tissue function and can, to an extent, replace lost or impaired tissues, they are not generally used as tissue

models. So, what is the difference between tissue modeling platforms and implant materials?

The answer is that they are usually made with different priorities in mind. There are very different requirements in the engineering of materials intended for tissue modeling, versus those intended as replacement tissues as an implantable material. Materials in tissue modeling, most typically, are used as a platform for understanding the basic biological response/mechanisms to an external stimuli (i.e. drugs, biomaterials). This is especially important in modern research where there is an almost infinite number of possible test variables. The testing of multiple variables would imply the priority for any model tissue is to be highly reproducible, with low variation between batches. To facilitate the generation of useful information from the models, it must be relevant to the target tissue, be easy to manipulate and is simple enough (in terms of its components) to understand the influence of individual variables on the test outcome; the option to build/increase complexity within the model will also be beneficial.

This contrasts with the priorities of tissues engineered for implantation (i.e. skin, bone, tendon grafts) where they **must**, first and foremost, be safe and biocompatible. The reproducibility of the construct is not often expected, as patient-derived cells are notoriously difficult to control. Nevertheless, it is assumed (in a cell-dense construct) that resident cells will create the necessary architecture, proteins and micro-environments, to replace the implanted scaffold material, as the new tissue gains biological function and integrate with surrounding tissues over time.

It is essential to make this distinction, and to make clear that this research is focused on the development of *in vitro* tissue models. Therefore the priorities for the model constructs are *reproducibility*, and *relevance to target tissues*.

1.3 Current types of tissue-models – *in vivo* and *in vitro*

Many tissue models exist to test and predict tissue response to an implant material. This section aims to provide an overview of the current approaches, and its associated advantages and disadvantages; to ultimately justify the need for developing next-generation, 3-dimentional, *in vitro* model systems.

1.3.1 *In vivo* models

The term *in vivo* is defined as processes performed or taking place within a living organism, and in biological research it often refers to animal models used to study biological processes and mechanisms within a complete and intact system.

For example, a common *in vivo* assays for bone-replacement biomaterials is the bone defect models, where part of the animal bone is surgically removed and replaced by biomaterials in a live animal model (Li et al., 2015). One of the advantages of an *in vivo* model is that implanted biomaterials will be subjected to physiological mechanical loading and biological reactions (i.e. inflammation) until the construct is removed for analysis.

The variables tested *in vivo* typically include the toxicity of new components and its effects on all organs/tissues of the body. However, the drawbacks associated with animal models include its complexity and limited accessibility. This means that tissue assays (apart from blood tests or skin biopsy etc.) are typically end-point, and require a large number of animals to study a range of variables, or temporal changes to the biomaterial and the surrounding tissue over time. This poses ethical, cost and time issues which needs to be justified.

The majority of the animal models in biomaterial research (especially in the

early stages of pre-clinical trial research) are laboratory mice because of the relative ease to introduce genetic modifications (i.e. disease specific models with similar pathologies to human disease), and reduced cost, space and time implications compared to other mammalian models. Typically, pre-clinical trials *in vivo* progress onto large animal models (with an improved resemblance to human physiology), only after preliminary tests in smaller animal models. The problem comes when the mice/rat model "inaccurately" predicts human tissue responses and give rise to false positive and negative results, leading to the abandonment of potentially useful biomaterials, whilst further developing materials which may potentially be non-compatible with humans (which are bound to fail with further testing) (Ennever et al., 1987) (McGonigle and Ruggeri, 2014). This questions whether the heavy reliance on animal models for biomaterial (and drug) testing can be justified.

Nevertheless, it is important to acknowledge that animals models are indispensable in testing systemic effects and overall safety of drugs/biomaterials, especially over a long period of time. But prior to this stage of biomaterial testing, reliable *in vitro* tests are needed to provide human tissue specific screening of biomaterials (to reduce false positive and negative results of material effect on the tissue) during their development.

1.3.2 *In vitro* models – 2-Dimensional VS 3-Dimensional

In vitro (or "in glass") refers to experiments carried out away from the intact living organism. The major benefit to isolating cells for culture *in vitro* is that it allows for a simpler model with isolated test variables, and easy access to the tissue components for analysis. *In vitro* models can refer to tissue sections (i.e. lung sections/biopsy) or cells, cultured both *on* (most typically coated tissue culture plastic (TCP)) and *within* a cell-adherent material. However, this

is where a distinction must be drawn between 2-dimensional (2D) (i.e. cells on coated culture plates, matrigel surface, etc) and 3-dimensional (3D) (i.e. cells within a biomaterial) culture systems.

2D systems typically refer to cell mono-layers cultured on a stiff and flat surface (i.e. tissue culture plastic). Examples of 3D soft tissue models include electrospun poly(ester urethane)ureas (Courtney et al., 2006) and 3D full thickness skin models based on silk and collagen (with studies of cross-talk between cell types in the skin model) (Bellas et al., 2012); where cells are embedded within a biomaterial.

The main differences *for cells* seeded in 2D culture and the natural tissue are:

- Spatial cues (including cell-matrix, cell-cell attachments)

- Substrate stiffness

- Concentration gradients (i.e. nutrients and growth factors)

In terms of mechanical properties, the stiffness of the cell substrate is notably different between 2D and 3D systems. Substrate stiffness is important as cells can exert and sense contractile forces via its cytoskeleton from the attached substrate. This ultimately affects cell behaviour such as migration, differentiation, etc. (Discher et al., 2005). Cell seeded in 2D cultures are usually attached to ultra-stiff tissue culture plastic, with very high resistance to cell contraction in one plane, whilst other surfaces are surrounded by a fluid environment, which offers little cell attachment sites, and even less resistance to cell exerted contractile forces (although it should be said that this is until cells (i.e. fibroblasts) on a 2D surface naturally produce ECM proteins, and transform their 2D environment into 3D over time). This contrasts with a true 3D environment where physiological stimulation is from *all dimensional planes* surrounding the cell.

As an example, studies comparing cell activity within 2D and 3D *ex vivo* lung cancer models (decellularised matrix seeded with human alveolar based epithelial adenocarcinoma A549 cell-line) have differences in cell proliferation and apoptosis rates. Differences in the metalloproteinase expression between the 2D and 3D models were also noted, where MMPs-1, -2 and -10 were at increased levels in 3D, and MMP-9 was *only* found in the 3D model. Importantly, cells nodules, the hallmark of lung cancer, were only formed within 3D constructs (Mishra et al., 2012).

The differences between findings from 2D and 3D *in vitro* models highlights the importance of cell-cell and cell-matrix interactions (Nyga et al., 2011), and other culture environment factors, such as the perfusion of the construct (i.e. microfluidics) (van Duinen et al., 2015). Just taking cell migration as an example, the changes in ECM topography (i.e. alignment of matrix and the ECM ligand density available for cell attachment) has been found to affect the migration rate and the extent of cell spreading and polarity. In 3D, the size of the interfibrillar space also dictate the rate of migration (Doyle et al., 2013) (Cukierman et al., 2001). Also, in terms of cell signalling, an upregulation in myosin II activity and cell migration rates can be seen within 3D matrices (Doyle et al., 2009).

The concentration of essential nutrients available to cells in 2D and 3D will differ due to the density of the culture environment. In 2D, the culture media (and so nutrients) are freely available to at least part of the cell surface. Within a 3D system, nutrients used up by cells will have to diffuse through the dense matrix, resulting in a concentration gradient for nutrients between the cells and the culture media outside the matrix. Although, note that the matrix can add to the complex cell signalling system by acting as a reservoir for soluble growth factors (Hynes, 2009).

In most cases, a 3D in vitro model system can be engineered to represent

a natural tissue environment as cells are naturally found embedded within the ECM (a 3D environment; with exceptions i.e. epi-/endothelial cells) composed of a wide range of ECM proteins; which supports cells within a structured scaffold and present environmental cues to interstitial cells (i.e. cell-matrix and cell-cell interactions, growth factors and cytokines).

Designing 3D *in vitro* matrices

Again, since cells in 2D (especially those cultured on TCP) receive non-physiological stimulation from their environment, their response/behaviour are unlikely to predict complex, natural, tissue responses. Therefore there is a need for 3D models with a cell environment representative of the natural tissue.

When designing the 3D model, it is especially important to consider:

- What the cell senses - is it 3D for the cell?

- What are the predominant environmental cues for cells in the target tissue

Cells are typically several tens of micrometer in size. The surrounding material/matrix must therefore also be in the same scale for cells to truly be embedded within a 3D environment. For example, if cells are embedded within a scaffold with pores measuring hundreds of micrometer, the smaller cells will only attach to part of the pore circumference. 3D spatial cues will therefore be lacking as cells are attached in one plane - effectively becoming a 2D surface to the cells.

Cells in 3D receive feedback regulation from its surrounding matrix. They respond, for example, to matrix stiffness, alignment, topography and chemical cues (i.e. the concentration of oxygen, nutrients and proteins). It is therefore clear that the structure and topography of cell substrate material has implication on cell behaviour, making it essential to consider the material used to

create the tissue model. It is important not to forget different tissue types (i.e. musculoskeletal, cardiac, kidneys, liver, skin, etc.) will involve different tissue organisation, components and cell-types; which will need to be taken into account when developing tissue-specific models.

1.3.3   Synthetic and natural materials in tissue engineering

Synthetic polymers are popular scaffold materials as they have highly controllable chemical compositions, and both physical and mechanical properties (i.e. typically much stronger than natural polymer derived materials, and can be designed to match the mechanical strength of host tissues). Additionally they are generally cost efficient to produce, have good availability and many synthetic polymers are already clinically approved for use within the body for other applications (i.e. PLGA are approved by the FDA for drug delivery).

Although there is a high degree of control over physical features and chemical composition of the material, the synthetic material itself will not integrate with the existing tissue in the body. In most modern TE applications, the synthetic polymers is used to deliver (or encourage cell migration into the scaffold), and support cells until it is eventually replaced by the cell-produced ECM; which is necessary for implants to obtain biological function (indirect tissue engineering (Brown, 2013b)). In such circumstances, the initial construct is usually non-physiological (apart from matching host tissue mechanical strength), and will only mature into a tissue-like construct with time. The implication of this is that the synthetic matrix would need to be designed with mechanical/chemical cues (such as tissue-like stiffness, cell-attachment site density, degradation rate, topography and/or growth factors and cytokines) to direct cell behaviour, to encourage the production and retention of ECM proteins.

A frequent problem in synthetic materials is the low rate of ECM deposi-

tion *in vitro*, meaning long periods in culture is necessary for its maturation (i.e. newly synthesised collagen is only slowly incorporated into the bulk tissue (Foroughi et al., 2008)). This could be due to the lack of molecular 'crowding' at the collagen deposition site because constructs are often culture in an environment which has limited macromolecule density (much lower than physiological levels normally found in the ECM environment). With sufficient macromolecule density in the culture environment, the excluded volume effect is found to accelerate the kinetics of protein assembly and fibril formation *in vitro* (Lareu et al., 2007).

The production of cell-synthesised extracellular matrix (ECM) is also highly dependent on the activity of resident cells. Once the synthetic material has degraded, the degradation products or active ingredients released from the biomaterials will be in contact with the surrounding tissues. Yet often the effects of such by-products on resident cells (of different cell-types), and the surrounding tissue, is not clear (i.e. is it carcinogenic or toxic to cells? does it cause fibrosis?). To add to the complexity, primary cell sources (i.e. autologous cells isolated from a patient) can have variable activity, with very different ECM production rates. This means that degradation rates of a biomaterial needs to be controllable (and customisable for each patient); especially in view of their use in the clinical setting.

Nevertheless, the ability to customise synthetic materials means it is effective for use as implant materials - when the variables to control cell-behaviour is known. This indirect tissue engineering method is, however, impractical for use in high-throughput model systems due to the long culture period for the ECM to be produced; not to mention the high level of cell dependency, leading to the high variability expected in cell-produced ECM.

Natural materials on the other hand, may be better suited as a substrate for model tissues. This is because the substrate is made of naturally existing pro-

teins of the ECM which contain the cell attachment sites, and physiochemical cues for cells. Examples of natural polymers used in TE include proteins naturally found within the ECM environment, such as collagen (most commonly types I and II), elastin, fibrinogen/fibrin and hyaluronic acid (at different quantities, depending on tissue type). Cell-attachment proteins such as laminins and fibronectins can easily be incorporated into protein scaffolds which will further provide tissue-like cues to cells, although the requirements for these ECM components will depend on the cell type incorporated into the tissue model. This category also includes other naturally derived materials such as polysaccharides and polyesters (Mano et al., 2007)) which can be extracted from non-mammalian animals, microorganisms or plants.

The main advantages of using natural materials to support cells in tissue models is that these molecules are naturally recognised by cells and are more likely to stimulate physiological responses in cells (similar to the natural environment i.e. migration, proliferation, remodeling of matrix). Additionally, many natural matrix-forming proteins are able to spontaneously (at specific conditions) form a scaffold *in vitro* (i.e. collagen hydrogels, fibrin scaffolds) because they contain precise amino acid sequences and structure which are difficult to replicate in the synthetic material.

However, there are also limitations to reconstituted proteins scaffolds. Particularly because these scaffolds are formed without cell involvement or cell-directed control of the matrix architecture; which may in turn affect cell behaviour (Cheema et al., 2011). The lack of mechanical properties of hydrogel based scaffolds can also be a problem, as it is one of the many physical cues cells detect from the ECM. However scaffolds can be made stronger by interventions such as chemical cross-linking of the protein. For example, cross-linked gelatin or fibrinogen have been found to support muscle myoblast cell line (C2C12) proliferation, despite initial cell damage due to cross-linking

(Sando et al., 2011).

Examples of *in vitro* 3D models taken from the natural tissue (i.e. *ex vivo*) includes the use of tissue sections or decellularised models (often top-down approaches of material fabrication); where tissues maintain the complex tissue structure whilst also having improved access for *in vitro* assays. For example, a decellularised lung model (with in silico modeling) found that cells in 3D had reduced proliferation rates (observed through ki-67 staining and cell counting) and were able to demonstrate cell-type differences in response to drug treatment (Stratmann et al., 2014) .

Although decellularised explanted lung tissue contain the complex tissue structures (not currently reproducible in artificial 3D constructs), the culture of these samples required constant perfusion and so currently have limited potential for up-scaling. Also since they are obtained from natural tissues, some variation between samples can be expected. On the other hand, 3D models built artificially (bottom-up fabrication) are considerably simplified compared to animal tissue models (Mishra et al., 2012), but are a step forward from 2D models and generally show improved physiological cell responses in drug screening compared to traditional *in vitro* 2D models (as reviewed by Nam et al. (2015)).

1.3.4 Regulations and international standards for biomaterial testing

The International Organisation for Standardisation (ISO) have published guidelines and regulation for the use of medical devices in biological settings to ensure a standard of animal welfare (ISO 10993-2), and patient safety during animal and clinical tests. ISO 10993 describes the international standards expected for biological evaluation of medical devices, with a total of 20 chapters to date (August 2016).

ISO 10993 aims to provide guidelines for the protection of patients from the use of medical devices, including biomaterials, by providing guidance in the systemic analysis and biological evaluation of medical devices (ISO 10993-1). The regulations encompass both natural and synthetic materials designed for long-term (i.e. more than 30 days) contact with human tissues, and is designed to assess and manage the risks involved with prolonged contact between bio-materials and human tissues.

Since the tissue models discussed in this thesis was not intended for direct human tissue contact (i.e. not intended for implant), the guidelines in ISO 10993 do not directly apply to the collagen model material described in this thesis. Instead, it describes potential test parameters for the model during *in vitro* biomaterial testing. For example, ISO 10993-9 describes the need for *in vitro* test on material degradation (may include chemical components used in the manufacturing process), which can also be studied in 3D tissue models as demonstrated in chapter 7 in this thesis. Other potential areas of application of the 3D model is in the study of cell response to the biomaterial and its components (i.e. cytotoxicity, genotoxicity and carcinogenicity; ISO 10993-5), and material degradation due to chemical alterations to the medical device (ISO 10993-13).

The successful implementation of 3D models as early biomaterial tests and screening, outside of animal models, will help to reduce the need for *in vivo* models. This thereby helps meet the principles of the National Centre for the Replacement, Refinement and Reduction of Animals in Research (NC3Rs), which aim to promote new technologies to replace, reduce and refine the use of animal models in research.

1.4 Collagen

Collagen is a family of proteins that is highly conserved between species during evolution. Collagen molecules are composed of three polypeptide chains arranged as a triple helix (Ramachandran and Kartha, 1954) (Ramachandran and Kartha, 1955). The composition of each chain (also known as α-chains) can vary, which is reflected in the chain nomenclature (i.e. $\alpha 1$, $\alpha 2$, etc.). To date, at least 29 types of collagen have been identified, most of which can be roughly divided into three groups depending on its function (Abraham et al., 2011) (Khoshnoodi et al., 2006) (Gordon and Hahn, 2010):

- Fibril-forming collagens - most common are types I (found most predominantly in load bearing tissues), II (cartilage) and XI (cartilage, intervertebral disc). All fibril forming collagens have long uninterrupted helical domains capped with N- and C- terminals containing non-collagenous propeptides, and provide the supporting matrix of most tissues

- Network-forming collagens - types IV (basement membranes), VIII (subendothelium of vascular walls) and X (endochondrial growth plates) are examples of network-forming collagens found within the body

- Fibril-associated collagens (FACIT) - such as types IX (cartilage, cornea), XII (dermis, tendons) and XIV (bone, dermis) can be found associated with underlying collagen fibres

The tissue models used throughout this thesis is based on **type-I collagen** - a type of fibril forming collagen.

This section aims to review current knowledge of the type-I collagen protein, in particular, its chemical composition, structure and its interaction with cells.

1.4.1   What is Type-I collagen?

Type-I collagen is one of the most abundant type of collagen in the body. It is a fibril forming collagen, and provides the structural integrity in most connective and load bearing tissues (skin, tendons, bones, etc).

The triple helix of each type-I collagen molecule is made of two α1, and one α2 chains. Each chain is composed of $\sim$1050 amino acids, with the main body of the chain consisting of repeating –Gly-X-Y– units; such that glycine (Gly) is found at every third amino acid along the chain. Glycine at every third position is important for an undistorted structure, as Gly at any other position is found to be highly destabilising (Brodsky et al., 2008) (Persikov et al., 2000).

Since it is often difficult to study the intact collagen molecule due to its tight structure (i.e. sterical hinderance), shorter fiber forming peptides ($\sim$36 amino acid residues) with variations in the –Gly-X-Y– sequence have been used to study the effect of amino acid sequence on its fiber forming propensities (O'Leary et al., 2011). Using these short sequences, it has been found that Proline (Pro) and Hydroxyproline (Hyp) are most commonly found in the X and Y positions respectively; with this configuration leading to the highest stability of the collagen triple helix (Persikov et al., 2000). Deviations from this Gly-Pro-Hyp sequence (i.e. to Gly-Pro-Pro) results in a less stable gel (Kar et al., 2006). The importance of Hyp in the collagen molecules has been highlighted in early studies in to the collagen molecule for stability (Gustavson, 1955) (Jimenez et al., 1973) (Berg and Prockop, 1973).

In mammalian tissue, type-I collagen molecules are produced within fibroblasts (and other cells, i.e. osteoblasts; depending on the tissue type), and are secreted into the extracellular space before they can be assembled into the ECM. Briefly, the biosynthesis of collagen molecules begin with the collagen α-chain production. Translated collagen chains are modified by post-

translational modification in the rough endoplasmic reticulum, where proline and lysine residues (in the Y position) are hydroxylated to form hydroxyproline and hydroxylisine. These hydroxilated amino acids are needed for triple helix stability (Ramachandran et al., 1973) and for intermolecular cross-linking.

As the three α-chains come together to form a triple helix, interchain disulfide bonds at the C-terminal of the α-chain aligns the chains into conformation (Doege and Fessler, 1986), allowing hydrogen bonds to hold the rest of the chains together. Both water bridges (Brodsky et al., 2008) and electrostatic interactions (Persikov et al., 2005) are also thought to have a role in stabilising the triple helix (i.e. the Hyp residue may form water bridges with carboxyl groups of adjacent chains (Suzuki and Fraser, 1980)). The triple helix at this stage is called the pro-collagen molecule (figure 1.1), and is packaged at the golgi apparatus for secretion into the extracellular space.

For collagen molecules to aggregate and form fibrils, the pro-collagen molecule must be cleaved at either ends of the molecule by N- and C-procollagen proteinase (Kadler et al., 1987), so that a relatively short non-helical region (telopeptides) remain at either terminal. The cleavage of procollagen terminals removes any steric hindrance, and enables the association of adjacent **tropocollagen** molecules (widely used in hydrogel formation) in a "quarter staggered" formation; such that adjacent and parallel collagen molecules are displaced by approximately 1/4 of the molecule length, which measures 67 nm (a D period). On an electron micrograph, this displacement can be observed as distinct banding patterns on the collagen fibre (Williams et al., 1978). This association of collagen molecules continue until fibres are formed (*in vitro*, fibres typically measure about $\sim$20-40nm in diameter (Williams et al., 1978)).

Further processing of the fibre is then needed for collagen fibres to achieve the level of mechanical strength found in natural tissues, so that it can support cells and other proteins within the matrix.
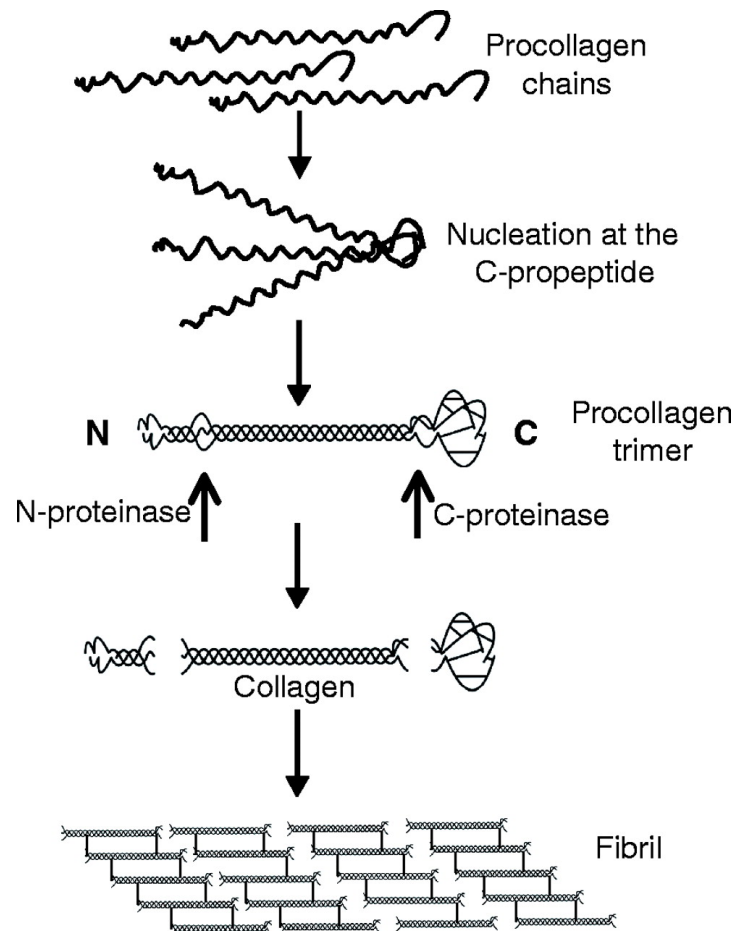
Figure 1.1: Schematic of procollagen processing derived from (Canty and Kadler, 2005). Individual collagen chains produced within the cells forms a triple helix through C-terminal disulfide bond formation. The resultant procollagen molecule is further processed by N- and C-procollagen peptidase which removes either terminals, allowing the collagen molecules to assemble into fibrils (with a quater-staggered arrangement) after secretion into the extracellular space.

1.4.2 Chemical alterations of the collagen structure – Cross-linking

Collagen molecules immediately after fibrillogenesis are only held together by weak labile bonds. For the collagen matrix to gain mechanical properties normally found in mature tissues, interfibrillar covalent cross-links between collagen molecules is necessary (Yang et al., 2008).

Interfibrillar cross-linking

Collagen molecules are naturally cross-linked together via two distinct processes. The first of which involves an enzymatic process mediated by lysyl oxidase to form divalent (and subsequent trivalent) intermolecular cross-links at defined sites along the collagen molecule. With age, non-enzymatic reaction with glucose result in the formation of advanced glycation products (AGE), leading to further cross-linking.

In enzymatic cross-linking, the residues involved will depend on the tissue type (i.e. the level of lysine hydroxilation within the collagen molecule) and age of the tissue. The majority of cross-links in adult skin and tendons are aldemine based. Lysyl oxidase causes the oxidative deamination of ϵ-amino groups of specific lysine residues of fibrils in the non-helical regions (telopeptides) of the molecule. The resultant lysine-aldehyde then reacts with opposing ϵ-amino groups of hydroxylysine in the helical region of the molecule. This type of cross-link is called dehydrohydroxylysinonorleucine (deH-HLNL) (Bailey and Peach, 1968). These then spontaneously reacts with histidine to form Histidinohydroxylysinonorleucine (HHL) (Yamauchi et al., 1987) which is a more stable trivalent cross-link.

Although there are many potential cross-link mechanisms, it is clear that deficiencies in hydroxilation or copper ions (causing decreased lysyl oxidase ac-

tivity) lead to tissues with decreased mechanical properties (Dahl et al., 2005).

The second mechanism is through non-enzymatic cross-linking. Prolonged incubation of collagen in excess glucose within an oxygen-rich environment led to an increase in cross-linking and browning of collagen constructs (Kohn et al., 1984). Reactive oxygen species was found to mediate glucose induced collagen cross-linking (Fu et al., 1992) (Fu et al., 1994) by forming advanced glycation products (AGE). The formation of AGEs is initiated by the formation of a schiff base between glucose and a protein amino group (i.e. lysine side chains), which then stabilises into an intermediate keto amine (amadori product). Further glycolysis over time leads to the formation of glyoxal, methyl glyoxal and 3-deoxyglycosone which reacts with ECM proteins to form AGEs (Snedeker and Gautieri, 2014). Evidence suggests that soluble AGE can directly stimulate cross-link formation in collagen (instead of simply being an end-product of cross-link formation) (Sajithlal et al., 1998).

However, for the direct engineering of collagen constructs *in vitro*, immediate and efficient methods to improves construct mechanical properties is usually needed. Artificial interfibrillar cross-linking of collagen fibrils (without enzyme action) is possible with chemical (i.e. gluteraldehyde; including photochemical agents such as riboflavin) or physical (i.e. dehydration) treatments. The mechanism and residues involved in these artificial crosslinking methods vary, but ultimately, all methods result in the interfibrillar cross-linking of collagen fibrils. Compared to natural cross-linking methods, these methods efficiently increases mechanical properties of collagen based materials (Chandran et al., 2012) (Olde Daminck et al., 1996) (Chan and So, 2005), but will also damage cells in the area of treatment.

Therefore, the current challenge is to introduce covalent cross-links into *in vitro* constructs in a *quick*, and *cell friendly* manner; for the production of scaffolds with increased mechanical properties. This challenge will be addressed,

and further discussed, in chapters 3 and 4.

1.4.3 *In vitro* collagen fibrillogenesis to produce hydrogels

Type-I collagen molecules in solution are surrounded by a water shell. When fibrillogenesis is triggered at physiological conditions *in vitro*, collagen molecules spontaneously assemble with neighboring molecules in a quarter staggered arrangement to form fibers.

Electrostatic interactions and hydrogen bonds (i.e. involving bridging water molecules) appear to be the driving force for fibrillogensis. Hodge and Schmitt (1960) identified narrowly defined clustered of basic and acidic polar groups on collagen molecules, which match the corresponding relative position on an adjacent molecule when displaced at the quarter staggered arrangement. The interprotein interactions are more likely to form in clusters, rather than uniformly throughout the collagen molecule. This is because some amino acids are better hydrogel bond donors (i.e. arginine and lysine) or receptors (i.e. glutamine and aspartate) than others (Streeter and de Leeuw, 2011). Packing of the collagen molecules optimises the alignment of hydrophobic side chains (Hulmes et al., 1973). Hydrophobic interactions between collagen molecules can potentially be stabilising (Streeter and de Leeuw, 2011), as a reduced amount of water shell on non-polar groups encourages interaction between adjacent collagen molecules.

The collagen fibrous matrix structure and organisation depend on the conditions of assembly (Comper and Veis, 1977). Nevertheless, all collagen hydrogel formation process begin with a nucleation phase, where polymerisation of the collagen protein begins in small clusters. Fibres form as collagen monomers in solution continue to aggregate, until fibrillogenesis is complete. Turbidity assays of collagen hydrogels often describe this as the lag phase

(before nucleation) and growth phase (formation of fibres), detected when the collagen solution turns opaque during the latter stage.

The hydrogel at this stage assumes a loose mesh-like fibrous structure, containing $\sim$ 0.2-0.6% (w/w) collagen protein, and mostly water in the interfibrillar space (with embedded cells, ECM proteins or biomaterials).

Factors currently known to influence collagen fibrillogenesis, and the stability of resultant hydrogels include:

- Collagen molecule structure (with or without telopeptides) and composition (i.e. in short peptide sequences)

- Solution pH

- Salt concentrations

- Gelling temperature

- Collagen density

- Presence of other proteins and macromolecules

Type-I collagen molecules used in hydrogel formation are usually native acid-soluble collagen (tropocollagen; with telopeptides), or collagen molecules cleaved of most of their telopeptide (atelocollagen). Both forms are derived from natural tissues, but are extracted using different processes. Tropocollagen normally extracted from young and growing tissues (using a weak acidic solution) are 'whole' collagen molecules with the telopeptides intact. Atelocollagen extracted from (usually insoluble) tissues using pepsin lack the complete telopeptide sequences normally found at the terminals of collagen molecules. Both are able to form hydrogels under similar physiological conditions, but at different rates; and result in gels with different physical properties. For example, atelocollagen has reduced ability to form well organised fibrils (Brennan

and Davison, 1981), aggregation rates, resistance to collagenase treatment (Walton et al., 2010) and thermal stability compared to tropocollagen derived hydrogels (Snowden and Swann, 1979).

Gelling conditions - pH, temperature and salt concentrations

Fibrillogenesis is described as an entropy driven process and is usually best at physiological temperature ($\sim$37℃). Temperatures too high can potentially denature the collagen protein into gelatin, whilst a low temperature will delay fibrillogenesis. Indeed, Comper and Veis (1977) found that the temperature can affect the nucleation (lag) phase of fibrillogenesis (but not the subsequent growth phase of gel formation).

Salt (NaCl) concentrations have been shown to influence the nucleation time (lag phase) during fibrillogenesis (Snowden and Swann, 1979); which may be attributed to changes in electrastatic interactions needed in nuclei formation (Comper and Veis, 1977). The presence of salts is important for the formation of structrually defined fibrils (Harris and Reiber, 2007), as fibrils formed without salts are less organised with spindle shaped aggregates.

Fibrillogenesis at neutral pH and physiological salt concentrations (pH6.5-8; in the presence of 150mM salt) led to stable hydrogels with fibers displaying the expected banding patterns, indicative of collagen molecule fusion with adjacent molecules at perfect alignment. At low pH ($\sim$pH 2-5), only poorly formed fibrils were produced. At pH 9, banding patterns of fibrils were present, but parallel bundling of collagen molecules appeared to be looser (Harris and Reiber, 2007).

Other molecules

The rate and extent of type-I collagen fibrillogenesis are susceptible to influence by other proteins and molecules, mainly, via changes in electrostatic interactions.

Changes in electrostatic interactions due to the presence of anions (especially chloridion and sulphates) affected the rate and extent of fibrillogenesis, possibly by altering the density of the hydration layer around collagen molecules. Although the exact effect depend on the type of anion and its concentration (Xing et al., 2011), the isoelectric point (pI) of collagen monomers are highly influenced by ion species (Li and Douglas, 2013). Some effects on the matrix structure and stability of the collagen structure was also noted.

Proteins naturally found within most tissues (i.e. proteoglycans and glycosaminoglycans (GAGs)) can also impact on collagen hydrogel formation. For example, GAGs such as dermatan sulphate added to the collagen solution prior to fibrillogenesis reduced nucleation time, increase rate of growth phase and increased the overall extent of collagen precipitation (Snowden and Swann, 1980) (Paderi et al., 2009). High density proteoglycans, on the other hand, increased nucleation time, but had little effect on other parameters of fibrillogenesis. They are also thought to exert influence on fibrillogenesis via electrostatic interactions (Mathews, 1965), where negatively charges on the polysaccharide interacts with the positive charges of the protein.

Another study found that the polysaccharide, ficoll, affected fibrillogenesis by increasing the lag time during nucleation, increased fibre growth rates and changed the architecture of the resultant matrix fibril (Dewavrin et al., 2014).

Other molecules, such as modified small leucine-rich proteoglycans (SLRPs) were able to delay fibrillogenesis in a dose dependent manner (Paderi et al., 2009).

Why use collagen hydrogels?

The main advantage of using collagen hydrogels in TE is the possibility of incorporating cells within an ECM-like matrix at *time-zero* (as the matrix is being formed) without direct cell involvement.

The reason collagen hydrogels enables cells to behave in a physiological manner is because they provide the interstitial cells with native tissue-like fluid and solid components, mechanical properties, topographical features and orientation cues - all of which changes with time in response to cell action (Brown, 2013a). The accessibility of the *in vitro* material will also enable the visualisation and study of cell-matrix interactions (i.e remodeling (Grinnell, 2003), cell attachment (Jiang and Grinnell, 2005), migration (Grinnell et al., 2005)).

The collagen matrix can be made more complex by building additional features into the basic hydrogel (bottom-up approach to TE (Brown, 2013b)). This makes it possible to isolate variables and tailor the model with tissue-specific features, which will ultimately impact on cell behaviour within the model tissue.

1.5 Plastically compressed hydrogels as tissue models

Cellular collagen hydrogels (typically containing >99% water) was first described by Elsdale and Bard in 1972 (Elsdale and Bard, 1972), and have since been a used to characterise cell behaviour within a 3D environment. The super-hydrated hydrogels, consisting mostly of water, have only weak mechanical properties and can quickly be resorbed when placed *in vivo* (Tabata et al., 2000). This means interstitial cells can potentially lose their surrounding supportive matrix.

Plastic compression of collagen type-I hydrogels is a technique developed

by Brown et al. (2005), where excess fluid trapped between fibrils of the hydrogel lattice during fibrillogenesis is expelled from the matrix by a combination of compressive load, gravity and capillary action (fluid absorbed into contacting blotting paper). This process increases collagen density within the construct to physiological levels, without altering its chemical composition. It is termed 'plastic' because compression expels the liquid non-reversibly, and water does not return to the collagen fibre lattice even on the removal of the compressive load (Brown et al., 2005).

The advantage of using plastic compression is their cell-compatibility when improving hydrogel collagen density. If, for example, the hydrogel is made from a collagen solution with a density of ~ 2mg.ml^{-1}, the resultant hydrogel will contain $\sim 0.2\%$ collagen, and 99.8% water. With a single plastic compression, collagen density typically increases at least 55 folds, to $\sim 11-18\%$ (w/w)(Brown et al., 2005) (Abou Neel et al., 2006) (Cheema et al., 2008). The resultant compressed collagen have been shown to persist for at least 5 weeks *in vivo* (Mudera et al., 2007). Cells can remodel and migrate through the construct, but the overall dimensions and shape remains relatively unchanged over the culture period (Alekseeva et al., 2012b).

There are currently two standardised methods to produce plastically compressed collagen gel, namely a) downward flow compression (Brown et al., 2005) (figure 1.2) and b) upward flow compression ((Alekseeva et al., 2011)) (figure 1.3); each referring to the predominant direction of fluid flow during compression. Both methods essentially result in compressed collagen constructs with similar μ-structures (figure 1.4). However, downward flow compression has the advantage of customisable shape and size of the final compressed construct (as the hydrogel can be made in customised moulds), whilst the upward flow method is optimised for constructs produced in multiwell-plates, which allows for increased reproducibility and through-put.
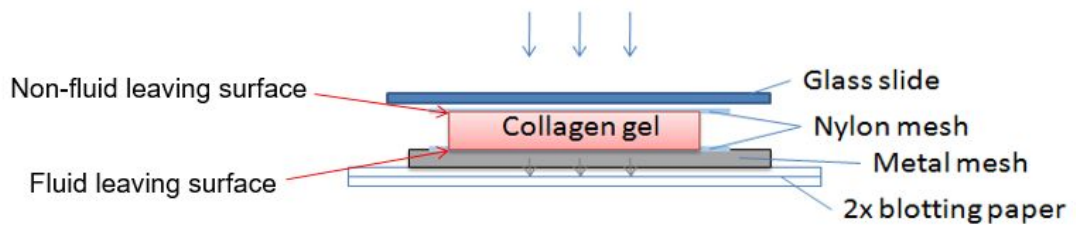
Figure 1.2: Schematic of downward flow compression of collagen hydrogels. Hydrogels are transferred from their moulds onto blotting paper, protected on either sides by nylon mesh (and a layer of metal mesh for easy handling). A load is then applied from top of the gel to expel excess fluid from the hydrogel, downwards onto the blotting paper.
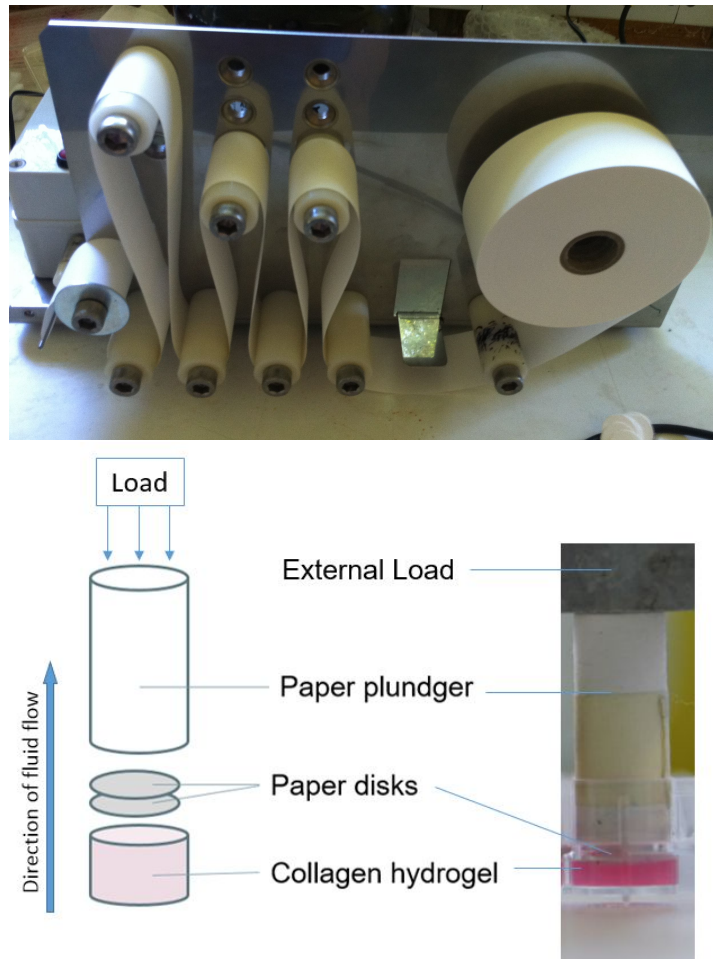
Figure 1.3: Setup for upward-flow plastic compression set within culture well-plates. (a) Custom-machine for rolling Whatman chromatography paper (4cm thick) to produce well-sized absorbent plungers. (b) Schematic of upward-flow plastic compression where absorbent plungers and an external load are placed onto the hydrogels (separated by blotting paper discs to protect the hydrogel). Fluid flows out of the hydrogel and travels upwards into the plunger.
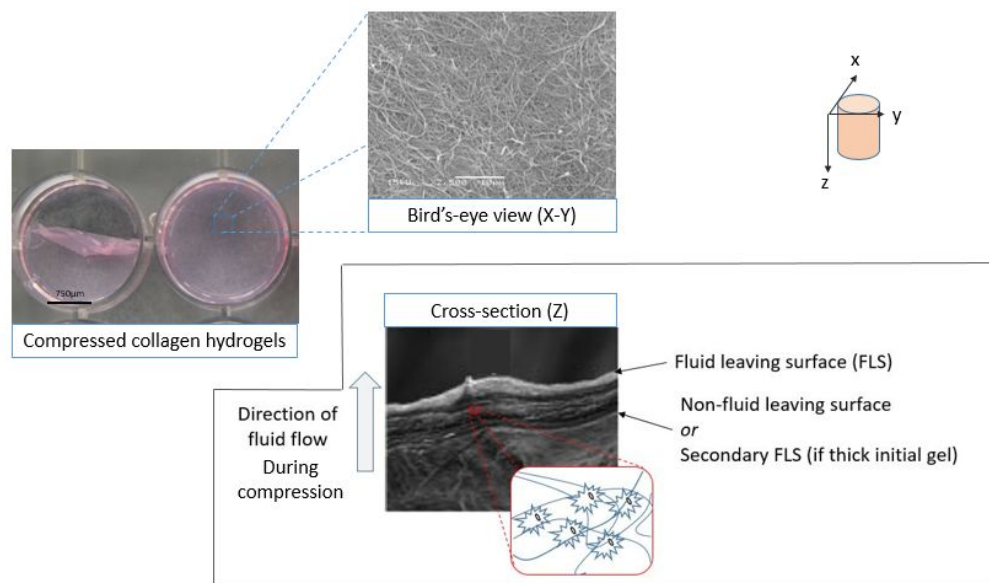
Figure 1.4: Collagen hydrogel compresses into a thin membrane-like material (typically between 50-150μm) with a mesh-like structure observable on the hydrogel surface (bird's-eye view (X-Y plane; SEM image). The cross-section SEM image (Z plane; adapted from Hadjipanayi et al. (2011a)) reveals that collagen fibrils are arranged into a lamellae-like micro-structure. The density of collagen fibrils/lamellae is non-uniform throughout the hydrogel cross-section, and is highest at the fluid leaving surface (annotated above; with schematic representation of cell entrapment *between* collagen fibres within the construct).

In all studies within this thesis, upward flow compression is used on the collagen hydrogels due to the high throughput potential and reproducibility, important for *in vitro* tissue model systems. Briefly, the process begins from the application of an absorbent paper discs and a plunger (made from a roll of blotting paper) onto the hydrogel. Note that the amount of pressure/load on the compression system only influences the compression rate at the initial stages of compression (Hadjipanayi et al., 2011a). One specific feature of the compressed collagen gel is the presence of a fluid leaving surface (FLS) (figure 1.4). This FLS consists of a dense concentration of collagen lamellae layers (1-5μm thick, observed in the cross-section (z-plane) view of the compressed gel). Although these lamellae are found throughout the thickness of the gel, their density was highest towards the FLS (Brown et al., 2005). The high density at the FLS, and so increased blockage/resistance to fluid outflow causes fluid flow to reverse, and escape through other surfaces of the hydrogel (further discussed in chapter 4, pg.125).

By default the surface opposite the FLS is the non-fluid leaving surface (NFLS), and usually contains a collagen matrix that is relatively less dense compared to the FLS. However, if the initial hydrogel thickness is high, a secondary FLS (with increased collagen density) forms in place of the NFLS, with an associated increase in resistance to fluid outflow through the secondary FLS. The finding that a secondary FLS forms at the surface directly opposite the FLS (i.e. the NFLS), and not at the sides of the hydrogel, suggests that fluid flow is subsequently directed towards the NFLS (i.e. the NFLS becomes a secondary FLS so that both top and bottom surfaces of the hydrogel has a high collagen density compared to the rest of the gel) (Tan, 2015). Note again that the NFLS only becomes the secondary FLS in gels with a high initial thickness, and can therefore be controlled to some extent, to create a defined collagen matrix microstructure within the collagen hydrogel.

The main advantages of using plastically compressed hydrogel constructs is the relative ease and speed in producing cellular, collagen-dense constructs (produced within minutes-hours, instead of weeks if reliant on cell migration and cell-ECM production). Additionally, the resultant constructs are thin and 'see-through', allowing the real-time monitor of model tissues (figure 1.4). The ECM structure (type-I collagen) is formed around the cells from time-zero (t0), negating the dependence on cells to migrate into dense collagen structures, and remodel (or produce) the ECM structure. Diverse cell types - such as those derived from skin (Hadjipanayi et al., 2009b), muscle (Kayhanian et al., 2009), bone (Bitar et al., 2008), vein (Hadjipanayi et al., 2011b) and nerves (Georgiou et al., 2013) - have been successfully cultured within compressed hydrogels.

Since cells are embedded within, and are supported by, a dense collagen ECM, the cues received from the compressed collagen matrix will be comparable (at least more physiological compared to 2D plastic plate cultures) to that of their native environment. Here, collagen type-I acts as a structural scaffold to which cells and other cell-influencing proteins/molecules can be incorporated to increase the tissue specificity of the model. These external ECM cues can then impact cell behaviour.

1.6 Interactions between cells and type-I collagen

For most cells, the ECM provides more than just structural support. Cells are able to attach to, and sense their surrounding environment - including both chemical and physical cues presented to the cells. For example, soluble growth factors (as a chemical cue) can be bound to the ECM which regulates their distribution, activation and presentation to cells within the matrix (Hynes, 2009). However, the main focus (in the first part) of this thesis is to create a physi-

ological **physical** environment by creating cell substrates that can match the natural tissue mechanical properties of stiff soft tissues; and in doing so, create a model tissue which produces physiological cell response to implanted biomaterials.

In terms of sensing their physical environment (i.e. matrix stiffness/ deformability and topography), cells interact with the ECM through attachment. Mechanical stimuli are converted into chemical signals, which in turn affect cell behaviour. This process of mechanotransduction can be via a range of cell-matrix attachments, with integrins being the most prominent and studied group of cell-matrix attachments.

Integrins are a family of cell surface receptors which link the cell external and internal environment. They can work with other proteins such as cadherins (involved in cell-cell attachment; (Gumbiner, 1996)), syndecans and selectins, to name a few, in order to produce cell-cell and cell-matrix interactions which are found in the natural tissue (Ramage, 2011).

The cell surface integrins $\alpha 1 \beta 1$, $\alpha 2 \beta 1$, $\alpha 10 \beta 1$ and $\alpha 11 \beta 1$ are known to associate with collagen molecules (White et al., 2004). The binding activity of integrins to ECM is regulated from inside the cell, but requires the formation of focal adhesion complexes to connect the cell internal and external environments. Focal adhesion and the process of mechanotransduction is complex and involves many proteins (upwards of 180 proteins (Kuo, 2013)) and pathways. Binding of talin and other adaptor proteins to β-subunit of the integrins has a key role in integrin activation within the cell (Legate and Fssler, 2009) (Mason et al., 2012) (β-subunits of the integrins regulate integrin activation through conformational change).

Binding of the integrins to the ECM proteins focuses clusters of integrin molecules within the plasma membrane. After initial activation, focal adhesions matures into multi-protein complexes at the cytoplasmic interface where

actin filaments and other intracellular signaling molecules are recruited (Hynes, 2002).

The ability of cells to sense matrix stiffness, or more accurately their deformability, is partly dependent on the contractility of the actin-myosin cytoskeleton, which is transmitted to the ECM through integrins and focal adhesions. Cells respond to the stiffness of their substrate by altering their cytoskeleton organisation, cell-substrate adhesion and other processes which affect cell behaviour (Mason et al., 2012).

For example, focal adhesion size linearly depend on local force exerted by cells. Mature focal adhesions elongate and orientate in the direction of actin stress fibres and applied force. Cell-substrate adhesion increases due to increased stiffness (Engler et al., 2004), and this change in adhesion alters cell shape which help regulate polarisation and alignment of stress fibers within cells (Zemel et al., 2010) (i.e. cells sense the tension of the material (Marenzana et al., 2006)). Similarly, cells also respond to changes in collagen fibril diameter and alignment (i.e. topography), and was found to increase matrix synthesis on thicker fibrils (i.e. 300nm diameter fibrils instead of 30nm) (Muthusubramaniam et al., 2012).

In order to produce a model that closely mimic the native tissue, it is important to understand the causes of cell behaviour changes, and the factors which cause physiological and tissue specific cell responses within the model.

1.6.1 Modeling of cell response within plastically compressed collagen hydrogels

As discussed in section 1.6, cells (such as fibroblasts), attach and respond to the cues provided by the collagen matrix. Examples (from the literature) of cell behaviour studied/modeled within the plastically compressed collagen

hydrogel 3D matrix are discussed below.

Cell viability

Cell viability is typically measured using live/dead cell staining and imaging techniques (East et al., 2010) (Wong et al., 2013) within the compressed hydrogel. Without other interventions, the cell viability within collagen hydrogels after plastic compression was found to be $\geq 90\%$ (Brown et al., 2005), with many studies reporting a higher percentage of viable cells (of different cell types) within the compressed gel. This high level of viable cells is likely attributed to the controlled compression of the sample, and the high permeability of the construct to cell essential molecules (constructs typically $\sim 100\mu$m thick). The thin sample also means that cells can be easily visualised when embedded within the matrix.

Generally, it is difficult to correlate the effects of cell-essential molecules, such as oxygen, to cell behaviour *in vivo* (due to the presence of other confounding variables). The simplified *in vitro* tissue model therefore acts as a powerful tool in studying the effect of oxygen concentrations (within a 3D construct), on cells. For the measurement of oxygen permeability, and its effect on cells, Ardakani et al. (2014) used a spiraled compressed cellular gel, with oxygen probes to measure the partial pressure of oxygen in the core, middle and outer layers of the construct. Cell viability within the construct remained above 70% even at the core. Although the partial pressure of oxygen was many times lower than the outer layers, this was not pathological. Another study by Cheema et al. (2008) showed that the majority of cells ($\geq 55\%$) remain alive within the core of a spiral collagen hydrogel constructs, even with a relatively low oxygen partial pressure, after 10 days in culture.

Anandagoda et al. (2012) also studied the effect of applying a layer of hyaluronic acid (HA) adjacent to a cellular compressed gel layer (spiraled to-

gether), and found a $\sim 88\%$ cell viability at the HA-collagen gel interface. Cells trapped in areas away from the HA saw a similar live cell count of $\sim 89\%$. The model was able to show that the HA component swelled as the compressed collagen gel got thinner, leading to the hypothesis that the dehydrating effect of HA on the collagen gel component caused the (albeit small number of) cell death, and the effect was therefore not due to toxicity of the HA material.

Migration

Migration of cells within the 3D construct with the appropriate directional cues, can be an indication of the extent of cell attachment to the matrix and the presence of chemical (or physical) gradients (i.e. oxygen, growth factors). Within the compressed hydrogel construct, cells migrated in response to oxygen concentration gradients (from an area of lower to higher partial pressure of oxygen) (Ardakani et al., 2014). Non-proliferating cells were also found to aggregate at the stiff-end of a construct which has been produced with a longitudinal collagen density gradient (material stiffness range between 1057-2305 kPa), demonstrating that cells will migrate in response to substrate stiffness (Hadji-panayi et al., 2009c).

The ability for cells to migrate within the type-I collagen derived constructs was also implied in the layer integration of hydrogels, as it was thought that cells drag and bend collagen fibrils as they migrate between layers (Meshel et al., 2005). Indeed, adhesive strength between two layers of collagen gels increased with culture time for cellular constructs (6-fold increase by 1 week in culture) (Hadjipanayi et al., 2009a), and not in its acellular equivalent. Since cells migrate between contacting layers, the adhesion strength will also depend on the contact surface area between the two layers (Marenzana et al., 2007) (and presumably the level of cell activity and number of cells present).

Proliferation

Cells naturally proliferate in growing tissues, and also for the maintenance of cell populations during cell-turnover. Proliferation of cells within the collagen hydrogel is typically measured through changes in the amount of total cell metabolic activity over time, through imaging, or more reliably through the quantification of total DNA content within the construct (as an end-point assay).

Within the collagen hydrogel, factors that influence proliferation rates include the initial cell seeding density; where a low density resulted in a relatively high proliferation rate (compared to cells within samples containing a high initial cell density; MG63 osteosarcoma cell-lines used in this study) (Bitar et al., 2008). This difference in cell proliferation rates was observed for up to 10 days, possibly when cell density within the 'low cell density samples' increased to a level where cell-cell inhibition occurred.

The link between high cell density and low proliferation rates was also observed in a study by Hadjipanayi et al. (2009b). The study found that the matrix stiffness surrounding the cells (not just the overall cell substrate) directly regulated proliferation rates, such that a graded increase in proliferation rates was seen with increasing collagen density.

Differentiation

The monitor of cell differentiation within the model will be essential to predict tissue development over culture time, particularly when cell types with the potential to differentiate into different lineages are involved.

For example, an obvious measure of long term success of an implant (other than in cartilage and ligament tissues) is the development of a blood supply. Previous studies have been able to demonstrate angiogenesis within the plastically compressed constructs with the co-culture of human dermal fibroblasts

(HDF) and human umbilical vein endothelial cells (HUVEC) (Hadjipanayi et al., 2010). Here, physiological hypoxia was identified as a factor which encouraged an angiogenic response, where endothelial cell clusters (positively stained for CD31 and vWF) were formed by 1 week within the capillary like structures.

Others

Other interesting measures of cell behaviour within the plastically compressed hydrogel include the regulation of protein/growth factor production, gene regulation and matrix remodeling.

Cheema et al. (2008) showed that cells respond to reduced oxygen partial pressures in their environment, by significantly increasing the level of vascular endothelial growth factor (VEGF) expression (at a maximum 151-folds). Importantly, the model was able to reflect the temporal change in VEGF levels over time, such that peak levels were seen at days 7 and 8, followed by an immediate drop in VEGF expression. In this study, it was also observed that cells may alter their consumption of oxygen in low oxygen environments. For example, partial pressure within the core of a cell-dense construct increased from ~ 25mmHg to ~ 60mmHg over time, with no obvious changes in cell numbers over several days in culture.

In terms of gene regulation by cells, Karamichos et al. (2008) showed that cells (primary HBMSCs) respond to matrix stiffness, and that the amount of serum within the collagen construct affected gene regulation and force generation. An increased matrix stiffness corresponded to a decrease in cell force generation, and increased lag time before the onset of hydrogel contraction (Karamichos et al., 2007). It was also found that the lag time to cell contraction, and the amount of force generated by cells, had some dependence on the amount of fetal calf serum (FCS) present within the cell environment. In the presence of 10% (v/v) FCS, an increase in matrix stiffness up-regulated

COL3 and MMP2 expression; whilst in 20% FCS, MMP2, COL3 and COL1 were unaffected (or slightly down-regulated) by matrix stiffness (Karamichos et al., 2008).

The remodeling of the matrix by cells can also be studied *in vitro* over time within hydrogel constructs. The kinetics of collagen fibril (enzymatic) degradation is strain/load dependent, affecting the rate of MMP secretion and collagen deposition (Hadi et al., 2012) (Collins et al., 2005). Over time in a cell-seeded construct, the remodeling action of cells gradually loosens the matrix (Tan, 2015, p.215). The overall shape of the compressed collagen construct, however, remains unchanged even after cell remodeling (Alekseeva et al., 2012b).

All in all, the above models have shown that cells respond to hydrogel:

- Matrix stiffness

- Matrix/cell binding site density

- Chemical gradients (i.e. growth factors, oxygen)

- Cell density

- Topography

1.6.2 Further engineering of plastically compressed hydrogels

Plastically compressed collagen gel is used as the basic model for next-generation models with added tissue-specific features. Therefore, it is important to review all methods of compressed hydrogel manipulation already in the literature; including chemical and physical features that has previously been incorporated into the basic model. Many of these features designed to build an increasingly complex model, to ultimately improve the relevance of the material to the target

tissue. These features provide environmental cues that are designed to direct cell behaviour, and can include **chemical cues** such as growth factors, cell-attachment proteins; or **physical cues** such as the structure (i.e. topography, anisotropy and alignment) and stiffness of the construct.

The examples listed below involve direct engineering of the collagen construct (predominantly free of direct cell involvement), and means that changes to the hydrogel (and therefore its effect on cells) are **instant and controllable**.

Mechanical properties

Multiple studies have shown the importance of matching native tissue and biomaterial stiffness for optimal construct-tissue integration (Moroni and Elisseeff, 2008). The mechanical properties of biomaterials are often quoted in stiffness (Young's modulus), shear modulus and the stress and strain until failure. A typical compressed collagen sheets have been reported to have a break strength of 0.6 ± 0.11 MPa and a Young's modulus of 1.5 ± 0.36 MPa (Brown et al., 2005). This value is often short of the nature tissue strengths (where individual hydrated collagen fibrils can have a Young's modulus of 0.2-0.5 GPa (van der Rijt et al., 2006).

Normally, standard methods to improve mechanical properties of collagen materials will involve some form of chemical cross-linking, such as with genipin or gluteraldehyde. However, the purpose of using plastically compressed hydrogels, instead of stiff and dense collagen materials (such as decelluarised collagen sponges), is their good initial interstitial cell viability immediately after fabrication. The use of harsh cross-linking methods defeats this purpose.

Photochemical cross-linking using photoactivated riboflavin is one possible way to cross-link cellular gels, as they are only activated when illuminated with blue light (Wong et al., 2013) (Rich et al., 2014). Topical application of riboflavin and its subsequent cross-linking resulted in some interstitial cell survival, which

then populate the hydrogel with time.

Alternatively, mechanical properties can be improved by further increasing the density of collagen within the construct. Double compression (second plastic compression of rolled compressed collagen sheet) achieved twice the collagen density (increased from 12.6% to 23.1% collagen), and resulted in a significantly increased break stress and modulus (Abou Neel et al., 2006).

Collagen fibril diameter within hydrogels was also reported to influence mechanical properties of the hydrogel. Cyclic loading (cycles of 20% strain and relaxation) encouraged side-to-side collagen fibril fusion in hydrogels, as seen by the increase in cross-sectional fibril diameters. After 144 cycles, the break stress, elastic modulus and break strain have increased 450%, 125% and 133% respectively (Cheema et al., 2007a).

Mechanical properties of the construct can also be improved by incorporating a supporting biomaterial within the hydrogel. For example, a PLGA mesh has been incorporated between collagen hydrogel layers before compression (Ananta et al., 2012) to produce a material that is easier to handle. Similarly Deng et al. (2014) have shown an increase in construct Young's modulus, from 2.31MPa to 70MPa, after aligned PGA fibers were incorporated within the hydrogel. This provided interstitial cells with temporary stress shielding from externally applied force. However, since the increased strength of the construct was dependent on the PGA fibers, the subsequent hydrolysis of the PGA (and so the lost of fiber continuity) caused a sharp decrease in the Young's modulus.

Anisotropy and topography

Another important consideration is the surface anisotropy and μ-structure of the construct **as perceived by resident cells**. This can impact on cell alignment, differentiation and construct perfusion for the long-term survival of cells within the construct.

Anisotropy within the collagen construct has been produced at different hierarchial/structural levels; from the nano-scale (i.e. alignment of the collagen fibrils) up to the micron-scale (i.e. embossing channels onto the construct during compression) (Kureshi et al., 2010). In the same study, alignment of cells (WI38; lung fibroblast-like cells) parallel to embossed grooves was also demonstrated.

Further guidance of cells within channels was explored using conical-shaped channels, created from soluble phosphate glass fibres which 'opened' at different rates when the glass fibres began dissolving from the thinner end. This produced a channel which opened towards the thicker end of the fiber with time (Alekseeva et al., 2012a), with the aim to ultimately encourage directional cell migration.

Alternatively, gross anisotropy of the compressed collagen gel can be achieved by topical surface cross-linking (i.e. applying directional stripes) of the collagen gel (Wong et al., 2013). This resulted in a doubled break stress in one axis of the hydrogel (parallel to the stripes).

Patterns (i.e. grooves) and channels can easily be embossed onto the hydrogel surface during plastic compression (Brown et al., 2005) (Alekseeva et al., 2012b) (Tan et al., 2014); or within the collagen construct (Alekseeva et al., 2012a) (Cheema et al., 2010). Note that for surface embossing, the above studies have found that pattern and shape of the mould is replicated most faithfully at the FLS (Alekseeva et al., 2012b), and surface patterns does not deform when additional layers are compressed onto the patterned surface (Tan et al., 2014). Grooves remained stable even in culture (with cell remodeling) over a test period of 14 days (Alekseeva et al., 2012b). This can potentially provide directional cues for cell migration and perfusion within thicker constructs Cheema et al. (2010).

Chemical cues

Another important consideration for *in vitro* tissue engineering is the impact of chemical cues found in the matrix environment, such as growth factors, on resident cells. Cells produce growth factors and other proteins with culture. Pre-cultured cellular compressed hydrogel construct can be used to deliver physiological levels (and combinations) of growth factors (i.e. for angiogensis in response to hypoxic culture conditions; such as HIF-1α, VEGF and matrix remodeling proteins such as MMP2 and MMP9) into a second construct. Hadjipanayi et al. (2011b) demonstrated that angiogenic growth factors (produced in response to hypoxic conditions; in the pre-cultured gel) diffused towards the new hydrogel by day 1, resulting in increased mean length of capillary like structures. Cell density in the initial growth factor delivering gel influenced extent of vascularisation (i.e. increased cell density (and presumably the amount of growth factors produced as a result) improved signs of vascularisation).

Others

Multiple layers of collagen hydrogels can be compressed together to build complexity within the tissue model (i.e. test migration of cells or interaction between two different cell types in adjacent layers). Layers were found to have good integration when compressed together (Tan et al., 2014). Topical crosslinking at the layer interface also further improved integration of compressed collagen sheets (Wong et al., 2013). The presence of cells within the hydrogel also improved layer integration as cells are thought to migrate across the layer interface whilst bending and carrying collagen fibrils across the interface (Hadjipanayi et al., 2009a).

1.7   Aims and objectives

The overall aim of this research is to produce next-generation, 3D hydrogel-based, **soft tissue models** with the ability to predict native tissue response to implant biomaterials. Since type-I collagen is one of the most abundant proteins found in human tissues, it is used as a tissue model substrate to provide physiological spatial cues for cells (i.e. cell-matrix attachments).

Overall, it is currently possible to generate tissue-like models using plastically compressed collagen hydrogels with:

- Dense extracellular matrix around various cell types

- Defined microstructures (i.e. FLS with collagen density gradient)

- Controllable matrix stiffness (within a modest range)

- Controllable surface topography

- Multi-layers with good perfusion of cell-essential nutrients

- Construct anisotropy

- Easy *in vitro* access for monitoring

Nevertheless, for the modeling of some soft tissues, such as skin and tendon, a matrix with increased stiffness and complexity will be required; and the production of the next generation with such features is the aim for the current study.

The objectives of the current studies are:

1. Increase mechanical properties of the collagen model substrate whilst retaining initial cell viability

2. Monitor biomaterial and cell response within a tissue-like model over time

1.7.1   Thesis overview

The aim of this study is to develop 3D soft tissue models with improved relevance to human tissues, and to study biomaterials within the accessible tissue-like model over time. All tissue models are based on plastically compressed hydrogels made of type-I collagen, the main structural proteins of most soft tissues.

This thesis is divided into two main sections. First involves the development of an *in vitro* model tissue with increased mechanical properties. The key feature of this model tissue is that it must contain an initial live cell population within the construct, have increased mechanical properties compared to traditional compressed collagen hydrogels, and has the potential for high through-put testing (in well plates). This was explored in chapter 3 by developing a novel hydrogel using a pre-crosslinked collagen (polymeric collagen, blended with traditional gel forming tropocollagen molecules) as the starting material for gel formation. Chapter 4 continues onto the characterisation of the resultant polymeric collagen containing gels. It was found that the blend gels collapsed quickly upon compression, leading to cell-damaging fluid shear stresses. Chapter 5 explores methods which can control fluid efflux rates from hydrogels by increasing the filtration effect (using macromolecules) at the FLS of the hydrogel.

The second part of the study looks into the applications of compressed collagen hydrogel based soft tissue models. Chapter 6 deals with the modeling of nanoparticle drug-delivery, and its effect on local tissues. Specifically, the growth factor, bone morphogenic protein-2 (BMP-2) is thought to be produced (in bone-like tissues) in response to statin drugs. Temporal changes to BMP2 protein levels was therefore tracked within the model. Chapter 7 studies the degradation of biomaterials (using fluorescent PLGA as a test material) within

a tissue-like environment. The degradation rates of the biomaterial in 2D and 3D (with/without cells), and the fate of the degraded biomaterial, are studied.

The methods common to all studies throughout this thesis are detailed in chapter 2. Finally, the main findings and conclusions of the studied models are summarised in chapter 8.

Chapter 2

Materials and Methods

Materials and methods used routinely throughout the project are listed in this chapter. Any variations to the methods (or methods specific to the study) can be found in the methods section of subsequent chapters.

2.1 Cells

Neonatal human dermal fibroblasts (HDF) and human osteosarcoma cell-line MG63 were cultured in 1000mg glucose Dulbecco's modified Eagle's medium (DMEM; Sigma, UK), supplemented with 10% (v/v) fetal calf serum (FCS; First Link, UK) and 1% penicillin streptomycin (Gibco Life Technologies, UK). Cells were removed from monolayer culture by washing with phosphate buffer saline (PBS) and incubating with trypsin (0.5% trypsin-EDTA; Gibco Life Technologies, UK) for 5 minutes at 37℃.

2.2 Collagen hydrogel preparation

Conventional collagen hydrogels were prepared, on ice, by neutralising 80% (v/v) rat tail acid-soluble type-I collagen (between 2.05 and 2.16mg.ml^{-1} in

70

acetic acid, First link, UK) containing 10% 10x Minimum Essential Medium (MEM) (Gibco life technologies, UK) using 5M and 1M sodium hydroxide (NaOH). The drop-wise addition of NaOH gradually changed the colour of the phenol red pH indicator (included in the 10xMEM), from yellow to fuchsia pink, when neutralised. The remaining 10% volume was made up with phosphate buffer saline (PBS) or DMEM (with or without cells). The neutralised collagen solution was gelled by incubation in 24-well plates at 37℃, 5%CO_2, for 30 minutes (gel volume depended on the study).

2.3 Polymeric collagen extraction

Polymeric collagen was extracted from tendons due to their relatively high polymerised type-I collagen content (see chapter 3 for further details). Fresh tendons were frozen at -20℃ for storage. 2 - 6g ostrich (2 years old) or calf tendons were homogenized in liquid nitrogen using a stainless steel mortar and pestle. The resulting tendon granules were pre-treated overnight at 4℃ in excess ($\sim$150ml per gram of tendon) 0.5M ethylenediaminetetraacetic acid (EDTA; Sigma-Aldrich) adjusted to pH 7.4, with at least one change (Steven, 1967). Treated tendon granules were washed twice in distilled water prior to expansion in 0.5M acetic acid ($\sim$100ml per gram of tendon). The solution was stirred constantly with a magnetic stirrer at 4℃ for at least 3 hours and the expanded collagen was recovered as polymeric collagen by stirring with a glass rod during neutralization (5 and 1M sodium hydroxide (NaOH)). This collected the polymeric collagen as it shear aggregated onto the glass rod. Collagen fibrils were suspended in 0.5M acetic acid, and re-precipitated at least twice to remove impurities trapped between collagen fibrils. Where necessary, the polymeric collagen solution was sterilized by mixing with an equal volume of chloroform (BDH Laboratory Supplies, UK). Collagen concentration was ad-

justed to 2mg.ml⁻¹ in 0.5M acetic acid before use (Wong et al., 2014).

2.4 Plastic compression

Following gelation, collagen hydrogels were plastically compressed based on previously described methods (Brown et al., 2005). A modified method more suited for up-scaling processes, namely in multi-well culture plates, was used for all plastic compression processes (Alekseeva et al., 2011). Briefly, absorbent paper roll plungers were made by rolling blotting paper (Whatman grade 1 chromatography paper, 93x4cm) into a coil ($\sim 15mm$ diameter; autoclaved for sterilisation when required). This was placed onto hydrogels formed in 24-well plates. The two components were separated by two well-sized paper discs (Whatman, grade 1 paper) to prevent the hydrogel from sticking to the plunger, and to prevent the unintentional embossing of the coil (plunger) pattern onto the gel. Weights of 21g per well was used where specified. After the completion of plastic compression, the plunger roll was removed. PBS or cell media were then added to each well immediately to keep the samples hydrated. The paper discs separating the plunger and hydrogel can then be removed at this point. Samples were then carefully detached from the base of the well, and used or cultured as required.

2.5 Rate of plastic compression

Rate of hydrogel compression was measured as the mass gained (fluid absorbed from the hydrogel) by an absorbent plungers with compression time. The plunger mass was measured every 30 seconds in the first 5 minutes of compression, and then every minute subsequently until no further mass gain was detected. No additional external weights was loaded onto the compres-

sion system in this part of the study.

2.6 Quantification of cell proliferation and cell toxicity

Alamar blue is a redox indicator used to quantify total cell metabolic activity within the sample. The alamar blue compound is also known as resazurin which is blue, and mostly non-fluorescent. However, it is reduced by cell mitochondrial activity to form a red fluorescent compound which can then be detected using a spectrophotometer. At selected time points, samples were incubated with 10% (v/v) alamar blue (AbD, Serotec) solution in phenol red-free DMEM for 4 h (500μl per well). Duplicates of 100μl of alamar blue solution from each well was transferred into a 96 multiwell plate, and absorbance was read with a microplate spectrophotometer (MR700 microplate reader, Dynatech Laboratories) at 510 and 590 nm. Samples were subsequently washed with PBS and returned to culture after culture media was added to each well.

2.7 Cell viability assay

Cell viability within compressed (or uncompressed) gels was confirmed by fluorescent imaging after a 45 minute incubation of the cellular hydrogel with stains consisting of 17μl ethidium homodimer (2mM; Invitrogen) and 20μl calcein-AM (4mM; Fluka Analytical) diluted in 5ml PBS (0.5ml of diluted stain solution in each well of a 24-well plate). Images were taken on the Olympus BX61. For each sample, images of three random fields of view was captured for cell counting. The number of live (green, calcein-AM stained) and dead (red, ethidium homodimer stained) cells were only included if the cells were within a digitally

superimposed frame (identical for each field of view).

2.8 Histology

Collagen constructs were prepared using a routine protocol. Samples were fixed with 4% paraformaldehyde for subsequent histological processing. Processed samples were embedded in paraffin wax and sectioned to a thickness of 8 - 10 μm. This was followed by standard haematoxylin & eosin (H&E) staining protocol. Briefly, sections were dried at 60°c overnight and de-paraffined the following day before rehydration through an descending alchohol series. The slides were washed gently in running water and was placed in haemotoxilin (Sigma, UK) for 10 minutes. Slides were dipped into acid-alcohol solution 5-6 times, washed and placed in eosin (Sigma,UK) for a further 10 minutes. The sections were then dehydrated with a ascending alcohol series and finally mounted in DPX (VWR, BDH Prolabo). Samples were subsequently viewed on a standard light microscope (Olympus, BH-2).

2.9 Scanning electron microscopy preparation

Samples were fixed in 2.5% glutaraldehyde (in 0.1M sodium cacodylate buffer) for at least 1 hour, and were subsequently washed with 0.1M sodium cacodylate buffer. Fixed samples were then dehydrated with a series of ascending alcohol concentration and hexamethyldisilazane (Aldrich, USA) treatment overnight. The dried samples were then sputter-coated with gold-palladium (K550, Emitech) and imaged as detailed below.

2.10   Microscopy

2.10.1   Light

In early samples, haematoxilin and eosin (H&E) stained sections were visualised and imaged using a Olympus BH-2 microscope and Olympus Camedia digital camera. Subsequent samples were visualised and imaged on the Zeiss Primovert microscope (Zeiss Axiocam 105 color camera).

Birefringence

On the Olympus BH-2 light microscope, a rotating light polarising filter was installed at the light source. Images were then taken using the Olympus BH-2 microscope and Olympus Camedia digital camera.

2.10.2   Fluorescence

Two different fluorescent microscopes have been used. Either the Olympus BX61 microscope with fluorescent light source from X-cite series 120Q, or the Olympus BH2-RFCA (with light source Olympus BH2-RFL-T3). In the latter, images were taken in black and white with a Hamamatsu digital camera (C4742-95). Images were subsequently processed using ImageJ to adjust colours to reflect those seen on the microscope.

2.10.3   Scanning electron microscope (SEM)

Sputter coated samples were imaged at 15-25kV on the SEM (JEOL JSE-5000 SEM, Japan)

2.11 Fluorometry

Fluorescent particles in solution were detected using a spectrophotometer. Earlier samples were analysed using a Perkin-Elmer LS50B fluorescence spectrometer (3ml samples in cuvette). Fluorescent hyaluronic acid nanoparticles (HA-NP) (from Uppsala University; see chapter 6 for more details) tagged with fitc were detected at an excitation and emission wavelength of 495nm and 520nm respectively.

An infinite M200Pro (Tecan) plate reader was used for later experiments, where fitc-tagged HA-NP were now measured at excitation and emission wavelengths of 485nm and 535nm. Rhodamine tagged PLGA materials were measured at excitation and emission wavelengths of 530nm and 590nm.

2.12 Statistical analysis

All studies were conducted with at least 3 samples per experimental variable, and data were represented as mean $\pm$ standard deviation, where appropriate. Unless otherwise stated, t-tests were used to compare two groups, and one-way ANOVA (analysis of variance; LSD post-hoc) were used in instances where more than two groups were being compared, assuming a normal distribution of data. The confidence interval was set at $P \leq 0.05$.

Chapter 3

Methods development for cellular polymeric collagen constructs

Mechanical properties of an acellular collagen hydrogel can be improved easily through the covalent cross-linking of the matrix. However, in order to efficiently create stiff tissue models, cell incorporation is important, and current challenges generally lie in the increase of hydrogel stiffness in a cell friendly manner.

In a collagen hydrogel (and other collagen derived materials), its stiffness depends on 1) the density of collagen, and 2) the extent of bonding (covalent and others) between adjacent collagen molecules. Although issues on collagen density within hydrogels can be overcome by plastic compression, current hydrogel materials (described in detail in section 1.5) are formed from monomeric collagen species, and lack interfibrillar covalent cross-links. This absence in collagen cross-linking leads to decreased stiffness in a typical hydrogel construct compared to the natural tissue.

Generally, improvements of material mechanical properties is achieved by forming covalent cross-links between collagen molecules. It is, however, important that cells within the construct remain viable for the use of a hydrogel as

a substrate to be justified. This rules out the use of most (if not all) chemical methods of artificial cross-linking, due to their cytotoxicity (chapter 1.4.2). In this chapter, a new solution to improving collagen material mechanical properties (without the use of artificial cross-linking) was studied. This is based on the use of a natural and highly polymerised form of type-I collagen (polymeric collagen) to produce cell-compatible and cell-supportive materials.

The focus of this chapter is on identifying the optimal collagen source and extraction process of polymeric collagen to form a stiff and cellular material at time-zero, so that it can ultimately be used as a 3D *in vitro* model of stiff tissues.

3.1   What is polymeric collagen?

All collagenous tissues containing type-I collagen will contain a fraction of collagen soluble in neutral salts and weak acid solutions (tropocollagen). This leaves a 'bulk' collagen mass composing primarily of a **polymerised form of type-I collagen** (i.e. polymeric collagen - representing the mature cross-linked bulk of tissue collagen) and some impurities. The proportion of polymeric collagen will depend on the tissue source (species, age, and tissue type), but often accounts for the majority of type-I collagen within the tissue.

In commercial collagen extraction processes, much of the polymeric collagen is treated as a waste product after acid-soluble collagen extraction, or are otherwise pepsin treated to produce smaller units of acid-soluble atelo-collagen (Rubin et al., 1965) (Drake et al., 1966) which can be reconstituted to form a hydrogel. This excess in polymeric collagen, and the general lack in commercially available polymeric collagen, goes to show that soluble collagen isotypes are often the focus of collagen research, as studies into the nature and uses of polymeric collagen fell out of general interest from 1980s

onwards (with virtual absence of publication). As a result, polymeric collagen has not previously been considered as a tissue engineering (TE) material (i.e. where cell-collagen materials were needed for tissue engineering, collagen gels based on acid-soluble collagen were used).

3.2 Polymeric collagen as a potential source of ready-made cross-links

Much of the work characterising polymeric collagen has been published in the 1960s-70s. However, issues with purity of extracted polymeric collagen were not solved until 1964, when it was reported that a Japanese technique (Nishihara method) was used to isolate purified polymerised collagen using pre-treatment of a tissue in crude α-amylase (Steven, 1964) (only crude preparations of α-amylase resulted in increased polymeric collagen purity so the result was attributed to contaminants within this preparation). It is noteworthy that the polymeric collagen in this report was extracted from aged, previously insoluble, tissues which comprise almost entirely of covalently cross-linked collagen fibrils. The collagen extracted by this method differed from acid soluble collagen in that it was an insoluble, highly cross-linked, form of collagen which could be suspended as a colloid in dilute acid. However, collagen fibrils from most tissues do not disperse fully in solution even with (crude) α-amylase treatment. It was therefore thought that other interactions must exist between collagen fibrils in the polymerised collagen (Mathews, 1965). Calcium ions were suggested as a possible further interaction between collagen fibrils as Steven (1967) later reported that collagen fibrils completely dispersed in a weak acid following treatment with a divalent cation chelating agent, Ethylenediaminetetraacetic acid (EDTA). EDTA is thought to remove calcium ions within polymeric

collagen, which stabilised its linkage with non-collagen protein (Spichtin and Verzar, 1969), and enabled the full dispersion of collagen fibrils. Indeed during the polymerisation of soluble collagen fibrils, the presence of small amounts of calcium ions accelerated the association of fibrils (Evans and Drouven, 1983), and suggest some involvement of the ion between collagen fibrils.

Observations from current studies concur in that EDTA treatment of less matured tissues improved the dissipation of collagen fibrils in solution; however, it was also observed that overly crosslinked tissues (i.e. decellularised collagen sponges) did not respond to EDTA treatment, as covalent bonds were unaffected by EDTA.

Once polymeric collagen was suspended in solution, it became possible to remove impurities from between its fibrils. It therefore represents an attractive source of collagen materials for biotechnological and tissue engineering as it is physiologically cross-linked and potentially strong and stable.

3.2.1 Extraction of polymeric collagen

Collagen composition of a tissue (i.e. procollagen, tropocollagen or enzymatically cross-linked polymeric collagen) depend on the age (Miyahara et al., 1982) (Wu et al., 2005), species (Angele et al., 2004) and the tissue source (Schofield et al., 1971). For example, polymeric collagen can be extracted without EDTA treatment from intestinal submucosa (Steven et al., 1969), but requires additional trypsin treatment for cartilage (Steven and Thomas, 1973).

Choosing the source of polymeric collagen depended on the polymeric collagen yield, which in turn is dependent on the extent of naturally occurring cross-links between collagen fibrils. In young tissues, cross-linking between collagen molecules is likely to be immature, involving acid-labile aldimine cross-links. Such bonds can be found between lysine-derived aldehydes and the e-

amino group of hydroxylysine, giving dehydro-hydroxylysino-noruleucine (deH-HLNL) bonds (Bailey and Peach, 1968); or between a free aldehyde of an activated histidine and an e-amino group of hydroxylysine within the collagen triple helix (dehydro-histidino-hydroxymerodesmosine (deH-HHMD) bonds) (Robins and Bailey, 1973). Such immature cross-links associated with recent synthesis are easily broken (Jackson and Bentley, 1960) (Kang and Gross, 1970), leading to their extractions as acid soluble collagen (and low yields of polymeric collagen). Only as the tissue ages, the acid labile cross-links are stabilised by insoluble bonds between the collagen fibrils (Bailey, 1969) (Miyahara et al., 1982). However, excessive cross-links between the collagen fibrils would be equally undesirable for the purposes of extracting polymeric collagen if the polymeric collagen cannot be suspended in dilute acid (and it would be less able to remove impurities trapped between fibrils). The ideal source of polymeric collagen would therefore likely come from fast growing and relatively young tissues (i.e. those with a moderate extent of interfibrillar collagen cross-links).

In terms of tissue types, polymeric collagen has been extracted from various soft tissues such as skin, tendon, sclera, cornea and intestinal submucosa (Schofield et al., 1971). However, in terms of type-I collagen donor source, tendons represent the optimal choice due to the relatively high proportion of type-I collagen within the tissue (therefore less impurities).

Tendon Source

Tendon was investigated as a source of polymeric collagen (as opposed to other tissue types, such as skin) due to its high percentage of type-I collagen, which could account for up to 85% of the tissue.

It is important to carefully consider the tendon source as the species, age and tendon type can impact on the extractability and yields of polymeric colla-

gen. Here, tendons from several different species (and in one case, different age) have been used for the extraction of polymeric collagen. Tendons under investigation included ostrich achilles tendons (at 6 and 24 months of age), calf achilles tendon (exact age unknown, from local butchers) and chicken feet tendon (sourced frozen from supermarket). Freeze-dried calf skin (kindly supplied by Devro, UK) was also tested for the extraction of polymeric collagen. Observations from each of the tendons under investigation are listed in the table 3.1, and further discussed after the methods detailing the extraction of polymeric collagen below.

Homogenisation

Tendons (except freeze-dried granules from Devro) were homogenised to start the extraction process. Homogenisation increased the surface area to volume ratio of the tendon for EDTA treatment and collagen fibril suspension in weak acid. Homogenisation of the tissue is sometimes used in collagen extraction processes (Liu et al., 2001), though not always necessary for tendons that are particularly susceptible to acid extraction (i.e. rat tails).

Several methods of homogenisation were tested and compared for their extraction efficiency, and ease of use.

(a) Cryostat

This method involved the cutting of tendon samples into thin sections to increase the surface area of the tendon exposed to the weak acid solution:

1. Tendons were cut into smaller pieces (measuring approximately 1-1.5 cm) and weighed

2. Each tendon piece was set horizontally in a block of ice (so that it was cut parallel to the collagen fibers)

3. The ice block was mounted onto a cutting block using optimal cutting temperature compound (OCT), and was left to set at $-30°c$ for at least 30 minutes

4. Tendon sections were cut at $\sim 10\mu$m

The tendons were cut sufficiently fine for polymeric collagen to be extracted. However, this process was found to be time consuming (and potentially labour intensive) and so lack efficiency for large scale polymeric collagen extraction.

(b) Blender

An alternative method attempting to increase cutting efficiency was tested (using a kitchen blender):

1. Tendons were placed in 0.5M acetic acid

2. The tendons were then blended using a standard kitchen blender until visibly homogensied (i.e. cloudy)

The problem with this method was that some tendons did not expand in the weak acid, and were difficult to cut. Prolonged blending in this case resulted in excess heat, which can denature collagen. The resultant collagen solution was frothy, viscous and solidifies spontaneously over time at $4°c$.

(c) Mortar and pestle (*method primarily used in this study)

An alternative homogenisation method was tested based on physical crushing of frozen tendons using a cold stainless steel mortar and pestle:

1. Up to 2g of tendon was placed in a pre-frozen ($-20°c$) stainless steel mortar and pestle

2. Liquid nitrogen was carefully poured into the mortar so that the tendons were covered

3. The pestle was slowly dropped onto the liquid nitrogen and frozen tendon

4. Immediately, a sledge hammer was used to apply force onto the pestle, which homogenised the tendon

5. This was repeated until the tendon was transformed into a fine power (in some cases only coarser granules of tendons could be obtained - e.g. tendons that are suspected to be highly cross-linked)

The mortar and pestle method was effective and efficient in generating homogenised tendon granules.

Overall, the use of physical force to crush frozen tendons (methods c) was more efficient in producing small granules of tendons. The mortar and pestle was used to homogenise tendons for any further experiments.

Extraction of polymeric collagen from homogenised tendons

The method used in this study for polymeric collagen extraction from tissues were simplified based on those published by Steven (1967). A flow chart of the methods used by Steven is displayed here for reference (figure 3.1).

```
        Tendon

  1  │  Cleaned

  2  │  Chopped

  3  │  Frozen

  4  │  Disintegrated

  5  │  Defatted in acetone

  6  │  Sample removed

  7  │  Equilibrated with 4% (w/v) chelating agents at 20°, pH 7.5

  8  │  Washed with water

  9  │  Homogenised with 0.2M acetic acid

 10  │  Stirred for 3 h ◄─────────────────────────┐

 11  │  Centrifuged at  8000 x g for 20 min        │      Repeat Step 10 and 11

           │                               │
           ▼                               ▼
       Supernatant                     Residue ──────────────┘
       (Dispersed collagen)

           │
           ▼

 12  │  Combined supernatants

 13  │  Add  1 M NaOH to pH 6-7
           │
           ▼
       Collagen fibrils
```

Figure 3.1: Polymeric collagen extraction method using EDTA-treatment prior to expansion in weak acid. This flow chart was obtained directly from Steven (1967).

The main differences between both methods is that, in the revised methods:

- Samples were not de-fatted with acetone

- Samples were not centrifuged to separate the suspended polymeric collagen and insoluble contaminants. Repeated suspension and shear aggregation of polymeric collagen from dilute acid appeared to be effective in separating polymeric collagen from insoluble contaminants

- Different concentrations of acetic acid and EDTA solutions were used (solutions were more concentrated in the modified methods to ensure maximum calcium chelation and yield of polymeric collagen)

Detailed methods used in this study for the extraction of polymeric collagen from homogenised tendons are as follows:

1. Homogenised tendons were placed in excess 0.5M EDTA solution overnight with at least one change of solution. EDTA (Sigma, UK) was dissolved in distilled water adjusted to pH 8 using NaOH. Once EDTA dissolved, concentrated hydrochoric acid (HCl) was used to adjust the solution to pH 7.5

2. Following EDTA treatment, tendon granules were collected by centrifugation at 2000rpm (2 minutes) and washed in distilled water (at least twice)

3. 0.5M acetic acid was added to the EDTA-treated tendons on a magnetic stirrer and left at 4 ℃ for at least 3 hours to allow time for the tendons to expand

4. On ice, polymeric collagen was collected by shear aggregation (using a glass rod or similar) during neutralisation of the solution using 5M NaOH (neutralisation on ice ensured that most acid-soluble collagen remained in solution). Polymeric collagen precipitated at ∼pH 6-7

5. The polymeric collagen was re-suspended in 0.5M acetic acid and precipitated at least two further times to reduce impurities trapped within the collagen fibrils

6. The solution was then sterilised by equal volume of chloroform if necessary, and stored at 4℃ for up to 1 week for future use

Polymeric collagen extracted from different sources

Species	Age (months)	Tissue source	Observations
Ostrich	6	Achilles tendon	Very soluble in weak acid (even without homogenisation and EDTA treatment). Low yields of polymeric collagen. Formed hydrogels when at $4 \degree c$ over 24 hours when neutralised.
Ostrich	24	Achilles tendon	Good polymeric collagen source with high yields.
Chicken	-	Feet tendon	Polymeric collagen extracted did not aggregate immediately upon neutralisation, and suggested the presence of impurities in the solution. Collection of polymeric collagen was difficult as collagen did not stick to stirring rod.
Calf	-	Achilles tendon	Extracted polymeric collagen visually appeared similar to that of ostrich tendons. Reduced yields as a proportion of the tendon did not expand in dilute acid (even after EDTA treatment).
Calf (freeze-dried)	-	Skin	Small yields during initial shear aggregation, but collagens precipitated with further and continuous agitation (on magnetic stirrer). Collagen appeared dense and sticky.

Table 3.1: Observations of polymeric collagen extracted from different sources.

Yields from 6-month old ostrich and chicken tendons were low due to the lack of polymeric collagen precipitation and difficulty in collecting the collagen. Some insoluble collagen was extracted from freeze dried calf skin, but the collagens did not aggregate immediately upon neutralisation. This indicated the possible presence of impurities which hinder the aggregation of the polymeric collagen. Good yields of polymeric collagen were obtained from both 24-month old ostrich and calf tendons, but were most reliably extracted from ostrich tendon. In some instances, homogenised calf tendons failed to swell in dilute acid even after EDTA treatment. This might be an indication of either more cova-

lent cross-links being present within localised areas within the calf tendons, or that other interactions between collagen fibrils exists (apart from the calcium ions that are holding and stabilising collagen fibrils within the matrix). There have been reports of localised, site-specific regions of mineralisation along the length of tendons (Kerns et al., 2016), which may explain the difficulty in extracting polymeric collagen from parts of the calf tendon. Although from a different collagen type and source, observations from cartilage tissues also indicate this differential swelling ability, where most of the tissue will not expand even with prolonged EDTA treatment, except those in the growth plate region (Brown and Byers, 1989).

Overall, extraction of polymeric collagen from 24-month-old ostrich tendons resulted in optimal yields, closely followed by calf tendons. Both tendon sources have been used to extract polymeric collagen, with initial studies based primarily on 24-month-old ostrich tendons, and later studies on calf tendons (switch in tendon source was due to the better availability of calf tendons).

3.2.2   Potential applications for polymeric collagen

Aligned polymeric collagen constructs

Shear aggregation of polymeric collagen was an efficient method of collecting polymeric collagen, and produced a material that was grossly aligned. This potentially provide directional mechanical cues for the control of cell behaviour.

This was particularly interesting for the prospects of generating a tendon tissue model as it potentially incorporates increased mechanical properties (provided by the covalent cross-links between the collagen fibril) and the alignment of the collagen fibres, which mimics the features seen in the natural tendon (although fibres within the tendon will be further arranged in bundles). Indeed, Puxkandl et al. (2002) showed that the intermolecular cross-link are essential

for the normal functioning of the tendon, without which, collagens were shown to have reduced tensile strength and increased strain to failure (which is also typical of very young collagen from rats).

Examples of other methods of generating constructs with an aligned matrix include the electrospinning of collagen fibres (Matthews et al., 2002), which can then be seeded with cells. But the drawback is that this is cell dependent and requires weeks of culture for cells to migrate into the construct. Even within hydrogels, there are ways to generate collagen fibre alignment, such as by cell induced internal tension on uni-axially tethered collagen hydrogels (Georgiou et al., 2013), or by external tension through repeated strain/relaxation cycles (Cheema et al., 2007a). But this also has the drawback (as seen in many other hydrogel based constructs, in that the collagen fibrils cannot be easily cross-linked due to the cell toxicity of artificial cross-linking methods.

Here, polymeric collagen contains pre-crosslinked fibrils and can be aligned (when extracted) from solution. It therefore has potential to address one of the current challenges of tissue engineering which is to generate a cellular, anisotropic and strong construct (with aligned fibres) in a short space of time. This was tested by adding cells in to the polymeric collagen solution, during neutralisation and shear aggregation to incorporate cells within the construct. The aim was to produce a cellular and aligned collagen material with increased mechanical properties (due to the presence of pre-crosslinked collagen), and a tissue-like structure detected at the cell level.

Optimisation of polymeric collagen collection

First, methods used to collect and align polymeric collagen was optimised. The main concerns to address here are the alignment and orientation of collagen fibrils, and the ease of use. For the repeatable collection of polymeric collagen, an even application of shear force was thought to be necessary; so manual

stirring was not reliable.

Using a magnetic stirrer attached to a glass rod (neutralisation using dialysis tube), significant proportions of polymeric collagen were collected, but most remained unaligned and remained stuck to the magnetic stirrer. This resulted in a mass of polymeric collagen being collected at the bottom of the flask with little being aligned by wrapping around the glass rod.

To overcome the issue of polymeric collagen collecting at the base of the construct, and improved alignment of polymeric collagen, a hand held device based on a simple motorised unit was designed and made as summarised in table 3.2. The shape of the polymeric collagen collection unit (generation 4b) eventually developed for use in experiments is shown in figure 3.2.

Methods for the collection and alignment of polymeric collagen using the custom made hand-held device. This part of the study was carried out with the help of Miss Danielle Baptista (summer placement student):

1. In a small glass beaker, 1-part 10xMEM was added to 9 parts polymeric collagen suspended in 0.5M acetic acid (2mg collagen/ml; at 4℃)

2. A motorised unit attached to a custom made collagen collector (see table 3.2) was switched on after submerging half the length of the collector in the collagen suspension

3. 5M (and later 1M) NaOH was added drop wise to the collagen solution until a colour changed from yellow to fuchsia pink (phenol red pH indicator contained within 10xMEM). Polymeric collagen aggregated between $\sim$ $pH6 - 7$

4. Once the solution was neutralised, the solution was stirred for an additional two minutes

5. Polymeric collagen was removed from solution and cut perpendicular to the fibril orientation to free the collagen sheet from the collector

6. The polymeric collagen was cultured in DMEM (supplemented with 10% (v/v) FCS and 1% (v/v) penicillin streptomycin), or was fixed for analysis

Shear aggregation of polymeric collagen during neutralisation using the custom made device (figure 3.2) produced aligned sheets polymeric collagen, as seen in the SEM and birefringence images (figure 3.3).
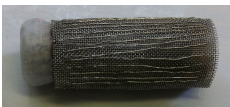
	Description	Image	Observations
Original	Magnetic stirrer attached perpendicular to a glass-rod using parafilm.		A significant proportion of polymeric collagen was not aligned as they collected on the magnetic stirrer instead of the glass rod.
Generation 1	Three needles arranged around a circular gear piece. Needles were $\sim 1cm$ apart.		Polymeric collagen only collected around individual needles. The gap between each needle may need to be shortened.
Generation 2	A metal mesh was rolled into a cylinder on top of a circular gear piece.		Collagen lacked alignment and often slipped from the mesh.
Generation 2.5	Stainless steel wires was sewn onto the wire mesh (perpendicular to the shear force) so collagen fibrils can 'grip' the wires and wrap around the cylindrical mesh.		Same problems were encountered as generation 2 (polymeric collagen did not grip on to the sewn wires).
Generation 3	Increased density of needles was used to shorten gap between needles.		Some (patchy) collagen alignment. There was a tendency for collagen to wrap around the needles, and to slip from the collector.
Generation 4a	A cap was added to the exposed end of the needles, and sealed with paraffin wax. Metal wire was wrapped around the needles to help prevent collagen slippage.		The additional cap prevented most collagen from wrapping around individual needles, and the collagen from slipping from the needles. There was visible alignment of polymeric collagen. It was difficult to separate the collagen from the extra metal wires.
Generation 4b	Similar to generation 4a, but without additional metal wire for easier retrieval of polymeric collagen from the collector after shear aggregation.		Yields of shear aggregated was similar to those collected in generation 4a, but without the added difficulty in retrieving shear aggregated collagen.

Table 3.2: Development of custom polymeric collagen collector unit for the shear aggregation and alignment of polymeric collagen fibrils during neutralisation of the collagen solution. A motor unit is connected to one end of the collector (as shown in figure 3.2).
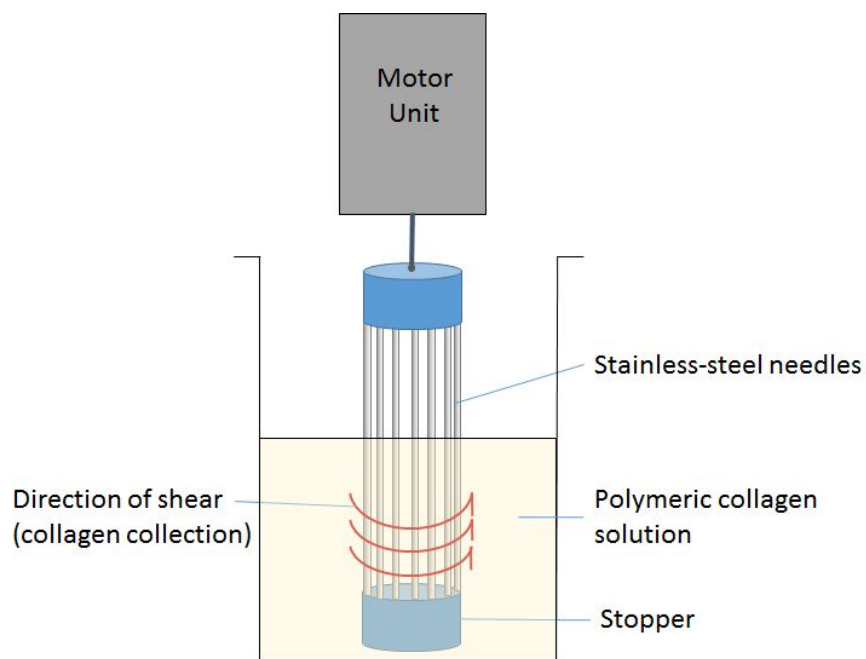
Figure 3.2: Schematic of custom-made machine and a collector unit made of stainless-steel needles (generation 4b; please refer to table 3.2) for collection of aggregated polymeric collagen from a beaker of polymeric collagen solution during neutralization. The red arrows denote the direction of shear during the collection of the aggregated collagen material from solution.
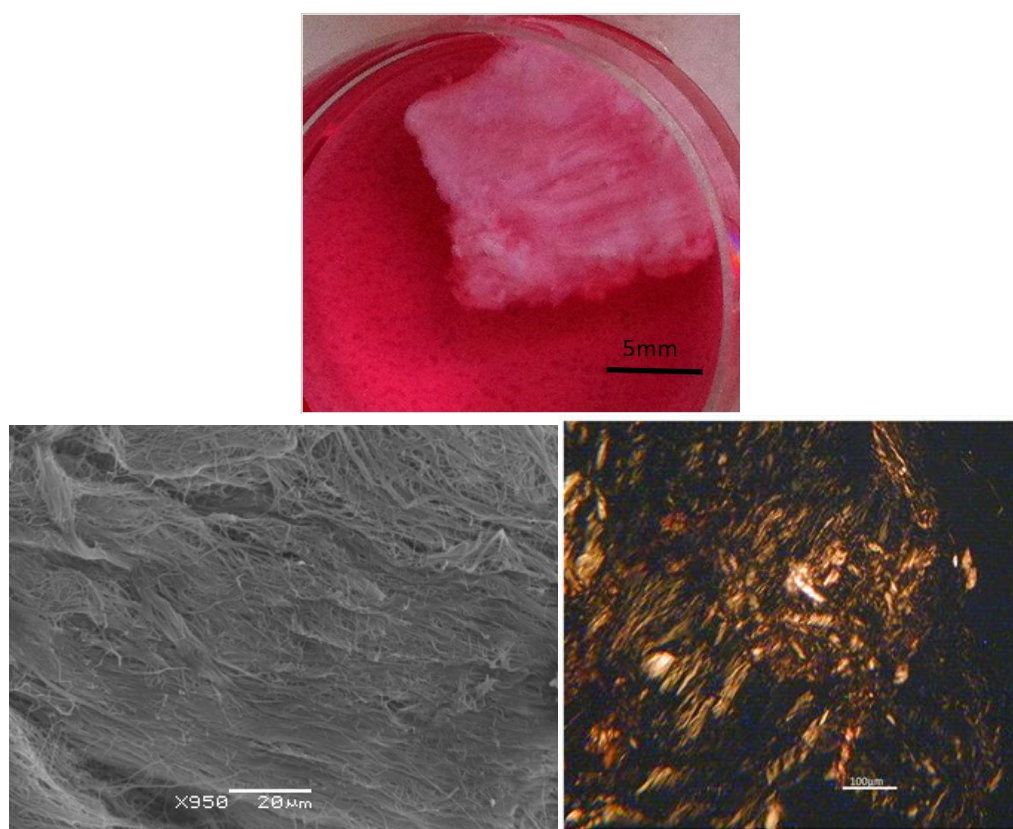
Figure 3.3: Shear-aggregated polymeric collagen. (a) Image of shear aggregated polymeric collagen material (b) SEM image of shear-aggregated polymeric collagen with highly aligned collagen fibrils. (c) Birefringence image of polymeric

This method was used to generate cellular constructs as cells were added into the collagen solution during shear aggregation (at step 3 in the methods below, as the polymeric collagen begins to aggregate).

The results from the H&E stained cellular polymeric collagen sections showed that apart from the presence of cells at day 0 (immediately after the fabrication of the construct), no cells were found in constructs with culture (figure 3.4). This indicated that although cells were incorporated into the construct, cells did not remain viable within the construct over time. This was thought to be due to the exposure of cells to acidic conditions (as cells were added to the solution at $\sim pH6$ when the polymeric collagen began to aggregate). Therefore a further test to study cell viability after cell exposure to acidic pH was carried out.

Fibroblast monolayers cultured in a 24-well plate (pre-cultured for 1 day to allow for cell attachment to the wells) were treated for a period of 0, 10, 20 or 30 minutes, in PBS adjusted to pH6 or pH5.5 (using hydrocholoric acid). The cells were stained (live/dead) and counted as described in section 2.7.

Figure 3.5 showed that the rate of cell death increased sharply when the pH of the cell environment was decreased from pH6, to pH5.5; and that the extent of cell damage was dependent on the length of exposure to the low pH. For example, the amount of cell death after exposure to pH5.5 for 10 minutes was ~50%, which increased to over 70% at 30 minutes of exposure.

Therefore, it was concluded that the exposure of cells to reduced pH conditions within the aligned construct was damaging to interstitial cells, and cells found in the H&E images at day 0 may require time as they undergo apoptosis.

Cells are an essential component of the tissue model, and so the aim of this part of the experiment is to find an alternative method to incorporate cells into the polymeric collagen material, without exposing the cells to sub-neutral pH.
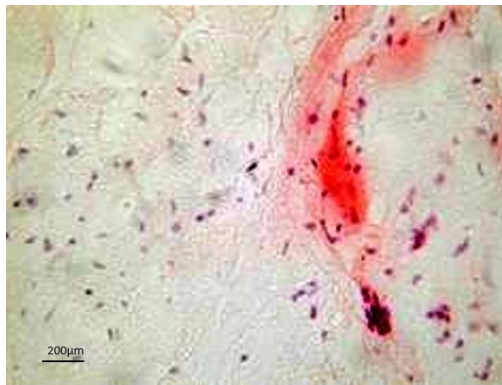
(a) At day 0 in culture
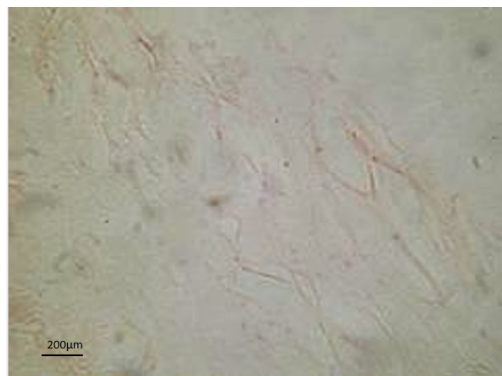
(b) At day 1 in culture
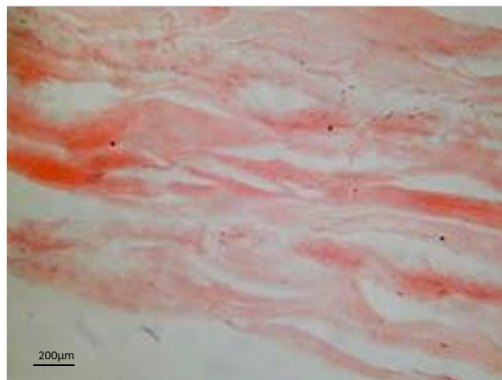
(c) At day 5 in culture
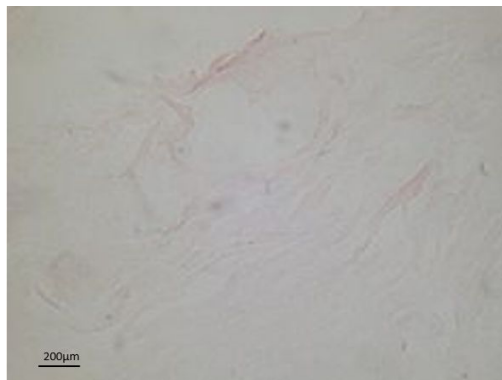
(d) At day 14 in culture

Figure 3.4: H&E images of shear aggregated polymeric collagen. Cells (HDF) were added during the neutralisation of the polymeric collagen solution. Constructs were cultured for up to 14 days.
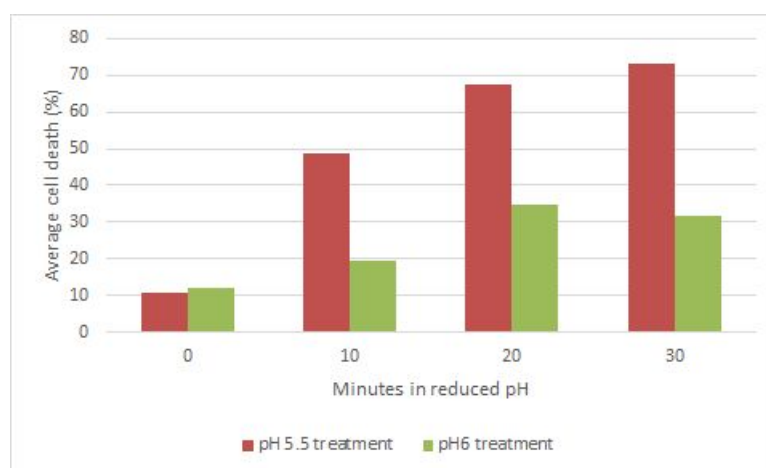
Figure 3.5: Cell viability after exposure to a solution of pH5.5 and pH6 for up to 30 minutes.

Therefore, an alternative method for incorporating cells and aggregated (aligned; $\sim$ 1x1cm) polymeric collagen was tested, and involved the incorporation of both the cells and aligned polymeric collagen construct between two pre-formed layers of conventional (acid-soluble) collagen hydrogels (i.e. like a sandwich), which was then compressed together to form a single, integrated, construct; and cultured for up to 14 days.

The hypothesis is that cells will preferentially attach to the stiffer collagen matrix (polymeric collagen), and so respond primarily to the mechanical cues from the polymeric collagen. Cells added to the hydrogel may, however, migrate towards the stiff polymeric collagen (Hadjipanayi et al., 2009c). Alternatively, if cells do not migrate towards the polymeric collagen, it may also benefit from the presence of polymeric collagen as cells have been found to respond to the stiffness of the surrounding matrix (Hadjipanayi et al., 2009b).

H&E imaging (at 1, 7 and 14 days of culture) of constructs with cells applied directly to the polymeric collagen, showed that cells were primarily attached to the polymeric collagen, and not the acid-soluble collagen hydrogels, at all time points (figure 3.6). Cells observed at later time points assumed a spindle-like morphology, typical of HDFs.

However, it was evident from the images that the distribution of the polymeric collagen constructs were highly variable within the construct, and differed in collagen and cell densities within, and between, samples. This meant that it would be of limited use as a tissue model.
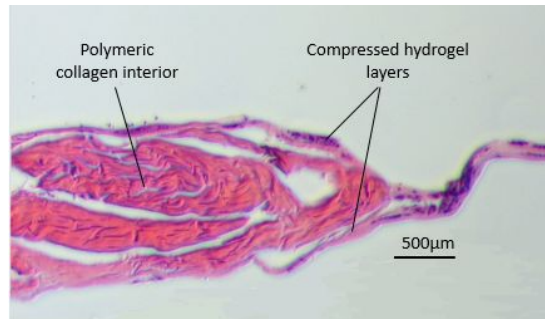
(a) Day 1
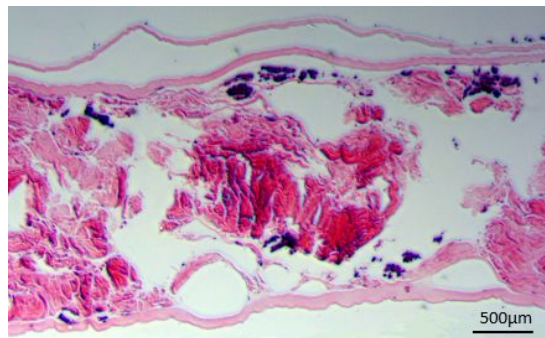
(b) Day 7
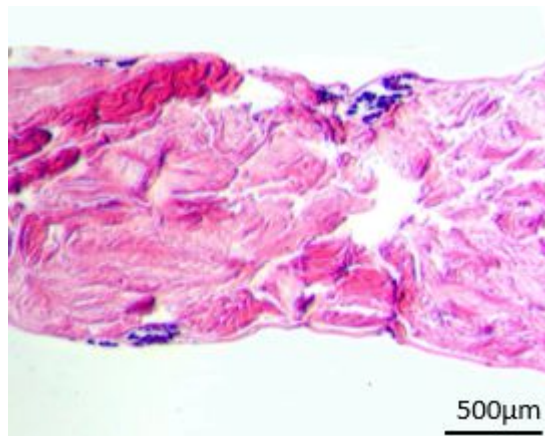
(c) Day 14

Figure 3.6: H&E stained histological images of cells and aligned polymeric collagen sandwiched between two layers of conventional hydrogel. Constructs were cultured for a) 1 day b) 7 days or c) 14 days.

Polymeric collagen containing hydrogels

A clue to an alternative method in using polymeric collagen came from initial studies on polymeric collagen extracted from young ostrich tendons (6 months old). The young tendons were found to produce collagen suspension which aggregated only slowly into a gel at 4c. This made it possible to seed cells into the fibrillar collagen at neutral pH prior to coalescing together into a stable mesh material. This was similar to conventional collagen gel formation from monomers except that the component fibrils were cross-linked.

Since the major difference between 6 month-old and 24 month-old tendons is the extent of stable cross-links between collagen fibrils (i.e. the younger tissues contain a greater proportion of acid-labile collagens), it was hypothesised that the soluble collagen interfered with the shear aggregation of the insoluble polymeric collagen, and allowed the polymeric collagen to remain suspended in solution even after neutralisation.

To replicate this delayed polymeric collagen aggregation effect, acid-soluble collagen (normally used in hydrogel formation), was blended with polymeric collagen extracted from older tendon tissues (previously aggregated immediately upon neutralisation). The aim here was to delay the aggregation of polymeric collagen from solution during the neutralisation of the collagen solution, so that cells can be safely added to the suspension at neutral pH.

Briefly, the methods used to blend collagens for the formation of polymeric collagen containing hydrogel was:

1. Polymeric collagen (extracted from calf or 24 month old ostrich) were suspended in 0.5M acetic acid at a concentration of $\sim 2mg.ml^{-1}$

2. The polymeric collagen solution was blended, for at least 3 hours on a magnetic stirrer, with acid-soluble tropocollagen (at a concentration of $\sim 2mg.ml^{-1}$) at a ratio of 1:0 4:1, 3:2, 1:1, 2:3, 1:4 and 0:1 (to give a

polymeric collagen proportion of 100%, 80%, 60%, 50%, 40%, 20% and 0%)

3. 10% (v/v) 10xMEM was added to the solution prior to neutralisation using 5M and 1M NaOH, until a colour change from yellow to pink was observed. Neutralised solutions were place at 4°c for up to 24 hours to gel

With the absence of monomeric collagen, polymeric collagen precipitated/ aggregated immediately during neutralisation. However, with the incorporation of monomeric collagen, the instant aggregation of polymeric collagen was prevented, and a hydrogel was formed as hypothesised. Samples containing more than 50% polymeric collagen were visibly less stable, and collapsed when disturbed. Therefore, only samples containing 20, 40 and 50% polymeric collagen were investigated further.

Shear aggregation of blend hydrogels resulted in some recovery of polymeric collagen. Samples discussed here were made with 2mg.ml^{-1} monomeric and polymeric collagen solutions, blended to give 0, 20, 40 or 50% polymeric collagen in solution (total volume of 25ml per sample). Contrary to expectation, samples with the highest amount of monomeric collagen (and least polymeric collagen (20%)) did not retain any polymeric collagen when shear aggregated (11.5mg out of 10mg of polymeric collagen in the hydrogel was extracted; i.e. all polymeric collagen including potentially some monomeric collagen). Increasing the polymeric collagen concentration within the gel resulted in increased retention polymeric collagen fibres (10.1mg out of 20mg, and 7.8 out of 25mg polymeric collagen in gels containing 40 and 50% polymeric collagen; figure 3.7).
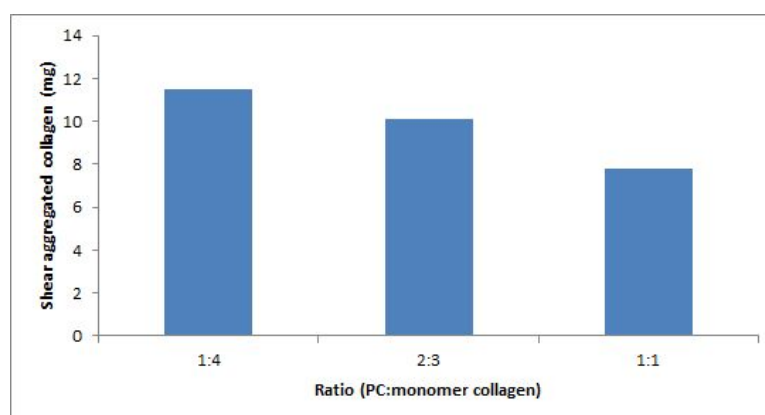
Figure 3.7: Mass of polymeric collagen shear aggregated during the neutralisation of blended collagen hydrogels. For all samples, a total amount of collagen within the sample was 50mg (a concentration of 2mg.ml^{-1}, in 25ml).

As a solution with a 1:1 ratio of polymeric and monomeric collagens was able to prevent the instant aggregation of polymeric collagen fibres, there was potential for cell incorporation after neutralisation of the solution, and before collagen fibril aggregation, at neutral pH.

The findings in this chapter show it is possible to incorporate living cells in a pre-crosslinked collagen matrix by developing techniques for handling and aggregating polymeric collagen fibrils (in this case by incorporating acid soluble collagen with the polymeric collagen). Although the use of shear aggregation did not result in reproducible gels suitable for use as a tissue model, it was possible to incorporate cells into hydrogel, in a manner similar to that of fibril formation used in making collagen gels; by blending-in of monomeric collagen to delay the aggregation of polymeric collagen during neutralisation. The result was a hydrogel with resident interstitial cells surrounded by a cross-linked, stiff, collagen matrix, as required.

Chapter 4

Results: Stiff skin and tendon model based on polymeric collagen

4.1 Introduction

As discussed in section 1.4.3, hydrogel based constructs have the major advantage of interstitial cell seeding at time zero, when it would otherwise require many weeks for cells to populate a porous scaffold, by conventional seeding. Natural proteins such as type-I collagen (which is also abundant in many natural biological tissues) contains binding sites recognised by cell membrane integrins. Particularly, for type-I collagen, $\alpha1\beta1$ and $\alpha2\beta1$ (see chapter 1) plays an important role in dictating cell behaviour. So, the presence of collagen molecules in the tissue model increases the biological relevance of the construct, and encourage cells to behave as they would in their native ECM environment.

In order to successfully model a tissue, which depends critically on cell-matrix interactions, it is important to match material stiffness to the stiffness

of native tissues to ensure cells receive similar environmental cues. Indeed the stiffness of collagen hydrogels, and many biomaterials, have been shown to greatly influence cell behaviour, such as proliferation (Hadjipanayi et al., 2009b), migration (Hadjipanayi et al., 2009c) and results in changes to gene expression (i.e. matrix remodeling genes) (Karamichos et al., 2008). The stiffness of the matrix is therefore an important consideration for eventual tissue function.

Mechanical properties/stiffness of a collagen hydrogel can be increased by plastic compression which increases collagen density (by expelling excess fluid) to $\sim 11 - 18\%$ (v/v) (Brown et al., 2005)(Abou Neel et al., 2006) (Cheema et al., 2008). This matches collagen densities of some tissues, such as skin (Brown, 2013a). However, adjacent collagen fibrils in a hydrogel are only held together by non-covalent associations soon after fibrillogenesis, rendering them weaker in terms of mechanical strength compared to native tissues (where fibrils are typically cross-linked enzymatically). In order for the hydrogel matrix to be a potential representative model of stiff tissues, such as skin and tendons, further improvements in the mechanical properties of the type-I collagen component of the matrix are needed.

The motivation of this study is therefore to generate a collagen hydrogel based construct with improved mechanical properties, but importantly, to also retain initial cell populations seeded within the construct at time-zero. This is because one of the main advantages for collagen hydrogels is the ability to create cellular constructs, as the construct is fabricated. In order to preserve cell compatibility of the hydrogel, artificial cross-linking methods are unsuitable as they tend to be cell lethal. Examples include glutaraldehyde, which is often used for cross-linking in many collagen material processes; for example, prior to the extrusion of collagen fibrils (in suspension) during electrospinning (Matthews et al., 2002). Other cross-linking methods include the use of

Genipin (Mekhail et al., 2011) and photochemical cross-linking agents such as riboflavin (Ibusuki et al., 2007) (Wong et al., 2013). However, such scaffolds then need a cell seeding stage which is time consuming, variable and are dependent on the cell type used. There is yet to be a non-cell damaging method for the cross-linking of collagen fibrils, also with the potential to be up-scaled for high throughput use.

The proposed solution to the lack of hydrogel mechanical properties (with the condition that cell viability is preserved) is to make hydrogels from collagens already with **pre-existing** covalent cross-links between their fibrils; namely, polymeric collagen. In essence, the proposed method involves use of pre-crosslinked collagen as a starting material to produce hydrogels; with the aim to improve overall mechanical properties of the construct and preserved cell viability.

In chapter 3, details regarding the development of a novel hydrogel made from a blend of acid-soluble tropocollagen and polymeric collagen has been described. The purpose of this study is to produce a tissue model which would be representative of stiff tissues, such as aged skin and tendons. To achieve this, the physical environment surrounding the 'living' cells will be altered by incorporation of pre-cross-linked type-I collagen. The hypotheses to test are:

- The hydrogel after the incorporation of polymeric collagen can be plastically compressed

- Polymeric collagen within the hydrogel increases the mechanical properties of the material

- Cells can be seeded within polymeric collagen containing hydrogels, retaining time-zero cell viability

- Cells behaviour, such as proliferation, are similar and representative of a native stiff tissue

It is important to note that two distinct processes have been described in chapter 3 to generate constructs containing polymeric collagen (please refer to figure 4.1; and result in materials with different physical properties. This chapter studies only the polymeric collagen containing hydrogels, generated through the blending of monomeric and polymeric collagens - where cell incorporation at neutral pH is possible.
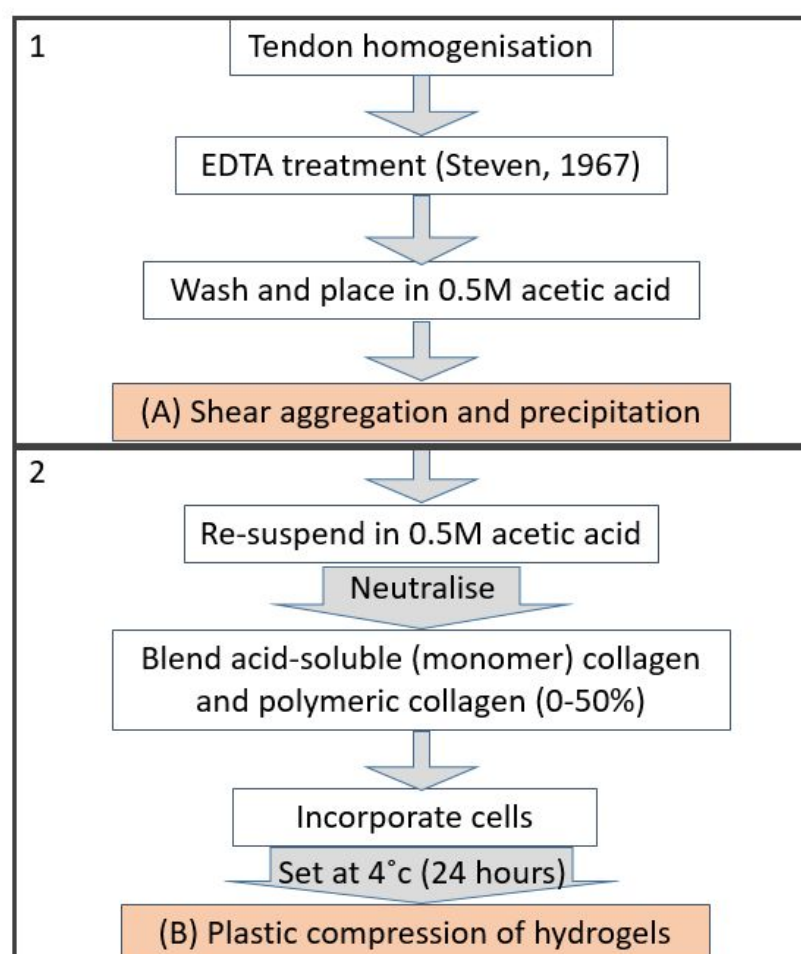
Figure 4.1: Flow-chart outlining the process for polymeric collagen extraction from a tendon source (box 1), and the use of polymeric collagen to produce cell-compatible blended hydrogels (box 2). The resultant polymeric collagen materials are either (A) non-cellular, aligned polymeric collagen fibers or (B) compressed blend collagen hydrogels (cell-compatible).

4.2 Methods

Methods listed below are specific to this study. Further methods common to studies throughout the thesis are listed in Chapter 2.

4.2.1 Polymeric collagen blend gel preparation

Collagen hydrogels were produced and compressed as mentioned in the method sections 2.2 and 2.4 above. Blended pre-crosslinked collagen hydrogels were produce by substituting half the volume of acid-soluble collagen with polymeric collagen (adjusted to $\sim$2mg.ml^{-1} in 0.5M acetic acid). Blends of 20%, 40% and 50% polymeric collagen (w/w to acid-soluble collagen) were neutralised, gelled and compressed as described.

4.2.2 Measurement of construct tensile mechanical properties

The Young's modulus of compressed hydrogels with and without polymeric collagen (50% w/w) was measured by dynamic mechanical analysis (DMA; DMA7e, Perkin Elmer) through static tensile loading at 50mN.min^{-1} until failure. Samples were cut to approximately 2mm x 12mm. To ensure sufficient grip of the sample onto the DMA clamps, steel meshes were folded onto both ends of the construct (secured with superglue). Each construct was then measured using a digital caliper for exact construct dimensions. Throughout tensile loading, samples were submerged in PBS to ensure they remain hydrated.

4.2.3 Measurement of collagen density within compressed gels

The density of collagen fibrils within compressed hydrogels was measured based on the mass difference between the hydrated and freeze-dried construct. Once the hydrogels were fully compressed within 24 well plates, PBS was added to each well for easy handling. It was therefore important to gently and quickly blot the hydrogel on blotting paper to remove excess fluid on the surface prior to measurement of the hydrated mass. All constructs were subsequently freeze-dried (Modulyo, Edwards) overnight and weighed for the weight of the dry solid fraction (i.e. collagen without the water).

4.2.4 Cell viability assay

Cell viability within compressed and uncompressed gels was confirmed by fluorescent imaging after a 45 minute incubation of the cellular hydrogel with stains consisting of 17μl ethidium homodimer (2mM; Invitrogen) and 20μl calcein-AM (4mM; Fluka Analytical) diluted in 5ml PBS. Images were taken on the Olympus BX61. For each sample, images of three random fields of view was captured for cell counting. The number of live (green, calcein-AM stained) and dead (red, ethidium homodimer stained) cells were only included if the cells were within a digitally superimposed frame (identical for each field of view).

4.2.5 Total DNA assay

Total DNA was measured using Hoechst 33258 (Sigma) based on previously published methods (Rago et al., 1990) (Rao and Otto, 1992). Cells within the hydrogel were recovered by digesting each collagen construct in 1ml 0.2% type-I bacterial collagenase (Gibco, USA) dissolved in PBS. Following a diges-

tion time of 1 hour at 37℃ (on a shaker), the suspension was centrifuged at 2000rpm for 5 minutes to collect cells. The cell pellet was re-suspended in 1ml distilled water and was repeatedly frozen ($-20℃$) and thawed to release DNA content from within the cells. 100μl Hoechst solution (2μg/ml) was added to an equal volume of DNA sample in a 96-well plate followed by absorbance reading at 460nm. A DNA standard curve was prepared using increasing concentrations of calf thymus DNA (Sigma, USA) in saline sodium citrate buffer adjusted to pH7.0.

4.2.6   Measurement of compressed hydrogel thickness

An optical method for measuring construct thickness was used on acid-soluble collagen derived, or 50% polymeric collagen blend gels. Previous work on compressed gel and optical thickness measurements have been carried out by Tan (2015). 2.5ml hydrogels were set and compressed in 24-well plates. PBS was added to each well to ensure samples remained hydrated prior to thickness measurement (as dehydration will reduce construct thickness). For the measurement, each sample ($n = 4$) was placed above a low powered (class 1, λ 1310nm) laser beam of a CTS-2 machine (Lein Applied Diagnostics, UK). The focal point of the laser (with a range of approximately 1mm) moves through the thickness of the sample whilst a detector within the machine detects any reflected light at the gel surface. Changes in the reflection index through the sampled area were registered as peaks of reflected light (converted into voltage) in the scan. A typical scan in this set-up registers two changes in reflective index; firstly between the plastic well-plate/compressed gel, and also between the compressed gel/air interface. These two interfaces distinguishes the upper and lower boundaries of the construct, and so measures the thickness of the compressed gel.

4.2.7 Statistics

Data were represented as mean $\pm$ standard deviation, and were subjected to one-way analysis of variance (ANOVA). The LSD post hoc test was used to identify groups with a significant difference. Confidence internals were set at $P \leq 0.05$.

4.3 Results

4.3.1 Mechanical properties of blend gels containing polymeric collagen

The main objective of this study was to produce constructs with improved mechanical properties compared to compressed collagen hydrogels derived from monomeric acid soluble collagen - which has been used in many tissue-like models and for the study of cell behaviour within a ECM like environment (Hadjipanayi et al., 2009b) (Hadjipanayi et al., 2009c) (Bitar et al., 2008) (Ardakani et al., 2014). So, first it was important to establish the mechanical properties of the novel polymeric collagen containing compressed hydrogels. Young's modulus (E) was used as a measure of stiffness, and was calculated as stress applied on the sample (σ) over sample strain (ε; change in length):

$$E = \frac{\sigma}{\varepsilon} = \frac{\text{force/cross-sectional area}}{\text{change in length/original length}}$$

Plastically compressed collagens without polymeric collagen had a Young's modulus of 0.36 $\pm$ 0.10 MPa when tested under tensile strain. The Young's modulus had increased 3-folds to 1.051 $\pm$ 0.377 MPa with the blending in of 50% w/w polymeric collagen ($P \leq 0.001$). Note that this compares well with (and surpasses) the Young's modulus of artificially cross-linked compressed

collagen gels as shown in the study by Rich et al. (2014), where constructs were photochemically cross-linked for 15 minutes in the presence of riboflavin (a photoinitiator which produces oxygen free-radicals upon activation with blue light) prior to compression. The Young's modulus of the riboflavin cross-linked construct was noted in the literature as 0.650 ± 0.073 MPa (Rich et al., 2014). Note also that sample dimensions were similar between riboflavin cross-linked gels and 50% (w/w) polymeric collagen blends where construct thickness (as shown in results below) were 50-60μm and $\sim$50μm respectively.

4.3.2   Collagen density within compressed polymeric collagen blend gels

The collagen density of the collagen constructs was measured by the weight of freeze-dried collagen mass as a fraction of the hydrated compressed hydrogel, prior to drying. As expected, the overall mass of freeze-dried collagen were similar across samples as the collagen concentration of both the acid-soluble and polymeric collagen were both adjusted to a similar concentration of $\sim 2mg$/ml. However, as the proportion of polymeric collagen increased, less water was retained by the construct during plastic compression (figure 4.2). Collagen density within the compressed hydrogel increased gradually from $12.0 \pm 1.1\%$ when no polymeric collagen was added, up to $20.8 \pm 5.1\%$ when half the collagen within the hydrogel was polymeric collagen (figure 4.2). In effect, the high volume of fluid loss from the polymeric collagen blend gels meant that the overall collagen density was highest in these samples. Collagen density of 20 and 40% polymeric collagen gels after compression were within this range, at 12.8 ± 2.0 and $15.1 \pm 1.7\%$ respectively.
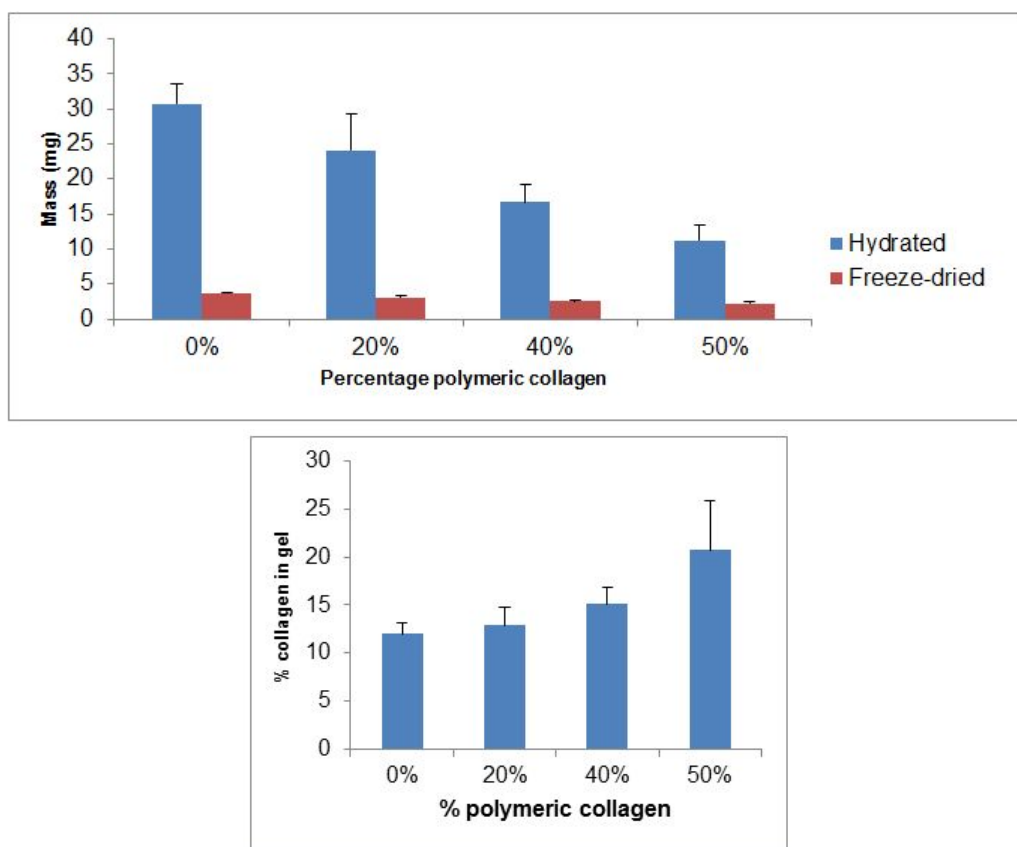
Figure 4.2: Hydrated and freeze-dried mass (mg) of compressed hydrogel blends. Collagen density within compressed gels were calculated as dried solid fraction over hydrated mass of compressed gels.

4.3.3   Construct thickness with or without polymeric collagen

Optical measurements of construct thickness found that an acid-soluble collagen hydrogel compressed to a thickness of 258 $\pm$ 48 μm. A blended gel of 50% (w/w) acid-soluble collagen and polymeric collagen significantly reduced construct thickness after compression to 49 $\pm$ 12μm ($P \leq 0.001$) (figure 4.3).
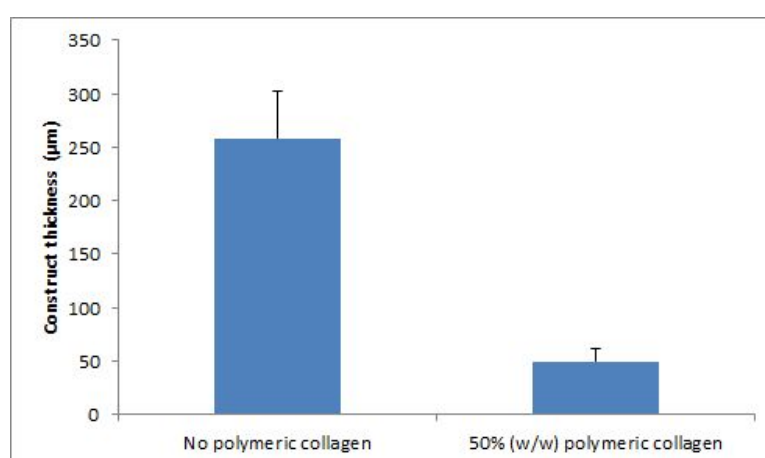
Figure 4.3: Compressed hydrogel thickness of acid-soluble collagen or 50% polymeric collagen derived hydrogels. Hydrogel thickness were measured optically and without further sample processing (i.e. no further dehydration, and represent a more accurate thickness value).

4.3.4   Compression profiles of polymeric collagen containing hydrogels

The rate of fluid loss from hydrogels was measured indirectly via the mass (i.e. fluid) gained by the absorbent plunger over time (figure 4.4).

Complete compression of acid-soluble collagen derived hydrogels without additional load (except plunger mass of $\sim 3g$ and weight of absorbed fluid) was found to occur over 19 minutes. The rate of hydrogel compression decreased

exponentially with time, and was the fastest between 0 and 30 seconds of compression, where the initial compression rate was highest at 0.723 ± 0.103 ml/minute (for non-blended gels).
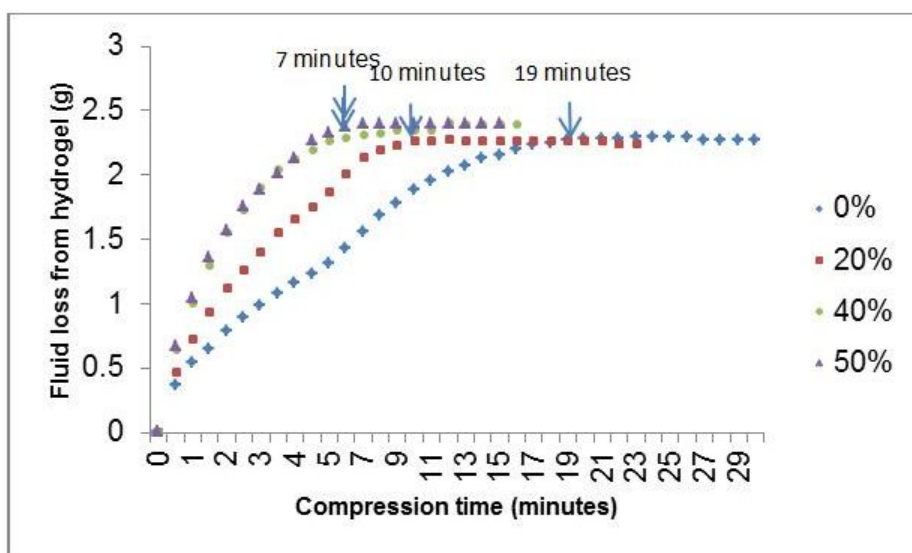
Figure 4.4: Compression profiles of collagen hydrogels with increasing proportions of polymeric collagen (0, 20, 40 or 50% w/w (polymeric collagen/acid-soluble collagen)) based on fluid absorbed by plunger during compression over time. Weight of plungers prior to compression was set as 0 grams. Arrows indicate the average time to complete compression for each blend.

With the substitution of 20% w/w of acid soluble collagen with polymeric collagen, the initial compression rates increased to 0.959 ± 0.092 ml/minute. Increased proportions of polymeric collagen within the hydrogel at 40 and 50% further increased initial compression rates to 1.308 ± 0.270 and 1.325 ± 0.152 ml/minute respectively. Note that the overall time for complete compression was much shorter in gels containing polymeric collagen, such that a gel containing 20% polymeric collagen was completely compressed by 10 minutes, and gels containing both 40 and 50% polymeric collagen were compressed by 7 minutes. It was observed that as initial rates increased (as found in gels with

high proportions of polymeric collagen), the total compression time required for complete compression decreased (figure 4.5).
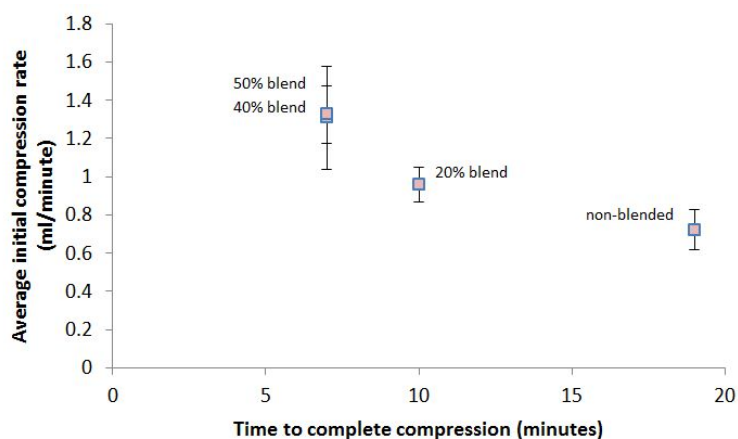
Figure 4.5: Average initial compression rates against average time required for complete compression for blended gels of up to 50% polymeric collagen.

4.3.5 Cell viability within blend collagen hydrogel

Increased compression rates, and therefore fluid shear stress, in polymeric collagen containing hydrogels was potentially damaging to resident cells. It was therefore important to study cell viability within blend hydrogels after plastic compression. Cell were either stained green by calcein-AM if it was living, with an intact membrane, or red in the cell nucleus by ethidium homodimer if the cell membrane was damaged and the cell was dead. Cells within compressed acid-soluble collagen derived gels were found to have a negligible proportion of dead cells of 3.1 $\pm$ 1.6%. 20% polymeric collagen blends (with modest increase in compression rates) had 16.0 $\pm$ 7.0% cell death at day 1 after compression. However, with further increases in hydrogel polymeric collagen content (i.e. 40 and 50% polymeric collagen), significant cell death was observed (80.3 $\pm$ 2.2 and 92.4 $\pm$ 5.6% respectively; table 4.1).

Polymeric collagen in hydrogel (%)	Day 1 average total number of cells	Day 1 average total live cell count (also in % of total cells)	Day 7 average total number of cells	Day 7 average live cell count (also in % of total cells)
0	71.8 ± 7.4	69.6 ± 7.5 (96.9%)	37.0 ± 13.8	46.0 ± 8.9 (100%)
20	56.0 ± 7.2	47.0 ± 7.2 (84.0%)	79.0 ± 16.7	78.2 ± 16.0 (99.1%)
40	48.2 ± 20.3	10.6 ± 8.0 (19.7%)	38.0 ± 15.6	36.6 ± 14.4 (96.3%)
50	61.3 ± 17.5	4 ± 2 (7.6%)	53.4 ± 12.0	52.0 ± 11.2 (97.5%)

Table 4.1: Average total number of cells, and number of live cells (in a field of view; determined by cell staining and counting) within blended collagen hydrogels at days 1 and 7 after plastic compression. Samples contain a blend of polymeric (0, 20, 40 and 50%) and monomeric collagen; with an initial seeding density of 15,000 cell/gel. Results are quoted as average number cells ± standard deviation (SD), including the number of live cells as a percentage of the total number of cells (i.e. both live and dead) detected within the compressed hydrogel.

Polymeric collagen in hydrogel (%)	Uncompressed sample cell death (%)	Compressed sample cell death (%)
0	0 ± 0	3.1 ± 1.6
40	8.1 ± 7.8	80.3 ± 2.2

Table 4.2: Percentage cell death (± standard deviation (SD); determined by cell staining and counting) within blended collagen hydrogels at day 1, with or without plastic compression. Samples contain a blend of 0 or 40% polymeric collagen, with monomeric collagen.

It is important to note that this level of cell death within blended gels was not seen prior to plastic compression (figure 4.6), with only 8.1 $\pm$ 2.2% cell death before plastic compression, and 80.3 $\pm$ 2.2% after compression (table 4.2). Cell death within compressed blended gels was therefore attributed to increased fluid shear stress experienced by cells during compression as opposed to the polymeric collagen itself used within the study.

Cell populations were able to recover and populate the compressed blended gels with culture time as seen in 50% polymeric collagen samples from days 1 through to 14 (figure 4.6). In terms of absolute numbers in the live cell count, cells increased an average of 66%, 345% and 1300% between days 1 and 7 (p≤ 0.001 for all samples), in samples containing 20, 40 and 50% polymeric collagen respectively. The highest rates of cell proliferation were observed in samples containing 40% and 50% polymeric collagen, and can be explained by the low baseline for change (i.e. low number of surviving cells at day 1), and increased physical space between cells (meaning less cell-cell contact and more space for new cells to occupy). The only exception was in samples containing no polymeric collagen, where the total live cell count decreased 34% between days 1 and 7 (p≤ 0.001; figure 4.7, table 4.1), which could be a result of a over population of cells at day 1, and so the number of cells adjusted according to the available space and nutrients. Additionally, by day 7 most samples (apart from 20% polymeric collagen samples) had a similar total cell count (despite the difference in the number of initially viable cells) suggest the samples share a similar limiting factor for cell proliferation (p=0.913 for 40% and p=0.079 for 50% polymeric collagen samples).
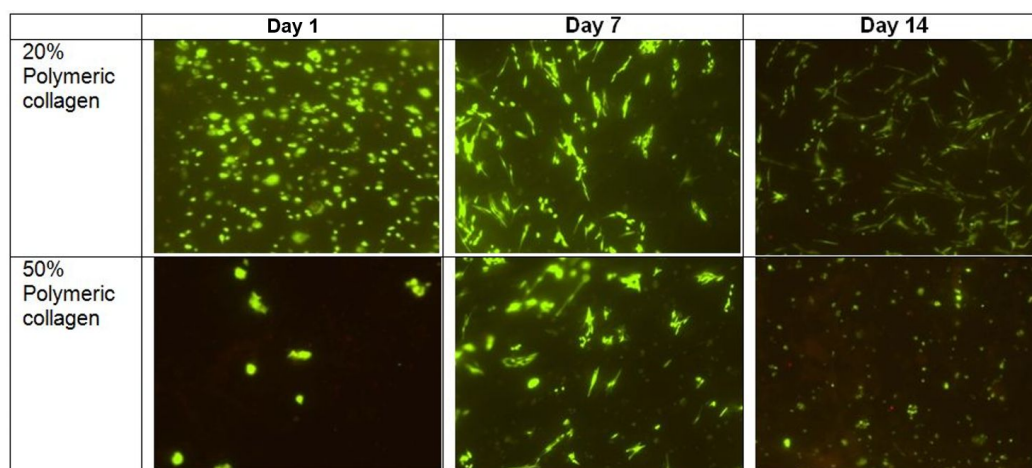
Figure 4.6: Representative images of live/dead stained fibroblasts seeded within compressed hydrogels at days 1, 7 or 14 days of culture. Hydrogels were blended with either 20% or 50% polymeric collagen.
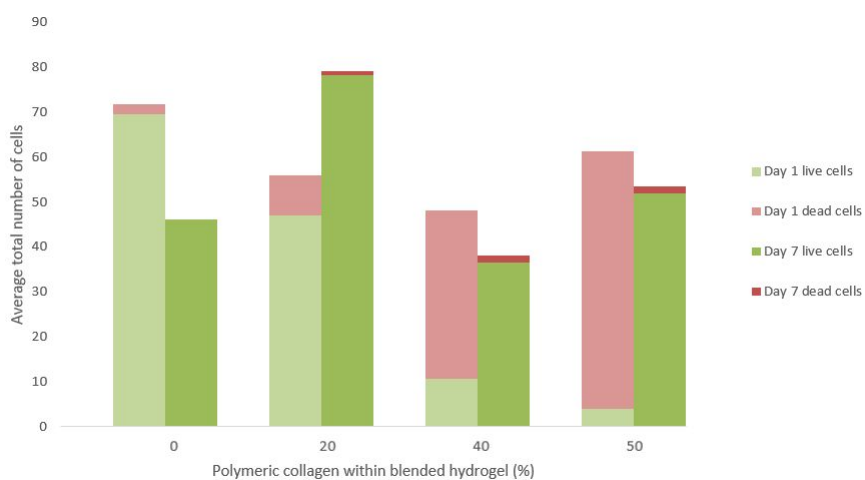
Figure 4.7: The average total amount of cell count within blended colla-gen samples (containing 0, 20, 40 or 50% polymeric collagen, blended with monomeric collagen) at days 1 and 7 of culture following plastic compression. Each column is segmented into two parts, showing the average number of live, and dead, cells found within the sample.

4.3.6   Cell proliferation within blended gels

The decrease in viable cells within blend gels was also reflected in the decreased total cell metabolic activity (as measured by alamar blue) and total DNA detected from constructs immediately after compression, especially in gels containing 40 or 50% (w/w) polymeric collagen (figure 4.8). In terms of cell proliferation within the hydrogel over time (between 1 - 7 and 7 - 14 days), cells in all samples (except 50% polymeric collagen) displayed a marked increase in metabolic activity ($P \leq 0.001$). A smaller increase in metabolic activity was noted in 50% polymeric collagen samples between days 1 and 7 ($p = 0.054$), which deceased with further incubation up to 14 days ($p = 0.037$). This result would imply a lack of cell proliferation, and indeed cell death, based on the metabolic activity alone. However, cell viability imaging (as seen in section 4.3.5 and figure 4.6) of 50% blends confirmed that more cells were present with the construct at days 7 and 14 of culture, and that most cells were alive. It was therefore important to also consider less variable measures of cell numbers such as total DNA within the construct. Indeed, a significant increase in total DNA was observed with incubation between days 1 and 7 for all samples, but was only significant for blended samples containing 40 or 50% polymeric collagen ($P = 0.033$ and $P = 0.006$ respectively).
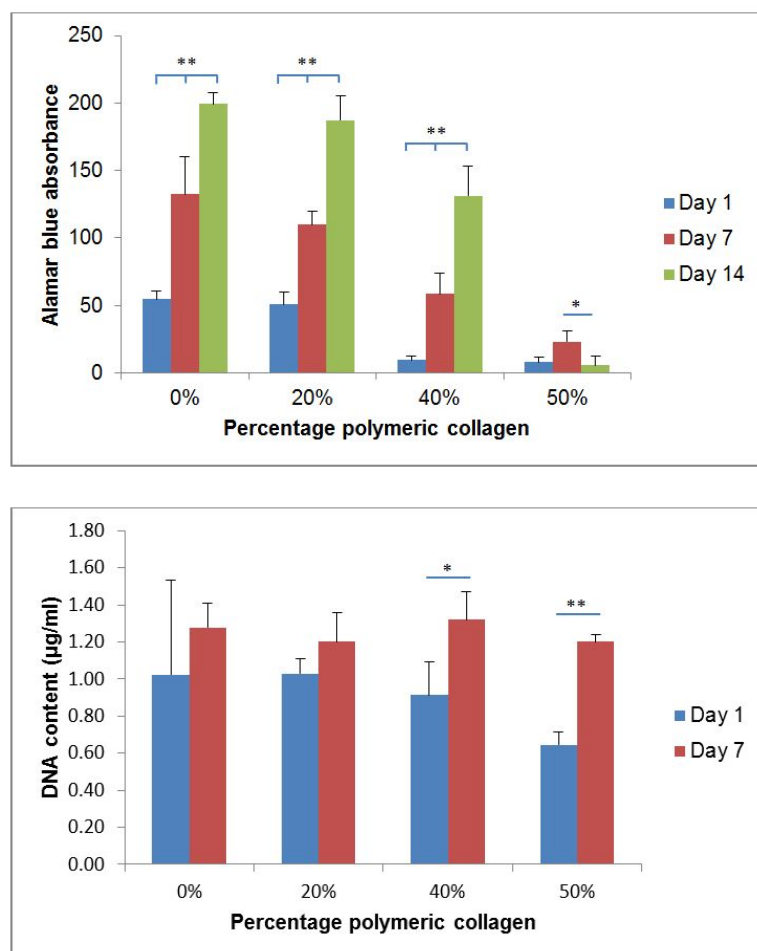
Figure 4.8: Fibroblast-seeded compressed hydrogels containing a blend of polymeric collagen (0, 20, 40 or 50% (w/w)) and monomeric collagen were analysed for a) total cell metabolic activity at 1, 7 and 14 days of incubation and b) total DNA within blend gels at 1 and 7 days of incubation (spectrophotometer readings were converted into μg/ml DNA using a DNA standard curve). ($*P \leq 0.05, **P \leq 0.005$)

4.3.7 Histological sections of cellular blend gels

Histological staining was carried out on 20 and 50% polymeric collagen blends which were incubated for 5 and 14 days to confirm the presence of living, adherent cells. Fibroblasts seeded within the hydrogel at time-zero were still present and visible within the blend hydrogels up to 14 days in culture. This again supports the observation that fibroblasts can be successfully seeded within polymeric-collagen-containing hydrogels, and be cultured over time (figure 4.9).
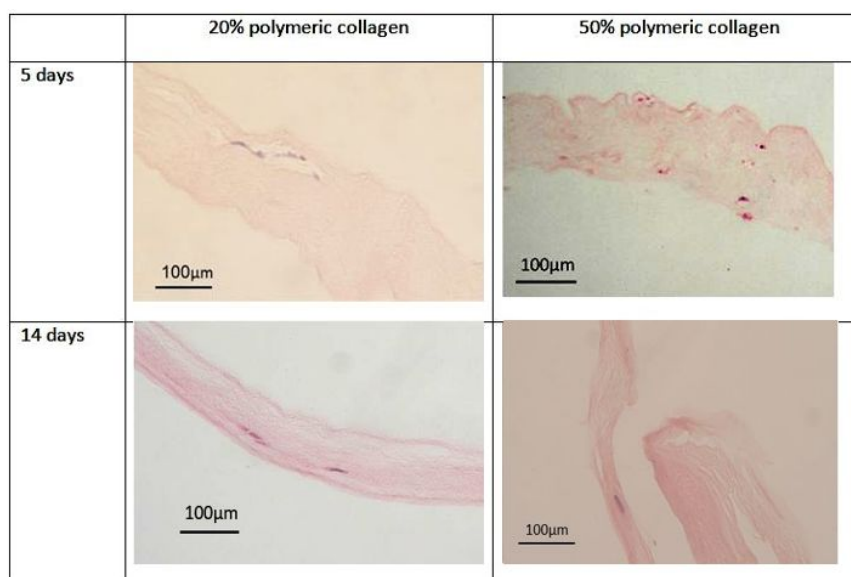
Figure 4.9: Histological staining (H&E) of cellular, compressed gels. 20 and 50% polymeric collagen blended samples were compared after incubation of 5 and 14 days.

4.4 Discussion

Currently one factor hindering the development of collagen hydrogel constructs for tissue engineering is the mismatch between initial cellularity and the general lack in mechanical strength for it to be physiologically relevant to native tissues. The main advantage of a collagen hydrogel is their ability to support interstitially seeded cells - incorporated into the hydrogel as it is formed. However, cells are known to be very sensitive to their environment, in particular, substrate stiffness which previously cannot be easily replicated in a hydrogel without cytotoxic cross-linking treatment. In this study, the aim was to bridge this gap by introducing pre-crosslinked polymeric collagen fibrils as a starting material, and in doing so, avoid artificial cross-linking of collagen fibrils.

This work is the first to systematically study the use of polymeric collagen in a hydrogel to produce *in vitro* tissue models with intrinsic covalent cross-links between collagen fibrils, and so improved mechanical properties. Plastic compression was used on blended collagen hydrogels to increase the overall collagen density to tissue levels, which also impacts on the mechanical properties (i.e. compare hydrogels before (0.02% collagen) and after ($\sim 12\%$ collagen) plastic compression). It was found that as the fraction of polymeric collagen increased (up to 50% w/w to acid soluble collagen), the overall collagen density within the compressed construct also increased. In a 50% polymeric collagen construct, collagen density almost doubled from 12.0% to 20.8% (compared to acid soluble collagen only constructs), which was reflective of their decreased ability to trap water within the construct. That said, this difference in collagen density was brought about by an increase in total water loss of $\sim 52\mu$l from within a blend gel (out of a 2.5ml hydrogel; based on the average difference in plunger mass at the end of plastic compression). However the relatively small difference in total volume had significant impact on hydrogel dimensions. In

terms of construct dimensions, blend gels were much thinner than the conventional hydrogel, despite similar starting volumes and collagen density. This also points to the reduced fluid trapping ability of the blend gel. Based on the thickness of the respective hydrogels, the total volume of the compressed gel can be calculated, as:

$$\text{Gel volume} = \pi r^2 h$$

Where *r* was the radius of the hydrogel, used to calculate the area of the circle (πr^2); and *h* was the height of the compressed hydrogel. Hydrogel thickness (height) were found to be 0.0258 ± 0.0045 and 0.0049 ± 0.0012 cm for compressed acid-soluble collagen and 50% polymeric collagen derived hydrogels respectively. Since all hydrogels were set and compressed in 24-well plates, the well diameter was taken as the gel diameter at 1.56cm (radius of 0.78cm), and the compressed gel volume was calculated:

$$\text{Acid-soluble collagen gel volume} = \pi r^2 h$$
$$= \pi (0.78)^2 \text{ x } 0.0258$$
$$= \mathbf{0.0493} cm^3$$

$$\text{Polymeric collagen blend gel volume} = \pi r^2 h$$
$$= \pi (0.78)^2 \text{ x } 0.0049$$
$$= \mathbf{0.0094} cm^3$$

The differences in average total volume within compressed acid-soluble collagen derived ($0.0493 cm^3$; or 0.0493ml) and polymeric collagen blend (0.0094ml)

gel was therefore $\sim$40μl. This was comparable to the differences in plunger mass after plastic compression for the respective hydrogel samples ($\sim 52\mu$m).

Apart from the increased collagen density, the incorporation of polymeric collagen into compressed hydrogels, as expected, increased material stiffness (Young's modulus) by $\sim$3 folds, to $1.051 \pm 0.377 MPa$. This was much improved compared to compressed hydrogels derived from acid-soluble collagen, and so offers a promising basis for a model of slightly stiffer tissues.

For all samples, the rate of compression was highest during the first 30 seconds of compression (hereafter termed the initial compression rate), and decreases exponentially with compression time. Initial compression rates increased substantially within gels containing 40 or 50% polymeric collagen. The increased compression rates in blended gels is likely due to a much diminished blocking of fluid outflow (from the FLS) as fewer small collagen species were present, therefore resulting in increased fluid shear stress (Hadjipanayi et al., 2011a) and cell death. The reasoning behind this is the long-standing suspicion that during collagen hydrogel formation, a proportion of collagen remains poorly associated and mobile. It was understood that during the early stages of collagen plastic compression, a dense mat of fibrils would be formed at the FLS to produce a 'ultra-filtration membrane', which would be predicted to catch (and so be clogged by) smaller mobile collagen aggregates, such as oligomers and non-aggregated molecules (for schematic representation, see figure 4.10). Increasing the proportion of polymeric collagen in these blended gels will radically and proportionally decrease the amount of small mobile species. This in turn decreased the membrane fouling effect, and so increases fluid efflux and shear across the stiff polymer fibrils. This is consistent with the measured increased fluid outflow for polymeric collagen containing (blended) constructs.
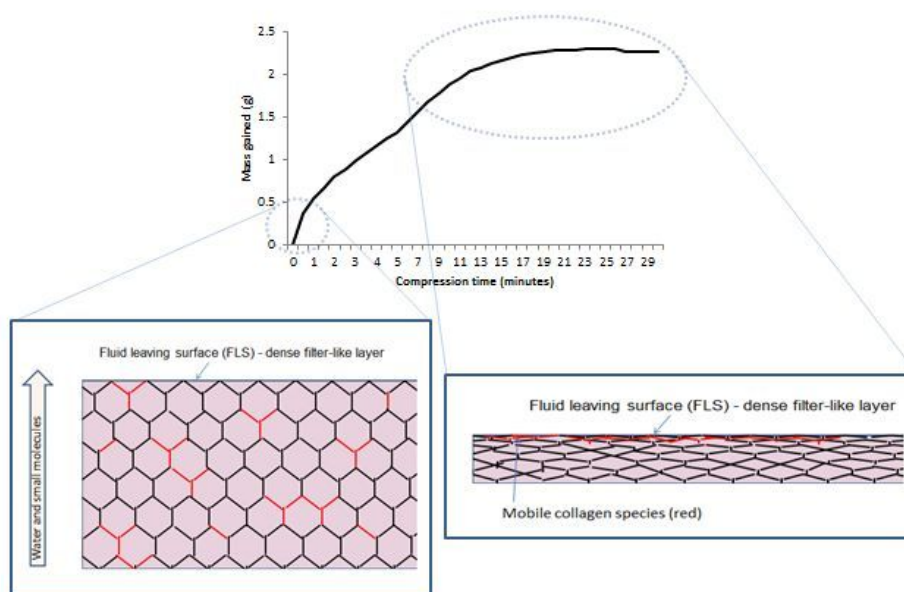
Figure 4.10: Schematic representation of collagen hydrogels during the beginning and later stages of plastic compression. Red lines within diagram represent mobile collagen species, such as monomeric or oligomeric collagen, which would be predicted to travel with fluid flow during plastic compression and becomes retained by the dense collagen layer at the fluid leaving surface (FLS) - further contributing to the filtration effect.

In terms of cell viability, cell damage is well known to be minimal during plastic compression of "conventional" acid-soluble collagen derived hydrogels (Brown et al., 2005), and a similar 97% cell viability was seen here following compression of non-blended hydrogels. However, significant cell death was observed after compression of hydrogels containing a relatively high proportion of polymeric collagen (40 and 50% at 80.3 ± 2.2 and $92.4 \pm 5.6\%$ respectively). It was also within these samples where a high compression rate was observed. The high fluid flow rates during compression of blended hydrogels were likely to have caused the cell damage by increased fluid shear stress.

Although cells naturally experience some fluid dynamics and flow (i.e. bloodflow), they are rarely damaged at physiological flow rates. Indeed the fluid dynamics may be essential to the cell function, such as inflammation or cell migration/alignment (Ng and Swartz, 2003). The mechanism by which at least some cell types sense fluid shear stress was via cell surface/membrane deformation and ion (i.e. Calcium) channels (Cunningham and Gotlieb, 2005); via focal adhesion when cells remain attached to the ECM. (McCue et al., 2004). The trigger of cell internal pathways can then affect cell essential pathways, such as MAPK signaling as demonstrated in mesenchymal cells (Glossop and Cartmell, 2009). However, when the fluid shear stress was sufficiently large, as thought to be occurring in the polymeric collagen containing hydrogels, cell membranes can sustain physical damage and undergo necrosis.

It was important to note that the cell population did recover with incubation time as reflected in the total DNA assay (figure 4.8), where an increase in total DNA within all samples was observed between days 1 and 7. This increase was however only significant for 40 and 50% polymeric collagen blends, suggesting a higher proliferation rate within the polymeric collagen containing gels. However, this finding was not consistent with the Alamar blue assay (for total cell metabolic activity within a sample), which has commonly been

used as a measure of cell proliferation. The Alamar blue assay indicated an increase in total metabolic activity for all samples except 50% polymeric collagen blends between 1 - 7 and 7 - 14 days. However, for 50% blends, there was a non-significant increase in cell metabolic activity between days 1 and 7, and a subsequent significant decrease in metabolic activity between days 7 and 14. Visual data of blended gels i.e. live-dead cell imaging (figure 4.6) would however indicate that total number of cells have increased with incubation time in 40 and 50% polymeric collagen blend gels (note also the change in cell morphology in 50% polymeric collagen blends). The presence of live cells within 50% polymeric collagen blend gels, coupled with the finding of decreased total metabolic activity may indicate the presence of quiescent cells. However, whether this change was indeed due to increased matrix stiffness or exposure to high fluid shear stress remains to be determined. Nevertheless, both assays agree that a higher proportion of polymeric collagen within the hydrogel caused a drop in initial cell viability immediately after plastic compression. Since this cell death was only observed after the compression of blended (fast-compressing) hydrogels, and that a rapid proliferation over 14 days was observed post-compression, it was concluded that polymeric collagen itself is cell compatible, and that the problem was the increased fluid shear.

Chapter 5

Results: Control of hydrogel compression rates using large molecules

5.1   Introduction

The generation of a novel, stiff and cellular collagen hydrogel matrix was described in chapter 4, where it has been studied for its potential use as a stiff tissue model.

This model is generated by including pre-crosslinked collagen into the structure of the hydrogel (so that the matrix is made of a mix of covalently cross-linked polymeric collagen and acid-soluble (conventional gelling) collagen. Plastic compression of these blended gels resulted in a construct with a three-fold increase in matrix stiffness relative to gels derived from acid-soluble collagen only (results in the previous chapter showed an increase in Young's modulus from 0.36 ± 0.10 to 1.05 ± 0.38 MPa). These blended hydrogels also supported the culture of resident cells *in vitro* over time. For a cell-rich gel, this improves the physiological relevance of the hydrogel as a 3D tissue model,

especially when the target tissue is relatively stiff.

However, as concluded in the previous chapter, the problem associated with the novel polymeric collagen blend gels was the unusual cell death that was observed during their fabrication. The cause of the cell death was pin-pointed to the increased fluid shear stress (i.e. increased flow rates) during the plastic compression of the new blended hydrogel; but it is important to stress that this cell death is not normally observed during the plastic compression of conventional, acid-soluble collagen, derived gels (Brown et al., 2005). Since plastic compression of the hydrogel is an essential step in generating a physiologically relevant model, this part of the study aims to devise a method to reduce shear stresses on interstitial cells, and prevent cell damage. For this, the relationship between fluid outflow during plastic compression and the factors that influence fluid flow within the hydrogel needs to be further investigated.

5.1.1   What influences fluid flow rates within a hydrogel?

The ability of the collagen matrix to hold water is interesting because the difference in size between the interfibrillar space ($\sim 10 - 50 nm^2$ or less, depending on the compressive load (Serpooshan et al., 2011)) and the water molecule (1.37Å ($\sim 0.14 nm$) (Zhang and Xu, 1995)) is at least 70 fold; and water should, according to its size, be able to easily flow through the hydrogel.

However during the plastic compression of collagen hydrogels, water only leaves the hydrogel partially, and slowly, across several minutes (even with external load). This suggests the presence of other factors from within the hydrogel is preventing the free flow of water from the hydrogel.

External factors that are already known to impact hydrogel compression rates include the amount of external load placed on the compression system, and the total surface area of the fluid leaving surface (FLS) (Hadjipanayi et al.,

2011a). However it is the factors within the gel that are thought to have the greatest influence on the ability of water, which is encased within the matrix, to escape.

Water within the hydrogel is held within a mesh of loosely associated collagen fibril. This means that water trapped within the hydrogel must leave the matrix through the spaces formed between collagen fibres during fibrillogenesis. Consequently the size of the interfibrillar space may affect the rate of water efflux from the gel. A typical hydrogel is made of $\sim 99.8\%$ (w/w) water, with the remaining mass that might potentially block fluid flow comprising of collagen molecules ($\sim 0.2\%$) and some neutral salts (negligible amounts).

Salts within the hydrogel typically include soluble salts (such as sodium and potassium chlorides) and molecules such as D-glucose, all of which are relatively small compared to the estimated size of the interfibillar space (ions are in the pico-meter range and glucose has a hydrodynamic radius of $\sim 0.46nm$ (Lim et al., 2014)). These molecules are therefore unlikely to contribute to the blockage at the FLS. Instead, it is thought that some collagen molecules are not fully incorporated into a single-bodied matrix during fibrillogenesis, but remained as monomers (or aggregated into small oligomeric collagen species), which are mobile within the hydrogel, and can then block interfibrllar spaces from within the hydrogel during compression (Hadjipanayi et al., 2011a).

Imaging of a fully compressed hydrogel sheet (cross-sectional SEM image adapted from Brown et al. (2005) (figure 5.1) shows that a collagen density gradient is formed within the hydrogel. The fact that collagen density was greater at one surface of the collagen sheet suggest a collection of mobile collagen molecules at the FLS (which acts as a ultrafiltration membrane). More specifically it is thought that at the first signs of compression, collagen fibrils at the surface of the hydrogel (at the fluid leaving surface) becomes compacted, minimising the interfibrillar space between these fibrils. This then acts as a filtra-

tion membrane whereby collagen monomers or oligomers, not small enough to squeeze through the narrowed space between the collagen fibrils at the FLS, are trapped at the 'filter' and contributes to the progressive blocking and reduced fluid outflow. A lamellar structure within the hydrogel is also interesting and may shed light onto the mechanism of micro-structure generation during plastic compression (further discussion section 8).
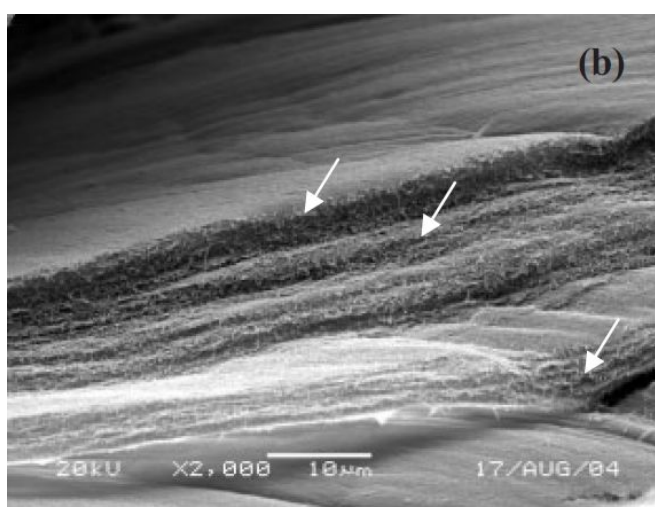
Figure 5.1: Cross-sectional SEM image of a fully compressed hydrogel adapted from Brown et al. (2005) (figure 4). Note the lamellar structure parallel to the FLS within the hydrogel.

Other potential ways to reduce fluid flow

Changes to the hydrogel structure may provide the necessary increase in the blockage at the FLS to reduce fluid flow. One possible change to the hydrogel structure is the fibre thickness. Collagen fibril diameter have been found to be $\sim 30nm$ when fibrillogenesis occured at $37^\circ c$ over 30 minutes (Cheema et al., 2007b). However, studies have found that collagen aggregation at lower temperatures resulted in increased fibre thickness (Wood and Keech, 1960). Increasing fibre thickness within a 'closed system' will be at the expense of the limited amount of collagen molecules and is likely to result in fewer, but thicker,

fibres and increased interfibrillar space.

Collagen density also potentially alters the fluid flow rate within the hydrogel, as increasing the amount of collagen fibrils will increase occupied space by the collagen fibrils, and result in smaller 'pores'. This would also lead to an increase in mobile collagen species that can contribute to the FLS clogging. Indeed, a collagen hydrogel containing $6mg.ml^{-1}$ atelocollagen required, on average, more time for complete compression compress (1ml gel, 41 minutes), compared to a $2mg.ml^{-1}$ collagen hydrogel of the same volume (6 minutes).

For the novel blend gel, reduced amounts of mobile collagen monomers/ oligomers (as half of the soluble collagen molecules were substituted with pre-crosslinked polymeric collagen) is expected to reduce FLS clogging, and would explain the rapid fluid outflow reported in the previous chapter. It was therefore hypothesised that replacing the molecules which contribute to the clogging of interfibrillar space (i.e. increase the clogging/filtration effect) will decrease fluid outflow rates, and so decrease the amount of fluid shear stress placed on resident cells during the compression of fast-compressing hydrogels; such as that seen in polymeric collagen containing hydrogels.

The main purpose of this study is to develop and understand methods for decreasing the rate of fluid efflux from hydrogels, particularly where compression is unusually rapid. The approach is to improve the FLS barrier formation (clogging) using artificially introduced mobile macro-molecules. Two basic mechanisms were tested within this aim. In the first, the tropocollagen (acid-soluble collagen) of the gel itself was progressively cleaved by incubation with pepsin, to generate potentially clogging atelocollagen species. In the second, selected polymer macromolecules were added to the gelling collagen mix as potential clogging agents.
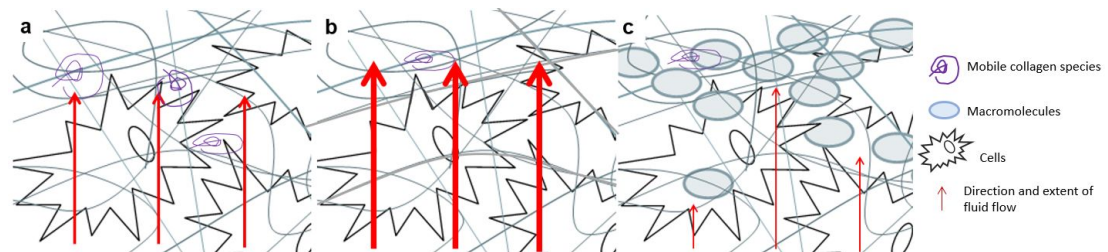
Figure 5.2: Schematic representation of fluid flow during plastic compression, within cellular a) conventional hydrogel b) polymeric collagen blend hydrogel and c) blend hydrogel containing large, FLS clogging, macromolecules (blue circles). Non-associated (mobile monomeric and oligomeric) collagen species, cells and water are normally enmeshed within the collagen hydrogel matrix following fibrillogenesis. However, the (intrinsically present) mobile collagen species are found in reduced quantities in blend hydrogels with a high polymeric collagen content (environments B and C). This causes a high fluid flow rate (though to be damaging to cells; environment B), but can be reversed when these mobile collagen species are replaced by large macromolecuels which contribute to the blockage to fluid outflow at the FLS.

5.1.2   Polymer macromolecules as clogging agents

The large polymers incorporated into the hydrogel, and tested in this study for its efficiency in blocking the FLS are as follows:

Fibrinogen

Fibrinogen (Sigma, UK) is a naturally occurring plasma protein normally involved in blood coagulation. The protein has a molecular weight of 340kDa . It can be converted into a fibrous mesh (Fibrin) by thrombin action.

Dextran

Dextran is a polysaccharide of polymerised glucose molecules made up to a size of 2000 kDa. In this study, Dextran with an average molecular weight of 500kDa was used (Fisher Scientific, UK).

Poly(ethylene)glycol (PEG)

PEG is a polymer made of polyethylene oxide, and are found in molecules of up to 8000 kDa (or more). PEG 400kDa and 1000kDa (both from Sigma, UK) were used in this study.

Ficoll™

Ficoll is a branched polymer made from the co-polymerisation of sucrose and epichlorohydrin. The molecules typically come in a size of either 70kDa or 400kDa. In this study, Ficoll™ 400kDa was used as a pore blocking agent.

The hydrodynamic size of the above mentioned polymers ranged from $\sim$ $11 - 42$nm, which are within the range of the interfibrillar space found between collagen fibrils within the hydrogel. Therefore they were chosen for use as a potential pore-clogging species.

5.2 Methods

Methods listed below are specific to this study. Further methods common to studies throughout the thesis are listed in Chapter 2. All hydrogels (both conventional acid-soluble collagen derived and polymeric collagen blended gels) were set within 24-well plates, with each well containing a gel volume of 2.5ml (except where specified). The rate of fluid efflux (i.e. compression rate) for all samples were measured as detailed in chapter 2.5.

5.2.1 Pepsin treatment of tropocollagen to produce atelo-collagen

Pepsin treatment was used to convert tropocollagen (conventional gelling acid-soluble collagen) into atelocollagen, which is a potential source of mobile collagen species. Collagen molecules without telopeptides associate less readily with adjacent collagen molecules during fibrillogenesis (Snowden and Swann, 1979) (Brennan and Davison, 1981), and so potentially increases the proportion of monomer/oligomer collagens which would remain mobile within the hydrogel at the time of compression.

Pepsin (porcine derived; Sigma-Aldrich) was dissolved in 0.5M acetic acid (2.5mg.ml^{-1}) and added in a ratio of 1:99 (w/w) to acid soluble type-I collagen at 4 ℃ (on stirrer). At 0, 1.5, 3, 4.5, 24, 48 and 72 hours after pepsin treatment, the collagen solution was neutralised and gelled following the method for acid

soluble collagen derived hydrogels (detailed in chapter 2). Compression rates for all gels were subsequently measured.

5.2.2 Macromolecules as clogging agents within the hydrogel

Macro-molecules (as mobile, clogging species) were incorporated into the hydrogels to increase blockage at the FLS. Fibrinogen (340kDa; Sigma-Aldrich) in 0.9% saline, dextran (500kDa; Fisher Bioreagents) or poly(ethylene oxide) (PEG; 400kDa or 1000kDa, Sigma-Aldrich) in deionised water, were made to a concentration of 0, 2, 5, 10 or 20mg.ml^{-1}. Ficoll™ 400 (Sigma-Aldrich) was made to 10, 50 or 100mg.ml^{-1} in deionised water. 10% (v/v) of the polymer solution was added to a neutralised collagen mixture containing 10% (v/v) 10xMEM and 80% (v/v) acid soluble collagen prior to incubation at 37 °c for 30 minutes. Compression rates of the hydrogels were subsequently measured.

5.2.3 Rate of fibrillogenesis

The rate of hydrogel formation (gelation), with or without the presence of large macromolecules, was measured using the change in light scattering of the hydrogel over time (gels became opaque as fibrillogenesis progresses).

3ml of the collagen solution, neutralised at 4°c, was transferred into a cuvette. It was immediately placed in a luminescence spectrometer (LS 50B, PerkinElmer, UK), where the solution would begin to form a hydrogel as it was exposed to room temperature. The absorbence of the solution was measured at an excitation wavelength of 450nm, and an emission wavelength of 700nm, every 30 seconds until no substantial changes in the values was observed.

5.2.4 Additional fibrin mesh at the FLS

Since fibrinogen was successfully introduced into the hydrogel as a interfibrillar 'pore' clogging agent, it was hypothesised that the topical application of thrombin (Sigma, UK; in water), a protease which converts fibrinogen into fibrin, to the FLS will result in a mesh-like structure which can contribute to the matrix's ability to retain water (i.e. increase matrix density at the FLS).

Fibrinogen containing hydrogels were produced as described above, where 5mg.ml^{-1} fibrinogen (in 0.9% saline) (10% v/v) was added to the neutralised collagen solution. After gelation of the hydrogel, 50μl of 1mg.ml^{-1} thrombin was applied to the hydrogel indirectly, by first applying the thrombin to a well-sized paper disc, before transferring the disc onto the hydrogel. The thrombin remained in contact with the hydrogel for 5 minutes prior to hydrogel compression. Compression rates of the resultant gels were measured and compared to fibrinogen containing gels without thrombin application.

5.2.5 Cell viability test in gels containing additional macro-molecule

The effectiveness of macro-molecule incorporation on slowing compression rates, and consequently on preserving interstitial cells viability was tested within conventional (acid soluble collagen derived slow-compressing) or polymeric collagen blend (fast-compressing) hydrogels. Hydrogels were made from 10% volume of 10mg.ml^{-1} PEG 400kDa (final concentration of 1mg.ml^{-1} within hydrogels), 10% (v/v) DMEM (Sigma-Aldrich) supplemented with 10% foetal calf serum (First Link, UK) and 1% penicillin streptomycin (Gibco, Life Technologies) containing human dermal fibroblasts (HDF; passages 8-9), 10% 10 x MEM and 70% (v/v) collagen solution.

After hydrogel formation (1.5ml gel; 15,000cells/gel) and compression, cell

activity within the gels was measured by Alamar blue assays as described in chapter 2.6.

5.2.6 Statistics

Statistical significance was determined by one-way ANOVA (LSD post-hoc) for data on compression rates. For all other experiments, an independent sample t-test was used. Confidence intervals were set at $p \leq 0.05$.

5.3 Results

The purpose of the study was to decrease compression rates of fast compressing hydrogels with the ultimate aim to preserve interstitial cell integrity. The approach adopted here was to increase the blockage of interfibrillar space, particularly at the FLS.

The typical compression profile of a hydrogel over time included a fast initial rate of fluid loss (in the first 30 seconds of compression), followed by a period of steady rate of fluid loss until it finally reached a plateau, when no further water left the gel (i.e. compression was complete) (figure 5.3a). When results from this compression profile was converted into rate of fluid loss from the hydrogel during compression (figure 5.3b), the initial time point (first 30 seconds) represented the highest rate throughout the compression process (in this case at more than double that of all other time points). Compression rates then decreased exponentially over time.

For polymeric collagen blended gels, the initial compression rate could be as high as 1.325 ± 0.152 ml/minute (as opposed to 0.691 ± 0.083 ml/min in conventional (cell-friendly slow compressing) acid-soluble collagen gels. Although compression rates quickly dropped with the progression of the compression

process, the short exposure of cells to high fluid flow rates was found (in the previous chapter) to be sufficient to damage resident cells.
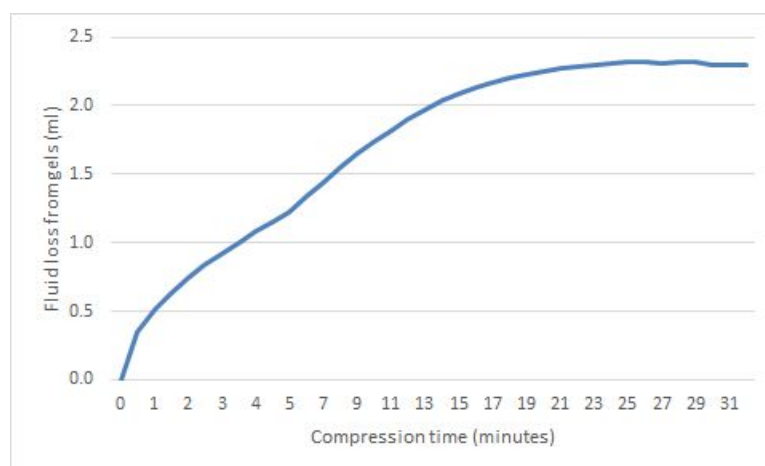
(a) Profile of fluid loss from hydrogel during plastic compression
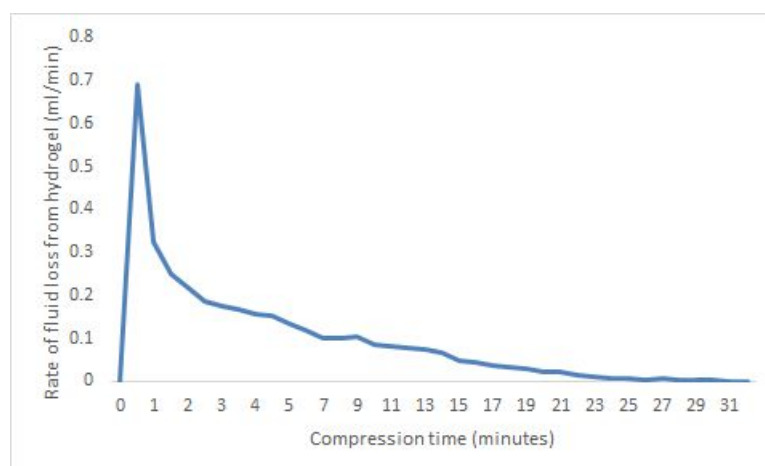
(b) Rate of fluid loss from hydrogel

Figure 5.3: Example showing the compression profile of a 2.5ml hydrogel set in a 24-well plate. a) Shows the cumulative amount of fluid loss (ml) from the hydrogel over time. b) A derivative graph showing the results in terms of rate of fluid loss (ml/minute) at each time point over the compression period. Note that the rate of fluid loss (compression rate) was highest at the beginning of hydrogel compression, and decreases exponentially as compression progresses.

5.3.1   Fluid flow rates after pepsin treatment

Pepsin treatment of collagen solutions did not result in decreased early stage (initial) flow rates. Instead, the rate of collagen compression increased with length of pepsin treatment, with a peak initial compression rates of 1.089 ± 0.152 ml/minute at 24 hours of pepsin treatment ($p \leq 0.001$) (figure 5.4; table 5.1). In addition, gels made from 24-48h pepsin digested collagen also produced increased outflow rates during later stages of compression (measured at 5 minutes into the compression process), at 0.184 ± 0.046 and 0.230 ± 0.152 ml/minute respectively, as opposed to 0.135 ± 0.024 ml/minute when no pepsin treatment was involved. With further pepsin treatment time, at 72 hours, the compression rates appeared to fall slightly relative to the peak rates seen in gels with 24-48 hours of pepsin treatment. These results suggest that any mobile species generated by pepsin digestion of tropocollagen (i.e. atelocollagen monomers/oligomers) did not block interfibrillar "pores" of the FLS, although it clearly did alter filtration rates in a complex manner.

Since pepsin treatment of tropocollagen produced atelocollagen which associate less readily with adjacent collagen molecules, the pepsin treatment may therefore have a greater effect on enlarging the "pores" within the hydrogel; potentially due to reduced fibril formation by the remaining tropocollagen and reduced amount of collagen species that are sufficiently large to clog pores (i.e. oligomers).

Pepsin treatment time (minutes)	n	Compression rate at 30 seconds	Compression rate at 5 minutes	Time to complete compression (minutes)
No pepsin treatment	9	0.691 ± 0.083	0.135 ± 0.024	26
0	6	0.616 ± 0.148	0.148 ± 0.024	25
1.5	6	0.743 ± 0.077	0.160 ± 0.025	20
3	6	0.791 ± 0.081	0.168 ± 0.010	17
4.5	3	**0.983 ± 0.248**	0.115 ± 0.092	14
24	9	**1.089 ± 0.152**	**0.184 ± 0.046**	13
48	9	**1.027 ± 0.160**	**0.230 ± 0.152**	20
72	6	**0.970 ± 0.173**	**0.146 ± 0.043**	19

Table 5.1: Average compression rates of hydrogels derived from acid-soluble collagen treated with pepsin for an increasing amount of time. Rates over the first 30 seconds (initial rate) and 5 minutes of compression are quoted as mean ml/minute $\pm$ standard deviation (SD). Time to complete compression are noted as the time where compression rates reached zero. Compression rates significantly different to non-pepsin treated gels are listed in bold font.
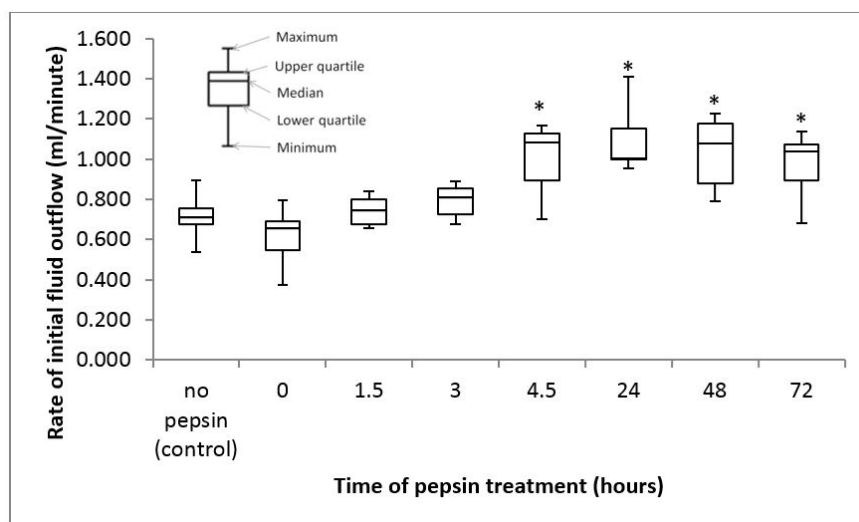
Figure 5.4: Box-and-whisker plot of initial (first 30 seconds) compression rate of hydrogels within increasing pepsin treatment time. Compression rate was significantly increased relative to control from 4.5 hours of treatment onwards ($p \leq 0.05^*$)

5.3.2 Fluid flow rates with macromolecule incorporation

Macro-molecule incorporation was more effective in slowing initial compression rates compared to the use of pepsin to produce mobile collagen monomer/oligomer species within the hydrogel (table 5.1 and tabel 5.2).

Macromolecule/ concentration	n	Compression rate at 30 seconds	Compression rate at 5 minutes	Time to complete compression (minutes)
No macromolecules	9	0.691 ± 0.083	0.135 ± 0.024	26
Fibrinogen 2mg.ml^{-1}	15	0.660 ± 0.114	0.139 ± 0.026	28
Fibrinogen 5mg.ml^{-1}	15	**0.582 ± 0.119**	0.141 ± 0.026	27
Fibrinogen 10mg.ml^{-1}	9	0.698 ± 0.097	0.138 ± 0.034	26
Fibrinogen 20mg.ml^{-1}	6	**0.915 ± 0.107**	**0.177 ± 0.025**	
Dextran 2mg.ml^{-1}	14	0.650 ± 0.085	0.124 ± 0.015	31
Dextran 5mg.ml^{-1}	15	**0.615 ± 0.090**	0.131 ± 0.022	32
Dextran 10mg.ml^{-1}	12	**0.618 ± 0.075**	**0.115 ± 0.013**	36
Dextran 20mg.ml^{-1}	9	0.631 ± 0.053	0.125 ± 0.027	36
PEG 400kDa 2mg.ml^{-1}	9	0.691 ± 0.085	0.144 ± 0.014	26
PEG 400kDa 5mg.ml^{-1}	9	**0.566 ± 0.080**	0.123 ± 0.017	35
PEG 400kDa 10mg.ml^{-1}	9	**0.456 ± 0.121**	**0.107 ± 0.018**	43

PEG 20mg.ml^{-1}	400kDa	6	0.636 ± 0.054	**0.097 ± 0.005**	50
PEG 10mg.ml^{-1}	1000kDa	6	**0.524 ± 0.028**	**0.103 ± 0.017**	50
PEG 20mg.ml^{-1}	1000kDa	6	**0.564 ± 0.051**	**0.095 ± 0.019**	71
Ficoll™ 10mg.ml^{-1}	400kDa	6	**0.846 ± 0.084**	**0.165 ± 0.038**	20
Ficoll™ 50mg.ml^{-1}	400kDa	6	**0.908 ± 0.089**	**0.172 ± 0.024**	16
Ficoll™ 100mg.ml^{-1}	400kDa	9	0.665 ± 0.153	0.146 ± 0.022	31

Table 5.2: Average compression rates of hydrogels with increasing concentrations of macromolecules. Rates over the first 30 seconds (initial rate) and 5 minutes of compression were quoted as mean ml/minute ± standard deviation (SD). Time to complete compression was noted as the time where compression rates reached zero. Compression rates significantly different to gels with no macromolecules are listed in bold font.

Optimal initial compression rates (for each macromolecule type) was observed at a polymer concentrations of 5mg.ml^{-1} for fibrinogen (0.582 ± 0.119 ml/min), 5mg.ml^{-1} or 10mg.ml^{-1} for dextran (0.615 ± 0.090 and 0.618 ± 0.075 ml/min) and 10mg.ml^{-1} for larger polymers such as PEG at 400kDa (0.456 ± 0.121 ml/min) and 1000kDa (0.524 ± 0.028 ml/min) compared to gels with no macromolecules (0.691 ± 0.083 ml/min). Importantly, the effectiveness of the blocking agent was generally found to be correlated with its Stokes radius (figure 5.5); and not the polymer molecular weight (figure 5.6). The hydrodynamic radius for fibrinogen, dextran, PEG 400kDa, PEG 1000kDa and Ficoll™ 400 were 10.95, 15.9, 26.56, 41.63 (adapted from Armstrong et al. (2004)) and 10nm respectively; with PEG 400kDa (26.56nm) (at 10mg.ml^{-1}) being most effective, of the polymers tested, in slowing the initial compression rates of hydrogels ((p $\leq$ 0.001; figure 5.7). Note that polymers were added to the hydrogel at a concentration of 1:9 (macromolecule : neutralised collagen solution), meaning a PEG concentration within the hydrogel of 1mg.ml^{-1}.

Smaller polymers (hydrodynamic radius) were less able to slow the compression rates due to the reduced blockage at the FLS. For example, PEG 400kDa (~ 26nm) was able to slow initial compression rates more effectively from a rate of 0.691 $\pm$ 0.083ml/min (where no macromolecules were present) to 0.456 $\pm$ 0.121 ml/min. Whereas dextran, a smaller polymer ($\sim$ 16nm), resulted in a maximum decrease of initial compression rates to 0.615 $\pm$ 0.090ml/min. Polymers larger than PEG 400kDa (i.e. PEG 1000kDa) did not further decrease the initial compression rate (p=0.147). Ficoll™ 400 was the only exception to the above observation, and increased compression rates when incorporated into the hydrogel (i.e. 10mg.ml^{-1}; p=0.002).

The data correlated with the line of best fit ($y = -0.007x + 0.764$) with a correlation coefficient of ρ^2= 0.5372, suggesting a moderate correlation to the line of best fit.
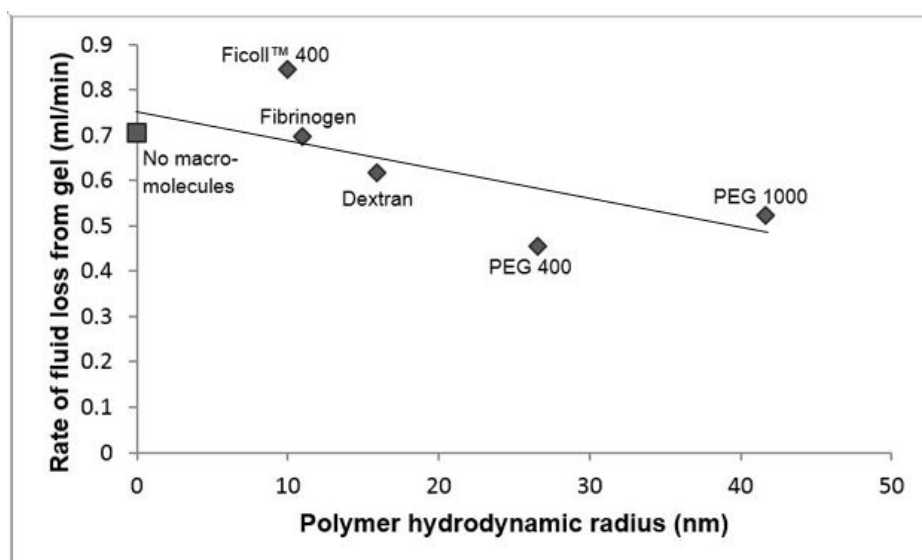
Figure 5.5: Correlation between polymer hydrodynamic radii and their respective initial (first 30 seconds) compression rates. All polymer concentrations were 10mg.ml^{-1}.
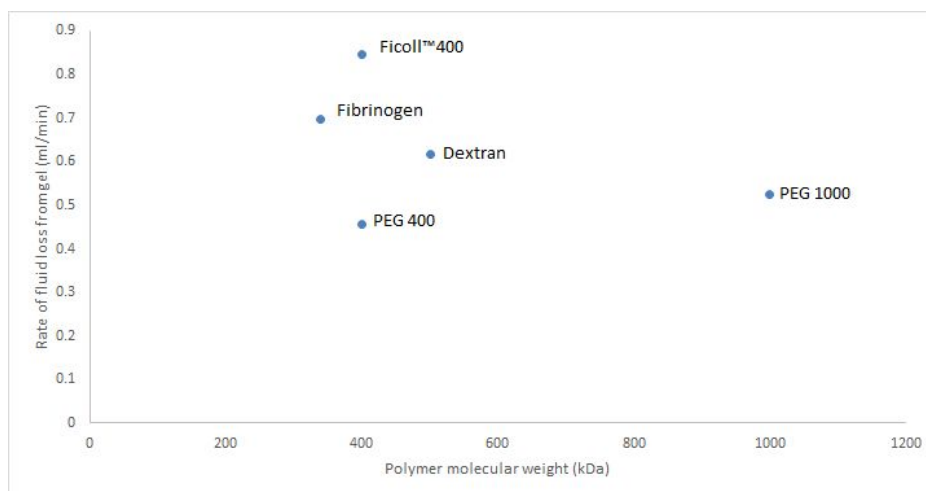
Figure 5.6: Initial compression rates (rate of fluid flow from the hydrogel) against polymer molecular weight. Correlation between initial flow rates and molecular weight of the macromolecule was weak.
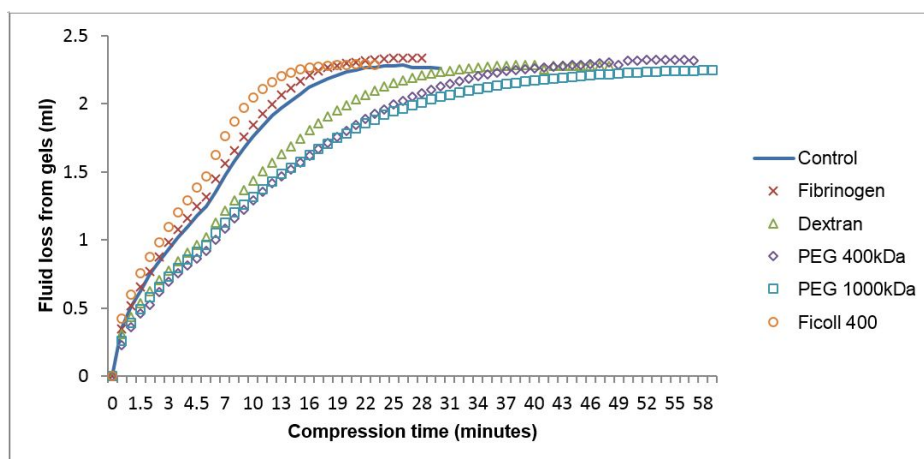
Figure 5.7: Compression profiles of hydrogels (2.5ml) containing 10mg.ml^{-1} polymers. Control gels with no macro-molecule additives are represented by the solid line. The extent of fluid loss from hydrogels during compression was measured as mass of fluid gained by the absorbent plungers (i.e. fluid loss from hydrogels) over time.

5.3.3   Gelation rates of hydrogels with macromolecules

Collagen hydrogels with no macromolecules showed first signs of fibrillogenesis after 2.5 minutes at room temperature. This was delayed until 3 minutes in samples containing PEG 400kDa. However, by 7 minutes into the gelation process for both samples, the absorbance reading (opacity of the gel) began to plateau suggesting fibrillogenesis was mostly complete (figure 5.8). In samples containing Ficoll™ 400, fibrillogenesis began sooner (from 1.5 minutes), and reached a higher absorbance reading compared to both plain and PEG containing gels by 5.5 minutes.

Whilst the incorporation of PEG 400kDa appeared to only affect the rate of hydrogel fibrillogenesis, Ficoll™ 400 may be altering the structure of the hydrogel, and led to a gel with a slightly higher opacity.
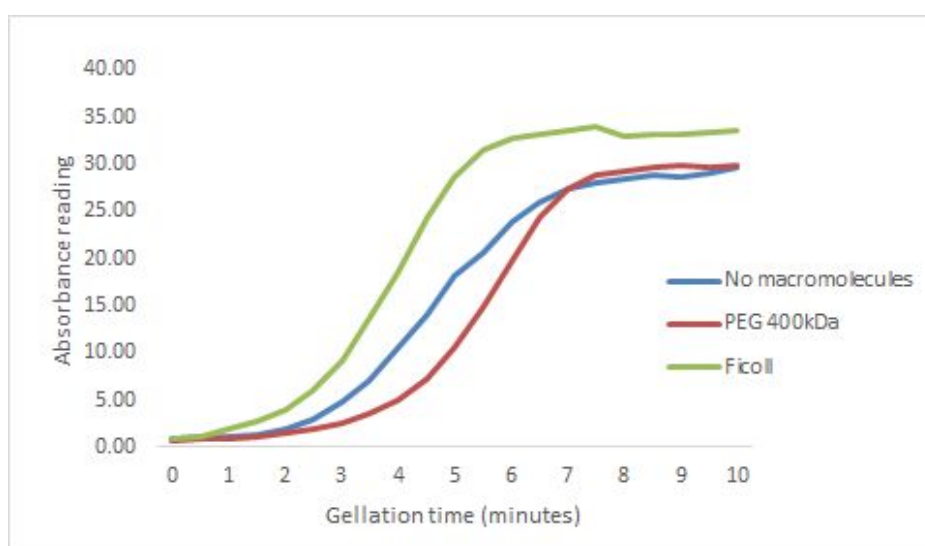
Figure 5.8: Absorbency of collagen solution over time during fibrillogenesis. Hydrogels either contained an overall concentration of 1mg.ml^{-1} PEG 400kDa or Ficoll™ 400; or contains no macromolecules.

5.3.4 Effect of additional fibrin at the FLS

The application of thrombin to the surface of the hydrogel (for the formation of a fibrin mesh) did not result in reduced compression rates. Instead, initial compression rates increased up to 0.943 ± 0.070 ml/minute compared to samples containing only fibrinogen (in its macromolecular form; 0.582 ± 0.119 ml/minute) (figure 5.9).
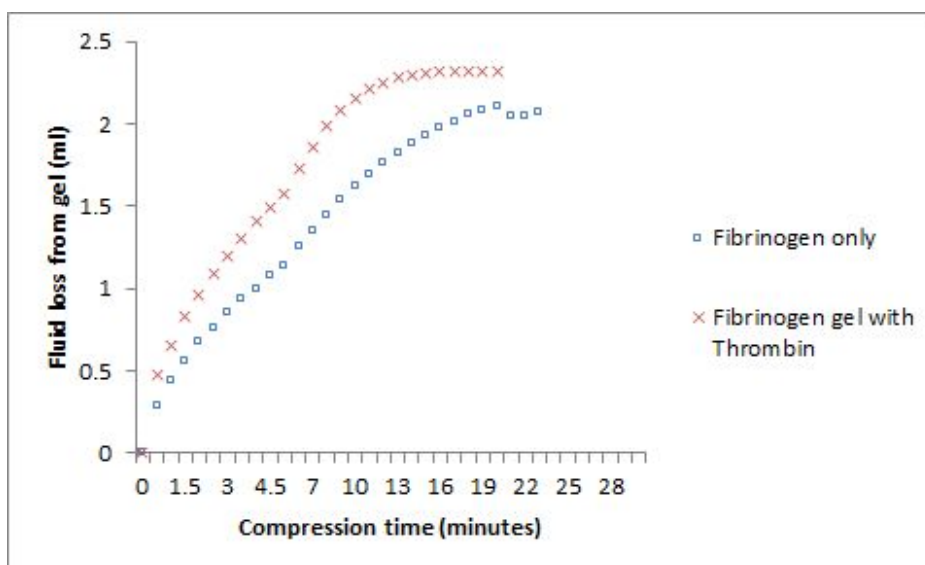
Figure 5.9: Compression rates of collagen gels containing 10% (v/v) 5mg.ml^{-1} fibrinogen, with or without added thrombin treatment on the gel surface. Where thrombin was use, 50μl of 1mg.ml^{-1} thrombin (in water) was added indirectly to the FLS via paper discs soaked in thrombin.

5.3.5 Proof of principle - protecting cells from damage within fast compressing hydrogels

10mg.ml^{-1} PEG (400kDa) (final concentration of 1mg.ml^{-1} within the hydrogel) resulted in optimal decrease in the initial compression rate, and was tested for its effectiveness in slowing compression rates within blended collagen gels (i.e. containing pre-polymerised collagen) containing interstitially seeded cells. Alamar blue readings of conventional (acid-soluble collagen) gels, with or without

PEG were similar at 25.35 ± 3.33 and 23.77 ± 1.20. Cell activity within blended (fast-compressing) gels was significantly reduced (as also seen previously in chapter 4 and in Wong et al. (2014)) in the absence of PEG (Alamar blue reading of 16.53 ± 1.98; p=0.017). However, interstitial cells were shielded from damage with the addition of PEG, resulting in a cell metabolic activity reading similar to conventional hydrogels after compression (figure 5.10). In effect, the addition of the PEG protected the resident cells from flow-related damage.
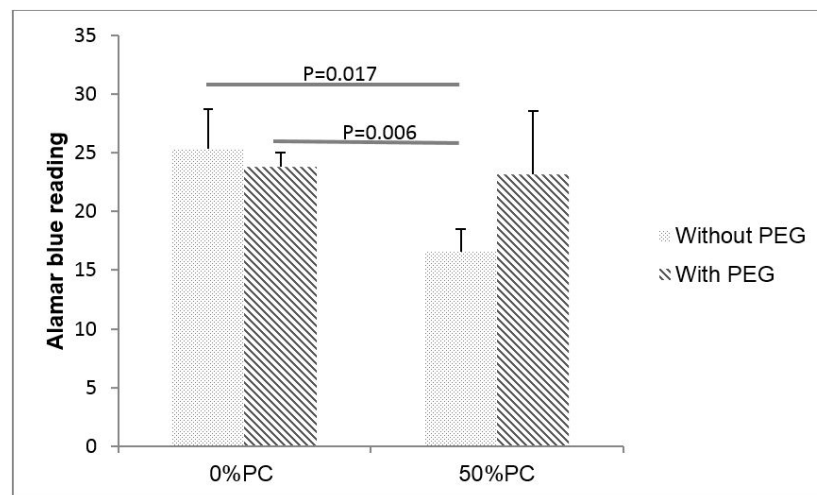
Figure 5.10: Total cell activity in polymeric collagen blend gels 1 day after compression. Cell activity within blend gels, with or without 10% PEG incorporation was compared to conventional (no macromolecules) monomeric collagen hydrogels.

5.4   Discussion

Results from chapter 4 showed improved material strength after the incorporation of polymeric collagen (and potentially any stiff fibres, as suggested previously (Deng et al., 2014)) into the hydrogel. However, initial cell viability was compromised within the compressed hydrogel by increased fluid shear stresses during hydrogel compression of the novel blend gel (Wong et al.,

2014). The aim of this study was therefore to reduce fluid shear stress on resident cells, and improve initial cell viability within the compressed hydrogel construct.

It was clear from the results of this study that some interventions were able to reduce fluid flow, such that fluid shear stresses remained within a physiological range. More specifically, **this study found that compression rates can be controlled through the utilization of the filtration effect at the FLS, to prevent loss of initial cell viability**.

Although simply increasing the density of collagen molecules within the hydrogel significantly reduced compression rates (i.e. by increasing the amount of mobile collagen species, and reducing pores size), it also resulted in a construct which was far more opaque compared to compressed hydrgels made from a collagen density of 2mg.ml^{-1} tropocollagen molecules; and potentially reduces the accessibility of *in vitro* assays to monitor cells within the hydrogel over time. Additionally, the increase in collagen density would also make it difficult to recover cells from the hydrogel, and prolonged digestion of the construct with a solution of 0.2% collagenase-I will be needed due to digest the collagen substrate. These problems associated within a high density gel may potentially hinder the use of a dense gel as an *in vitro* tissue model, and other methods for reducing fluid flow will need to be considered.

The two methods used to increase mobile macromolecular species capable of contributing to the clogging of the FLS within the hydrogel included the use of pepsin, or large macromolecules (which do no associate with the collagen matrix during fibrillogenesis. The former method involved the pepsin digestion of acid-soluble collagen solutions converted tropocollagen into mobile atelocollagen species, which could travel towards the FLS and contribute to the blockage.

It has been noted in the literature that loss of telopeptides from tropocolla-

gen (i.e. by pepsin action) impedes the rate of collagen self-assembly (Snowden and Swann, 1979), so an increasing amount of collagen molecules, in theory, remained as mobile monomers within the hydrogel at the time of compression. Since atelocollagen associates less readily with adjacent collagen molecules, the less extensive interfibrillar branching of the collagen oligomers (Whittington et al., 2013) may therefore explain the decreased efficiency in clogging the FLS; as the molecules are less likely to be trapped between interfibrillar spaces. As a result, even with the increase in mobile atelocollagen molecules, compression rates did not decrease as expected, but increased with pepsin treatment time (at least up to 24 hours; table 5.1). This increase in compression rates may be exacerbated by the reduction in gel-forming tropocollagen species (as it is converted into atelocollagen), leading to a looser fibril network.

Interestingly, the rate of initial compression did not increase linearly with pepsin treatment time. Instead, a slight fall in initial compression rates was observed with further pepsin treatment beyond 48 hours (figure 5.4). A study in 1970 by Leibovich and Weiss has shown that fibril morphology changes with pepsin digestion, where prolonged treatment resulted in increased symmetrical tactoidal fibrils/aggregates (Leibovich and Weiss, 1970) (Bard and Chapman, 1968). This suggests the time dependent change of pepsin treatment on hydrogel compression rates may also be due to fundamental change in collagen fibril assembly, instead of purely changing the amount of mobile collagen species within the hydrogel. However, since the use of pepsin treatment to produce interfibrillar space clogging species was not effective as a method to control fluid flow rates within the hydrogel, the use of other 'pore' clogging species was considered.

Artificially introduced pore-blocking macromolecules, such as PEG or dextran, were added to hydrogels to contribute to the ultrafiltration membrane at

the FLS.

In terms of the effectiveness of artificially introduced macromolecules in controlling initial compression rates, the size and concentration of the blocking agent influenced the extent of reduction in compression rates. More specifically, the polymer Stokes radius (hydrodynamic size), rather than its molecular weight, was generally found to correlate with the initial compression rates.

Small molecules, such as water and oxygen, are known to be able to diffuse freely through the thin compressed hydrogel layers (Cheema et al., 2008), whilst larger molecules (in the micrometre scale; including cells) can be caught, and entirely retained, by the collagen fibril network (Hadjipanayi et al., 2011a). Hence the size of the optimal FLS clogging species will likely be within this range (i.e. large macromolecules that can be trapped within the collagen matrix) - with some consideration on the balance between fluid flow rates and the time required by the hydrogel for complete compression.

From figure 5.4, it appears that the range in which the macromolecule affects compression rates was between $\sim 11-27$ nm. This was within the estimated size range of interfibrillar space from Serpooshan et al. (2011). In this study, polymers with stokes radius less than $\sim 11nm$ (fibrinogen) did not effectively contribute to the accumulation of molecules at the FLS, so only moderate effects on initial hydrogel compression rates was observed (rates were similar to samples with no added macromolecules). Increasing the macromolecule size between $\sim 11nm$ and $\sim 27nm$ appeared to linearly reduce initial compression rates of hydrogels. PEG 400kDa (Stokes radius 26.56nm) resulted in optimal rates, but further increases in polymer size beyond $\sim 27nm$ did not yield further reduction in compression rates, potentially because these species are generally less mobile and are trapped in the interfibrillar space of the matrix, far from the FLS (as demonstrated in larger molecules (Hadjipanayi et al., 2011a)).

Late stage compression rate results do suggest some influence of macromolecule size, on its mobility within the hydrogel during compression. For example, it was observed that the rate of fluid flow was higher at initial compression stages (first 30 seconds) for gels with PEG 1000 kDa (at 0.524 ± 0.028 ml/min instead of 0.456 ± 0.121 ml/min observed with 400 kDa PEG); despite its larger size. This would mean that more fluid was leaving through the FLS in the first 30 seconds of compression when 1000kDa PEG was present within the hydrogel. However, by 5 minutes into the compression process, samples with either PEG 400kDa and 1000kDa had almost identical compression rates (i.e. the blockage at the FLS have reached a similar level). This suggests that the PEG1000kDa may be beyond the size at which polymers were freely mobile through the collagen network (i.e. slower to move through the hydrogel), and so was less efficiently accumulated at the FLS. The effects of larger polymers was still observed further downstream of the compression process (i.e. at 5 minutes), suggesting a longer travel time for PEG 1000kDa to reach the FLS.

Note that the total compression of a sample containing PEG 1000kDa was longer (50 minutes instead of 43 minutes when PEG 400kDa was present); and suggests that overall, the larger macromolecules may eventually offer a more complete blockage of interfibrillar space at the FLS. However, the delay in the macromolecules traveling towards the FLS meant that fluid flow rates at the initial time point remained high, and so was not useful for the purposes of decreasing exposure of cells to high fluid flow rates.

Although the results did suggest an increased molecular size generally resulted in the decrease in initial compression rates, it was not possible to rule out whether the presence of macromolecules may affect the structure of the collagen matrix (i.e. by occupying space within the collagen solution) during fibillogenesis. The presence of PEG 400kDa appeared to only increase the

lag time prior to fibrillogenesis, but other macromolecules such as Ficoll™ 400 appear to change the hydrogel structure at a more fundamental level, as the gelation time and resultant opacity after filbrillogenesis differed in comparison to plain samples (without macromolecules).

Since the macromolecules were essentially providing physical blockage of the interfibillar space to fluid flow, the effectiveness of each macromolecule can be measured in terms of the hydraulic resistance of the FLS to fluid outflow (R_{FLS}; i.e. caused by the blockage of interfibrillar space at the FLS). (R_{FLS}) of samples, containing interfibrillar space clogging species, was mathematically modeled based on Darcy's law (Hadjipanayi et al., 2011a) (Tan, 2015). The calculations for R_{FLS} was carried out with the help of Dr. Noah Tan.

$$R_{\text{FLS}} = \frac{A.TMP}{\mu.Q}$$

The hydraulic resistance (R_{FLS}), measured as FLS surface area (A) and transmembrane pressure (TMP) over the dynamic viscosity (μ) of water at $20\,°c$ (1.001x$10^{-3}Pa$) and Q, rate of flow in millilitre per second. Here, the change in mass of the fluid absorbing plunger is assumed to be very close to the TMP, and so the increase in plunger mass is substituted for the TMP function.

a)
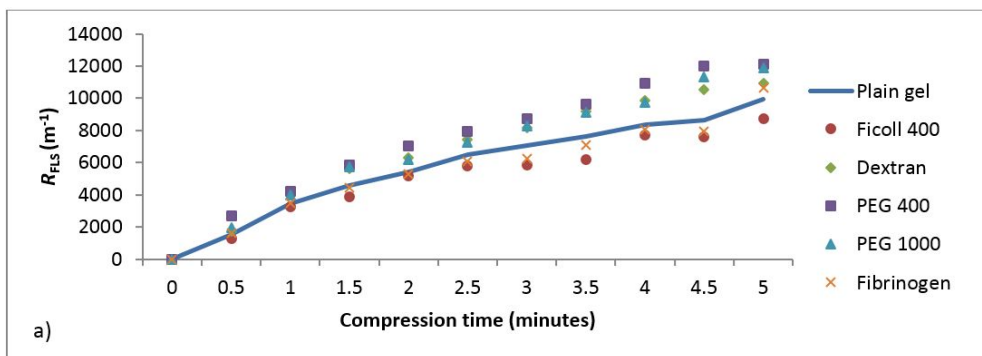
Figure 5.11: Average R_{FLS} during plastic compression of hydrogels containing artificially introduced macro-molecules over the first 5 minutes of compression.

Resistance to fluid outflow generally increased with hydrogel compression time, as more and more macromolecules (or other pore-clogging species) were caught at the ultrafiltration membrane (FLS). During initial stages of compression (first 30 seconds), R_{FLS} was highest in gels containing 10mg.ml^{-1} 400kDa PEG, although the difference did not reach significance compared to plain gels (p=0.090) (figure 5.11). However, when R_{FLS} was modeled in terms of rate of change, PEG 400 (P$\leq$0.001) and PEG 1000 (P=0.013) had significantly increased R_{FLS} gradients compared to plain hydrogels at 0 - 1 minute (figure 5.12). The high R_{FLS} for PEG 400kDa containing samples corresponded to a optimal decrease in initial compression rates.

Hydraulic resistance to fluid leaving the hydrogel continued to increase 4.5 - 7 fold between 30 seconds and 5 minutes of compression for all samples (p $\leq$ 0.001), with R_{FLS} at 5 minutes being highest in samples containing PEG 400kDa (p=0.002) and 1000kDa (p=0.009) compared to plain gels. Only hydrogels containing PEG 400 maintained an increased R_{FLS} rate of change compared to plain hydrogels between 2.5 - 4 minutes (P=0.026). The high initial rate of R_{FLS} was thought to be due to the low baseline for change in the FLS at the start of the compression process, where there was no increased density of collagen molecules at the beginning. It was only after the start of the compression process, and throughout the early stages of compression, that previously mobile macromolecules have traveled with the fluid flow, and collected at the FLS - causing an increase in resistance to fluid outflow.

The modelled rate of change in R_{FLS} within the first 4 minutes of compression for all samples suggest blockage at the FLS was built up at different rates, with the fastest being at the FLS of PEG400 and PEG1000 containing hydrogels in the first stages of hydrogel compression (figure 5.12). Importantly, this increase in resistance to fluid outflow corresponded to a decrease in compression rate as expected.
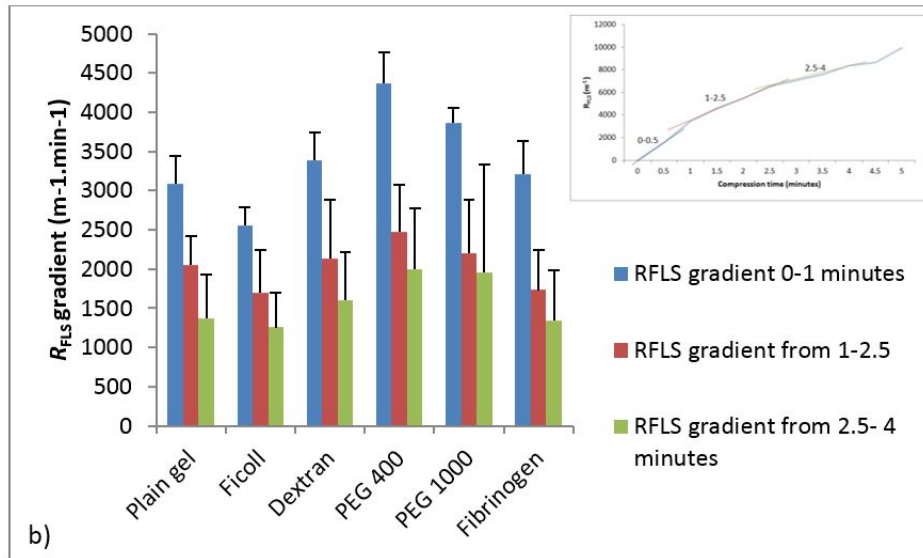
Figure 5.12: Comparisons of R_{FLS} rate of change at 0-0.5, 1-2.5 and 2.5-4 minutes in samples containing different macromolecules.
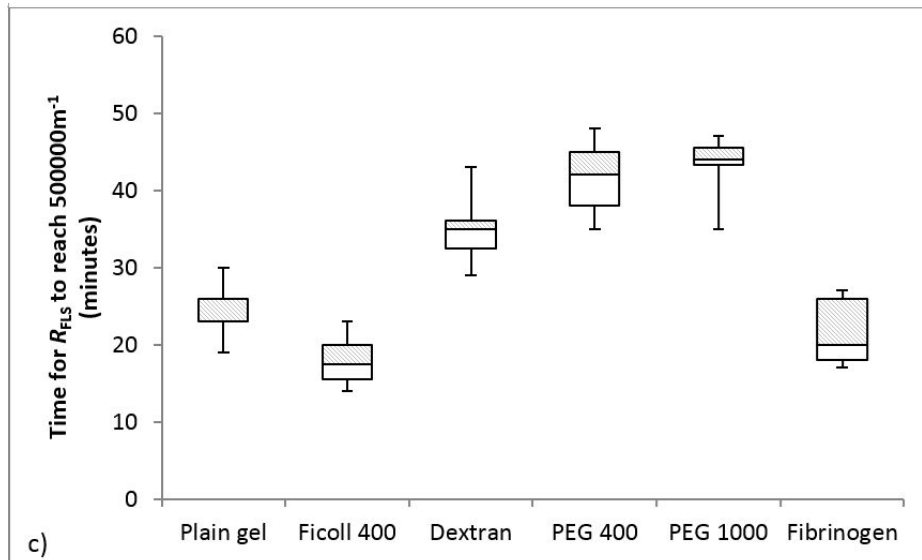
Figure 5.13: Box and whisker plot showing the time required for R_{FLS} to reach 500,000m^{-1} at later stages of compression, in the presence of different macromolecules. Samples were compared against R_{FLS} of hydrogels within no addition of macromolecules.
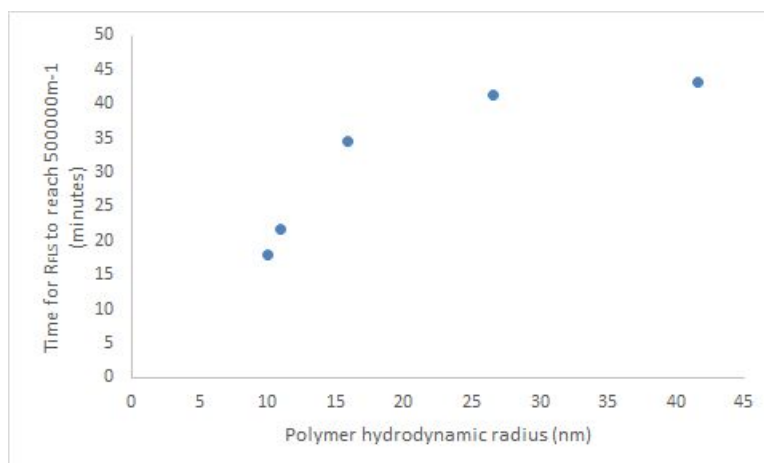
Figure 5.14: Time required for R_{FLS} to reach $500,000 m^{-1}$ in the presence of macromolecules with different hydrodynamic size. This high R_{FLS} reflects later stage compression of the hydrogel.

The time for resistance to fluid flow to reach 500,000m^{-1} (nominal R$_{FLS}$ value all samples reached towards the end of compression) was measured as an indication of the R$_{FLS}$ response at late stages of compression. Within a plain hydrogel, the time for R$_{FLS}$ to reach 500,000m^{-1} was 24.2$\pm$3.6 minutes. The presence of dextran, PEG 400 and PEG 1000 increased the time to 34.5$\pm$3.9, 41.3$\pm$4.7 and 43.2$\pm$4.3 minutes respectively; which meant that the time for the FLS to acquire the same level of blockage was longer in the presence of these macromolecules. This corresponded with the size of the macromolecules, suggesting the mobility of the molecules within the hydrogel affected the time it requires for R$_{FLS}$ build-up at the FLS (figure 5.14). Only hydrogels containing Ficoll™ 400 decreased the time it took for R$_{FLS}$ to reach the nominal end value to 18.0 $\pm$ 3.9 minutes (i.e. Ficoll containing gels were completely compressed much sooner; figure 5.13). This may be a result of ficoll effects on collagen fibrillogenesis described as molecular crowding agent (Dewavrin et al., 2014) (Lareu et al., 2007)

Overall, the incorporation of large polymers were therefore found to be effective in slowing compression rates of blended gels, apparently by replacing the mobile collagen molecules initially present within the standard, non-blended hydrogels. Artificially added polymers (i.e. PEG) replaced the absent monomer/oligomer collagen, and contributed to the blockage of the FLS. The resultant filtration through the clogged FLS slowed compression rates (to cell compatible levels) and shielded cells from damage during plastic compression (figure 5.10).

It was found that compressive load was the primary determinant of fluid efflux during initial stages of compression (Hadjipanayi et al., 2011a). However, with further compression, FLS collagen density was linearly correlated with R$_{FLS}$ where increases in hydraulic resistance resulted in decreased fluid efflux rates.

Anomalies within the trend for compression rates, against macromolecular size (hydrodynamic radius) was Ficoll™ 400. Due to its relatively small hydrodynamic radius ($\sim 10nm$), it was predicted to have little or no effect on compression rates. However, Ficoll™ 400 in fact caused an increase in compression rates, compared to (control) gels without macromolecules, when incorporated into hydrogels. This was surprising because if it simply did not contribute to the clogging effect at the FLS, the compression profile of the Ficoll™ containing gels should be similar to that of the plain collagen gel. The increase in compression rates was therefore thought to be caused by a change in the fibrillogenesis of the hydrogel (Dewavrin et al., 2014). Indeed, alteration of fibrillogenesis by the added polymers was a possible factor in many cases, especially where they are present at high levels.

This highlights the point that changes to the matrix will likely alter the requirements, in terms of blocking agent size, for efficient FLS blockage (i.e. as seen by the contradictory behaviour of Ficoll™ as a blocking agent, and the highest levels of added polymers (20mg.ml⁻¹)). Therefore there will be a need to consider, and control, factors which alters fibril diameter; and consequently interfibrillar spacing. Other factors discussed in chapter 1.4.3, including temperature, ionic strength and pH during fibrillogenesis, are some of the factors known to affect collagen matrix structure, and will need to be controlled for constant matrix structures.

Since the aim of the study was to improve initial cell viability within fast compressing hydrogels (i.e. to protect cells from damaging fluid shear stress), PEG 400kDa was introduced into cellular fast-compressing hydrogel (blend gel) for optimal reduction in initial compression rates. It was found that in the absence of PEG 400kDa, a significant amount of cell death was observed immediately following compression (reflected in the reduced total cell metabolic activity detected from the samples). However, when PEG 400kDa was added

to the blend hydrogel, cell viability remained close to 100%, similar to that of the conventional hydrogels as observed through the level of total cell metabolic activity detected from the gels after plastic compression.

This was the most important finding from this study, where it was found that **it was possible to reverse the effects of high initial compression rates/fluid flow rates (as seen in polymeric collagen blend gels) by incorporating FLS clogging large macromolecules; and such interventions was sufficient to protect interstitial cells from damage by reducing fluid shear stress**. This enabled the fabrication of tissue models, with increased stiffness (provided by the pre-crosslinked polymeric collagen) and interstitial cells (which will remain viable through the compression process).

This finding is significant in that it may also be applicable to other materials based on a fibrous matrix as the sensitivity to cell damage under rapid fluid flow is likely to be common to many protein materials with interstitial cell seeding.

Chapter 6

Results: Model of cell response to drug delivery in nanoparticle cargo

6.1   Introduction

Targeted delivery of drugs are increasingly studied to improve efficacy (i.e. lower drug dose and improve tissue response) of drug treatment, and reduce systemic effects on non-target tissues/organs.

Nanoparticle drug carriers (and other carrier materials i.e. liposomes, polymeric micelles) can offer advantages such as:

- Targeted delivery (i.e. by selective attachment to cells, or by an enhanced permeability and retention (EPR) effect)

- Time-controlled delivery

- Drug dosage control

- Minimise required dose for effect (reduce undesirable side-effects)

Nanoparticles used in cancer treatment, for example, are gaining popularity due to the 'enhanced permeability and retention effect (EPR)' in highly vascu-

larised tissues (i.e. tumors), which enhances nanoparticle-drug specificity to cancerous tissues. Drug carrier can also often be produced with time-release properties for a regulated and constant delivery of drugs to the tissue over time (see (Vllasaliu and Singh, 2014) for a review of the characteristics of nanoparticles used in drug delivery systems).

Here, compressed collagen hydrogel is used as a 3D *in vitro* model to study the effects of drug delivery (as a nanoparticle cargo) on cells; more specifically, the stimulation of growth factor production. This model will test hyaluronic acid nanoparticles (HA-NP) as a biomaterial carrier for the delivery of drugs.

The objective is to study the delivery of the nanoparticle cargo into the model tissue, and later to study cell response (i.e. growth factor production) to drug (i.e. simvastatin) delivered to the tissue in hyaluronan nanoparticles (HA-NP). The study will include information on the retention of the nanoparticle in the model tissue, the effect of the NP biomaterial, and drug-cargo on local cells. Subsequently the amount of BMP2 produced in the presence of Simvastatin was measured using ELISA assays to quantify BMP2 protein in the cell matrix and culture media.

6.1.1 Hyaluronan-nanoparticles (HA-NP) for drug delivery

Hyaluronic acid (HA; or hyaluronan) is a linear, high molecular weight polysaccharide made of repeating units of N-acetyl-D-glucosamine and D-glucuronic acid. This glucosaminoglycan is a major component of the ECM, and is important in cell adhesion to the ECM amongst other cell functions. Cell receptors such as CD44 recognises and interacts with HA (Kim et al., 2008); which is incidentally over-expressed in some cancer cells, making HA an attractive material for targeted drug-delivery.

Cross-linked HA has been shown to be good carrier of drugs and proteins

(such as growth factors) in different tissue models (i.e. bone (Bae et al., 2011), cartilage (Ramesh et al., 2014)). Cross-linking of HA is often necessary to reduce its rate of dissociation/degradation and resorption because their natural turn-over rate can be very short (hours to days; depending on the tissue type).

Here, a fluorescent hyaluronan-nanoparticle (HA-NP) drug carrier material is tested for drug-delivery efficacy, and cell response (triggered by these drugs) within plastically compressed collagen hydrogels (i.e. the tissue model). These HA-NP carriers are developed and supplied by a group in Uppsala university; with the HA-NP particles without the drug cargo (i.e. empty HA-NP particles; average of 485.3nm diameter) supplied by D. Ossipov; and HA-NP containing 9% (w/w) simvastatin cargo supplied by O. Varghese (average 680nm diameter).

The HA-NP material is formed by functionalising the HA molecule with thiol and hydrazide groups. Cross-linking between the hydrazide functional group, and an aldehyde group in an adjacent HA molecule, led to the formation of a hydrozone network/hydrogel (Varghese et al., 2009). This hydrogel (with a 2% solid content) can be formed within 30 seconds. A hydrophobic cargo (which is necessary for later stages of nanoparticle assembly), such as the fluorescent marker (fluorescein isothiocyanate; FITC) or pyrene (an aromatic hydrocarbon), is cross-linked to the hydrogel via thiol groups (Ossipov et al., 2010) (Yang et al., 2011). For the material to form nanoparticles, the hydrogel must be enzymatically digested into smaller units by hyaluronidase. Nanoparticles then form by hydrophobic interaction, with the cargo now on the interior of the nanoparticle surrounded by a HA shell (which can be cross-linked to improve stability). Previous reports have shown that aromatic durgs (i.e. doxirubicin) can be incorporated into the HA-NP by electrostatic or hydrophobic association/aromatic stacking of the nanoparticle pyrene cores (process depending on the electrostatic charge on the drug) (Yang et al., 2011). The resultant HA-

NP is then sized by dynamic light scattering (DLS) or SEM imaging, and are lyophilised for storage.

6.1.2   Simvastatin HA-NP and BMP2 production

Simvastatin is a drug (prodrug) currently used to lower blood concentrations of low-density lipoproteins (bad cholesterol) and triglycerides. When hydrolysed into its active form (β-hydroxuacid/simvastatin acid) (Aarthy et al., 2014), it functions by inhibiting the enzyme 3-hydroxy-3-methylglutaryl Coenzyme A (HMG-CoA) reductase (Garrett and Mundy, 2002).

Interestingly though, the drug also appeared to increase bone mineral density and turnover (among other side-effects such as muscle myopathy) in patients (Montagnani et al., 2003) (Maritz et al., 2001), through the production of BMP-2 (Mundy et al., 1999) (Garrett and Mundy, 2002).

The growth factor, Bone morphogenic protein (BMP)-2, is known to be osteoinductive and enhances bone formation and repair. Prolonged exposure to BMP-2 led to bone-like structure formation with associated increase in osteoblast differentiation and improved mineralisation of constructs (Kisiel et al., 2013). However, in systems where BMP-2 are not natrually produced (or are in insufficient quantities), the growth factor must be administered frequently for optimal bone-like formations. This mode of administration (i.e. directly via the culture media (*in vitro*), or systemically (*in vivo*)) is less efficient, meaning excess growth factors are needed for therapeutic concentrations of BMP-2 within the scaffold. Potential issues for the above method are:

- Cost

- High dosage

- Potentially uneven exposure of *in vitro* scaffolds to BMP-2 if construct not

permeable

- Scaffolds potentially exposed to cyclical BMP-2 concentrations over time (peak at each administration, with BMP-2 subsequently used up/degraded before next dose)

New methods of nanoparticle (NP) preparation (mentioned in section 6.1.1 above; Uppsala University) means that aromatic drugs, such as Simvastatin, can be loaded within nanoparticles made from the natural protein - hyaluronic acid. These HA-NP can then be incorporated into the bone-like scaffold for slow and sustained release of drugs; in effect, used as an indirect method of BMP-2 delivery within the scaffold (i.e. BMP-2 produced when simvastatin is gradually released as the HA-NP degrades).

Local administration of the drug (in NP format) potentially lowers the dose required to generate significant osteogenic properties. Additionally, the sustained levels of BMP-2 contact with bone-scaffolds may be more representative of the *in vivo* environmental BMP-2. This may provide a better model for testing the efficiency of bone scaffold materials as an *in vitro* model. The osteogenic cells can then mineralise the scaffold to generate a bone-like structure. It is postulated that extended and sustained BMP-2 contact with cells will improve speed, and extent of mineralisation (and eventually calcification), of bone-scaffolds compared to manually administering BMP-2 growth factors. However, this is outside the scope of this study, as the NP are tested as a potential delivery method for drugs. The aim here is to monitor cell activity via the level of growth factor produced within these model tissues.

It is hypothesised that HA-NP will be retained by the tissue model during plastic compression (based on previous work by Tan (2015); which found a 19% retention of HA-NP after plastic compression), which can be improved by alterations of the compression process/hydrogel; also that the HA-NP-S

(with simvastatin cargo) will lead to BMP-2 production by resident bone-derived cells. Importantly, it is hypothesised that the 'single-dose' of HA-NP-S will gradually and sustainably release simvastatin within the scaffold, which will stimulate a steady level of BMP-2 production over time.

6.2 Methods

Methods listed below are specific to this study. Further methods common to studies throughout the thesis are listed in Chapter 2.

6.2.1   HA-NP preparation for use

Two different hyaluronan-nanoparticle (*HA-NP*) formulations were used. For initial studies, lyophilised HA-NP (485.3nm diameter) was prepared and provided by D.Ossipov from Uppsala University. Subsequent functional studies of NP within compressed collagen hydrogels was carried out using HA-NP containing a 'cargo' of simvastatin drug (*HA-NP-S*) (9% (w/w) of material mass; 680nm diameter), which was provided by O.Podiyan of Uppsala University. All NP were conjugated with fluorescein isothiocyante (FITC), which enabled detection through their fluorescence.

Lyophilised HA-NP material were stored at 4 °c in the dark (within a dissicator). Prior to use, HA-NP were re-suspended in sterile filtered deionised water, to give a concentration of 1mg.ml^{-1}. A rolling machine (at 37°c; dry incubator) was used to disperse NP evenly in solution (for 30 minutes). Immediately prior to use, the NP solution was mixed gently by inverting the container.

6.2.2 Cells

Human osteosarcoma cell-line (MG63 cells) were cultured in 1000mg glucose Dulbecco's modified Eagle's medium (DMEM; Sigma, UK), supplemented with 10% (v/v) fetal calf serum (FCS; First Link, UK) and 1% penicillin streptomycin (Gibco Life Technologies, UK).

To transfer cells into collagen hydrogels (for the creation of cellular tissue models), detached cells were counted and suspended in a known amount of supplemented DMEM, and incorporated into neutralised (HA-NP containing) collagen solution as described below.

6.2.3 Collagen constructs containing HA-NP

Methods for incorporating HA-NP into collagen hydrogels was based on that described by Tan (2015).

Acellular collagen hydrogels were produced by neutralising 80% (v/v) acid soluble collagen (2mg.ml^{-1}) and 10% 10xMEM using 5M and 1M NaOH. 10% (v/v) 1mg.ml^{-1} HA-NP particles in sterile deionised water were added to the neutralised collagen solution. The final concentration of HA-NP within the collagen solution was 0.1mg.ml^{-1}.

1ml samples of the HA-NP-collagen solution were set in 24-well plates by incubation in 37 °c, 5% CO_2 for 30 minutes.

Cellular gels were produced similarly with a further 10% of the acid-soluble collagen being substituted for cells (500,000 cells.ml^{-1} of hydrogel) suspended in DMEM.

The resultant hydrogels were plastically compressed within their wells using upward flow compression described in section 2.4.

6.2.4   Detection of HA-NP from gels

Readings of fluorescence intensity have previously been found to reliably quantify concentrations of HA-NP (Tan, 2015, p.80).

Collagen samples were digested with 0.2% collagenase-I (Gibco, USA) at 37 °c for 20-40 minutes to release fluorescent HA-NP nanoparticles from the collagen matrix. Samples were either measured for fluorescence (fitc conjugated to the HA-NP nanoparticles) on a fluorescence spectrometer (Perkin-Elmer LS50B; 3ml samples in a cuvette) at an excitation and emission wavelength of 495nm and 520nm respectively; or when specified, on a microplate reader (Infinite M200Pro; Tecan) at excitation and emission wavelengths of 485nm and 535nm.

6.2.5   Improving HA-NP retention within compressed hydrogel constructs

Nanoparticle retention in the 'porous' hydrogels during plastic compression had been previously found to be at 19% (Tan, 2015). This was thought to be due to their small size relative to interfibrillar pores, allowing outflow of nanoparticles from the hydrogel.

In order to improve retention of HA-NP nanoparticles, and hence efficiency of nanoparticle delivery into the tissue model, changes to the collagen matrix, nanoparticle solution (non-chemical changes) or the plastic compression process were studied for their effectiveness in improving NP retention. Details of the test variables are listed below.

Changes to the collagen hydrogel

- **Gelling temperature** of 4℃ (instead of 37℃) was likely to result in a collagen matrix made of thicker fibrils (Christiansen et al., 2000). It was hypothesised that the matrix formed at 4℃ will decrease the extent of nanoparticle outflow by providing an improved filter for small particles (i.e. HA-NP) during plastic compression.

  For this study, HA-NP containing hydrogels were produced as described in the methods section above, except hydrogels were incubated for 24 hours in 4℃.

- **Incubation environment** can potentially affect fibrillogenesis and matrix architecture due to pH changes (although buffers are found in the MEM solution). Hydrogels were routinely incubated in 5% CO_2 during fibrillogenesis. CO_2 solubilisation can lead to a slight reduction in pH as it dissociates in solution into H^+ and HCO_3^-. To test if this change in pH within the hydrogel will affect hydrogel matrix structure (and hence HA-NP retention), samples were incubated at atmosphereic CO_2 levels at 37℃.

- **Density** of the collagen solution used in standard hydrogels was originally 2mg.ml^{-1}. 6mg.ml^{-1} (type-I atelocollagen; Collagen Solutions) was used in this test to increase collagen density, and reduce interfibrillar space between fibrils. It was hypothesised that the increased collagen matrix density will produce a greater filtration effect at the FLS during plastic compression, and lead to a greater proportion of HA-NP retention within the compressed gel.

- **Presence of macromolecules** was found in chapter 5 to control plastic compression rates of hydrogels by increasing the filtration effect at the

FLS. 400kDa poly(ethylene) glycol (PEG) dispersed in water was added (10% of the total hydrogel volume; final concentration of PEG at 1mg.ml^{-1}) to a neutralised solution of type-I collagen (70% (v/v)), 10% (v/v) 10xMEM and 10% (v/v) HA-NP solution. For direct comparisons, control hydrogels were produced by substituting the PEG solution with deionised water.

Changes to the compression process

- **Plunger material** with different densities and fluid absorption rates was tested to see if this affected nanoparticle retention. Plant fibre plungers (TAP Biosystems, UK) were cut to 4 cm cylinders, and used in place of the paper plungers from the standard compression protocol (made of Whatman grade-I chromatography paper).

- **0.22μm filter discs** (Millipore, UK) were used in place of Whatman paper to separate the hydrogel and the plunger. Paper discs in the compression setup was in direct contact with the hydrogel during compression, so the addition of a fine filter layer between the hydrogel and the plunger was thought to potentially contribute to the filtration effect (on top of the effect observed at the FLS).

Changes to the HA-NP solution

- **Nanoparticle size** of HA-NP-S (with simvastatin cargo) was compacted during treatment in a basic solution. Briefly, lyophylised HA-NP-S was suspended in a solution of PBS (1mg.ml^{-1}) already brought to pH12 by addition of NaOH. After 30 minutes on a rolling machine, 0.2M HCl was used to neutralised the solution. The 30 minute treatment in a pH12 buffer altered the nanoparticle diameter, and compacted the nanoparticle to ~200-250 nm. Samples containing the larger non-pH12 treated

HA-NP-S (680nm diameter) were used as direct comparisons. Retention of the nanoparticles was thought to be affected by the nanoparticle diameter, and larger nanoparticles was hypothesised to have improved nanoparticle retention within the compressed gel.

6.2.6 Cellular HA-NP-S drug cargo containing constructs

Constructs containing HA-NP-S nanoparticles, with simvastatin drug cargo, were produced as described for cellular hydrogels above. Each 1ml construct contained 500,000 MG63 cells (passage 9-14). Construct were cultured in 1ml supplimented DMEM at 37 ℃ and 5% CO_2 for up to 14 days. The culture media were collected (snap frozen in liquid nitrogen and stored at -80℃) and replaced every 2 days. For studies of BMP2 trapping within the tissue-like constructs, collagen gel samples were snap frozen separately from the culture media samples and were stored at -80℃. Prior to the ELISA assay, the compressed collagen samples were homogenised and suspended in 1ml PBS.

6.2.7 ELISA assays for BMP2

A sandwich ELISA assay (Quantikine BMP2 assay; R&D Systems) was used to detect and quantify the levels of BMP2 proteins trapped within the collagen construct, or released into the surrounding culture media over time. The assay was carried out as per the manufacturer's instructions. All additional materials required for the ELISA assay were obtained from the DuoSet ELISA ancillary reagent kit (R&D Systems). All steps were carried out at room temperature with a washing step between each reagent (3 washes with a wash buffer made of 0.05 % Tween®20 diluted in water).

Briefly, 96-well plates were prepared by coating the wells with $100\mu l$ BMP2 capture antibody (1μg/ml; in PBS) overnight. All wells were then emptied and

washed before 300μl of 1% bovine serum albumin (BSA) was added to each well as a blocking reagent.

Samples (culture media or homogenised collagen construct in PBS; 100 μl per well) were added to the wells for 2 hours. The wells were washed before 100μl BMP2 detection antibody (1μg/ml in 1% BSA) was added to each wells for incubation (2 hours).

In the dark, working concentrations of streptavidin-HRP (100μl; diluted in 1% BSA) was added to each washed well for 20 minutes. Wells were then washed and treated with equal volumes of hydrogen peroxide and tetramethyl-bezidine (total volume of 100μl per well) for 20 minutes to develop colour (which can be detected on a plate reader) in reaction to the horse radish peroxidase (HRP) molecule from the previous step. Finally, without emptying and washing the wells, an additional 50μl of stop solution (sulphuric acid) was added to stop further colour development.

Plates were immediately measured on a microplate reader (Infinite M200Pro, Tecan) at a wavelength of 450nm (with wavelength correction at 540nm).

BMP-2 standard curves were produced using serial dilutions of the BMP-2 protein from initial concentrations of 3000pg/ml (in 1% BSA). The BMP-2 solutions (at 3000, 1500, 750, 375, 188, 93.8, 46.9 and 0 pg/ml) were plated in the extreme right and left columns on each plate together with the samples. Each well is subsequently processed and measured as described above. The readings were plotted against BMP-2 concentration in order to obtain a standard curve for each plate.

6.2.8 Statistics

One-way ANOVA was used to compare data on HA-NP retention using different interventions. For all other experiments, an independent sample t-test was

used to test for statistical significance. Confidence intervals were set at $p \leq$ 0.05.

6.3 Results

Preparation of HA-NP and HA-NP-S involved dissolving lyophilised pellets of the nanoparticles in deionised water to form a bright yellow solution of known concentrations (i.e. 1mg.ml^{-1}). Hydrogels were produced as described section 6.2 above. The resultant hydrogels were visibly yellow-orange in colour (instead of fuchsia pink), which gelled within 30 minutes when incubated at 37°c.

6.3.1 Retention of HA-NP within constructs after plastic compression

The first step in producing the tissue model with nanoparticles is to establish the presence and retention of HA-NP nanoparticles within the hydrogels during plastic compression.

As an example, in one set of experiment quantifying the retention of HA-NP after compression, the uncompressed hydrogel was found to have an average fluorescence intensity of 154.64 $\pm$ 26.54 arbitrary units (a.u.) in solution after the hydrogel was digested in collagenase. As seen in figure 6.1, this dropped to 17.70 $\pm$ 1.01 a.u. after plastic compression (p= 0.001).

The average percentage of HA-NP retention within the hydrogel after the plastic compression process was therefore:

$$\% \text{ HA-NP retained within gel} = \frac{\text{fluorescence within compressed gel}}{\text{fluorescence within uncompressed gel}} \text{ x } 100$$

$$= \frac{17.70}{154.64} \text{ x } 100$$

$$\textbf{= 11.4 \%}$$

Repeats of this experiment set showed that HA-NP retention ranged between 10.1 $\pm$ 1.7 and 16.6 $\pm$ 1.2 % after plastic compression. The overall average percentage retention of HA-NP nanoparticles was *13.5 $\pm$ 1.5%*, which was used as the baseline retention of HA-NP to asses the effectiveness of interventions used to increase nanoparticle retention within the hydrogel (unless otherwise stated).
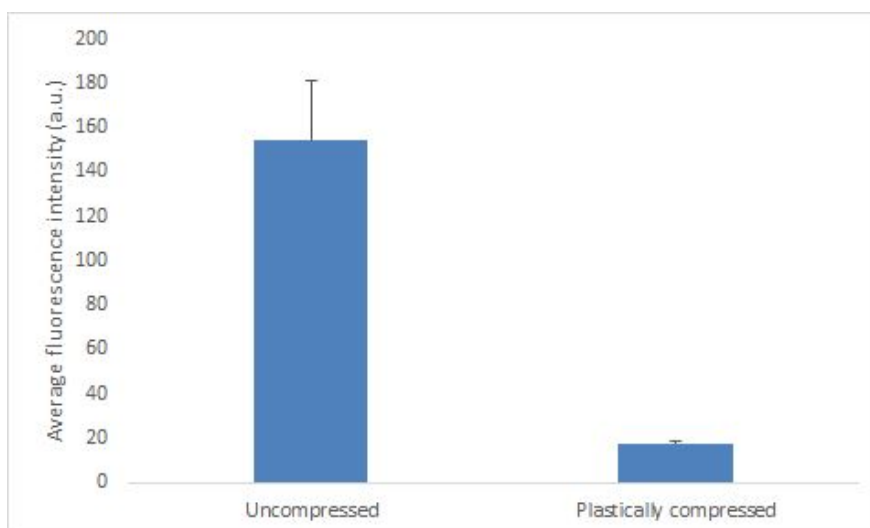
Figure 6.1: Average fluorescence intensity of fitc conjugated HA-NP within hydrogels, before and after plastic compression. Prior to fluorescence measurement, all hydrogels were digested in 1ml type-I collagenase. Volume of digested compressed gels were adjusted prior to measurements to account for the water lost during compression.

6.3.2   Attempts to improve HA-NP retention within compressed gels

Plastic compression was a key process in producing collagen constructs with physiological ECM density. However, the high rate of HA-NP loss from the hydrogel during compression was not desirable, especially when materials difficult to synthesise or isolate were used. To improve HA-NP retention within the compressed collagen hydrogel, various adaptations of the methods regarding the compression process, the hydrogel composition (structural and chemical) and the HA-NP solution were tested.

Changes to compression setting

Changes to the plunger material did not result in any changes to HA-NP retention within the compressed hydrogel (p= 0.549). However the replacement of paper discs with 0.22μm filter discs between the hydrogel and plunger appeared to have a small, but significant (p= 0.027) effect on HA-NP retention during plastic compression; which increased from 13.5 ± 1.5 % to 20.1 ± 2.8 % (figure 6.2).
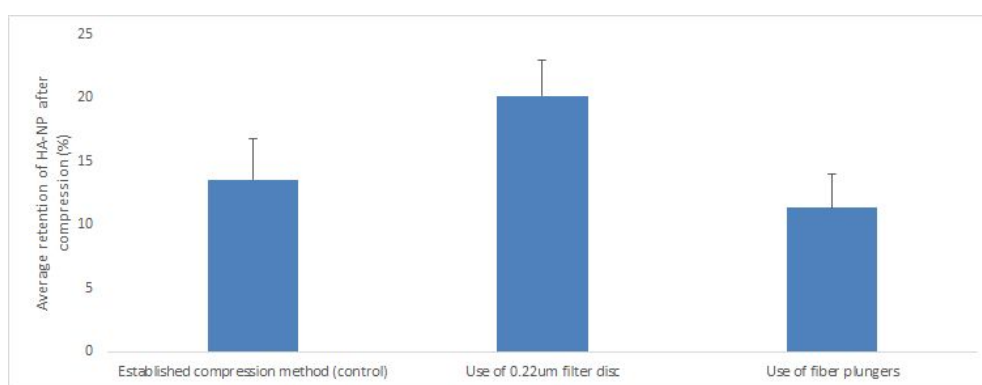
Figure 6.2: Average percentage retention of HA-NP after plastic compression of hydrogels with changes to the compression process. The use of fibre plungers did not affect the amount of HA-NP trapped within the gel. But placing 0.22μm filter discs between the hydrogel and plunger successfully increased HA-NP retention by about 7% (p=0.027).

Changes to hydrogel

Changes in gelling conditions such as temperature and environmental CO_2 concentrations did not result in a significant increase in HA-NP retention (p= 0.269 and p= 0.211 respectively; figure 6.3). However, a 2.5-fold increased HA-NP retention (from 13.5 ± 1.5 % to 33.5 ± 12.7 %) was observed when the density of the starting collagen material was increased from 2mg to 6mg (p $\leq$ 0.001).
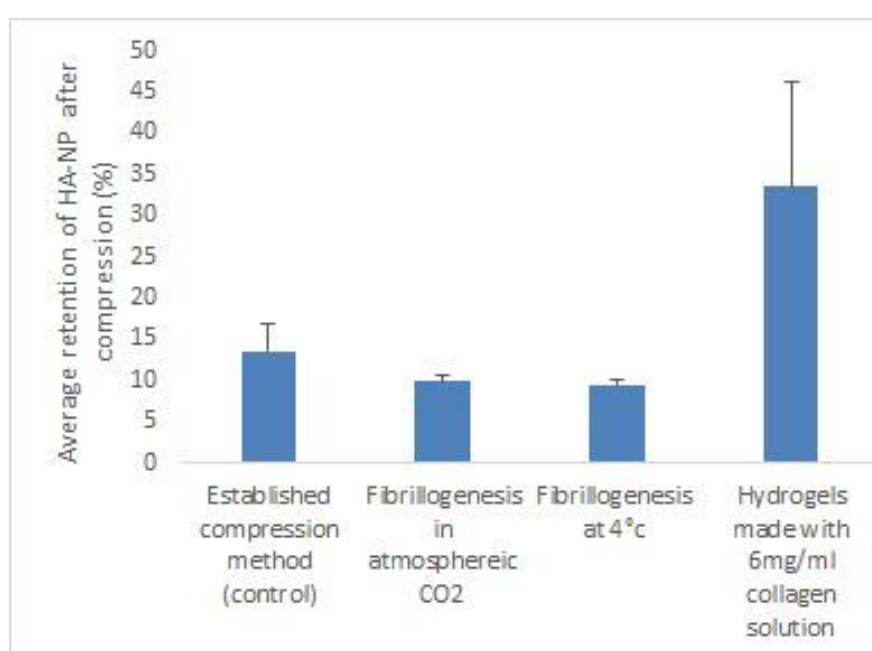
Figure 6.3: Average percentage retention of HA-NP after plastic compression with variables in the collagen hydrogel or fibrillogenesis conditions. Hydrogels set in atmospheric CO_2 and 4 °c did not improve HA-NP retention. However, increased collagen density improved HA-NP retention (p≤0.001).
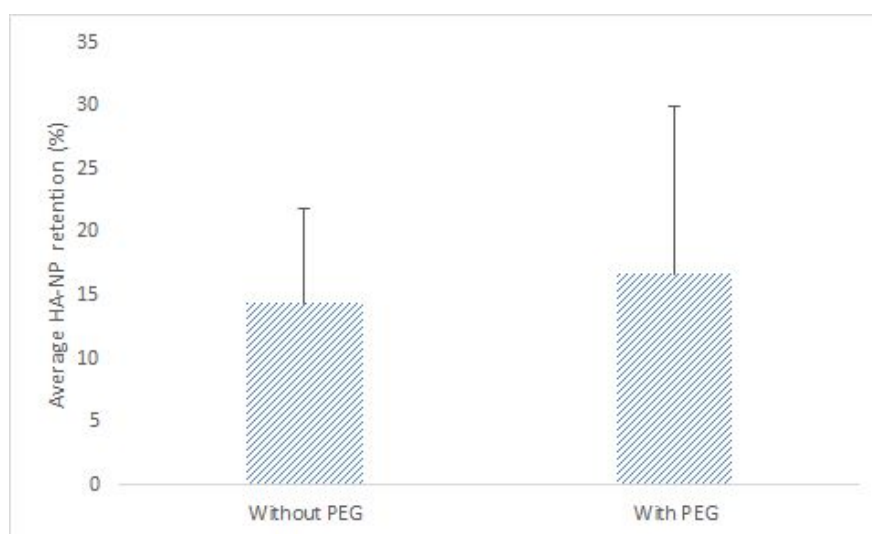
Figure 6.4: Average percentage retention of HA-NP within the compressed hydrogel, with or without PEG 400kDa incorporation. No significant differences were observed between either sample group (p=0.448).

Contrary to expectation, the incorporation of PEG 400kDa did not significantly increase nanoparticle retention within hydrogels during plastic compression (p=0.448). The variability within the sample group was high, with HA-NP retention averaging 14.4 ± 7.6 % in samples without PEG,and 16.7 ± 13.3 % in samples with PEG incorporation (figure 6.4).

Changes to HA-NP solution

HA-NP size also had an effect on the retention within the compressed gel. HA-NP-S (with simvastatin cargo; 680nm diameter) had improved retention rates (41.6%) compared to 'empty' HA-NP particles (p$\leq$ 0.001). The trapping rates of HA-NP-S were also significantly higher, compared to their smaller, pH12 treated HA-NP-S counterparts at 35.4% (200-250nm diameter; p=0.005; figure 6.5).
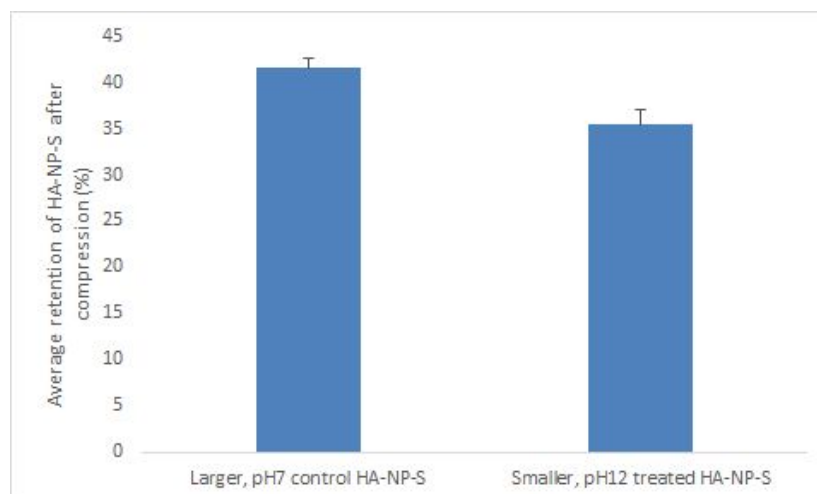
Figure 6.5: Average percentage retention of HA-NP-S, dissolved in pH7 or pH12 solutions, after plastic compression. pH12 treatment for 30 minutes led to alterations in the nanoparticle diameter and reduced retention of the compacted HA-NP-S within the hydrogel.

6.3.3 BMP2 production within tissue model

Measurements from the ELISA assay was converted into BMP2 protein concentration using a standard curve with a line of best fit across, where recombinant BMP2 of known concentration were plotted against spectrometer readings (separate for each plate) (for an example see figure 6.6a).
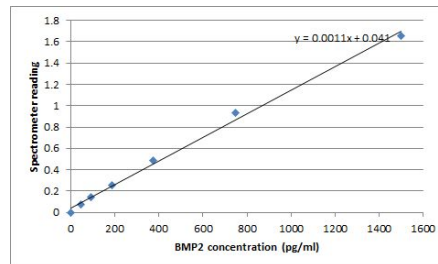
(a) BMP2 standard graph against spectrometer readings
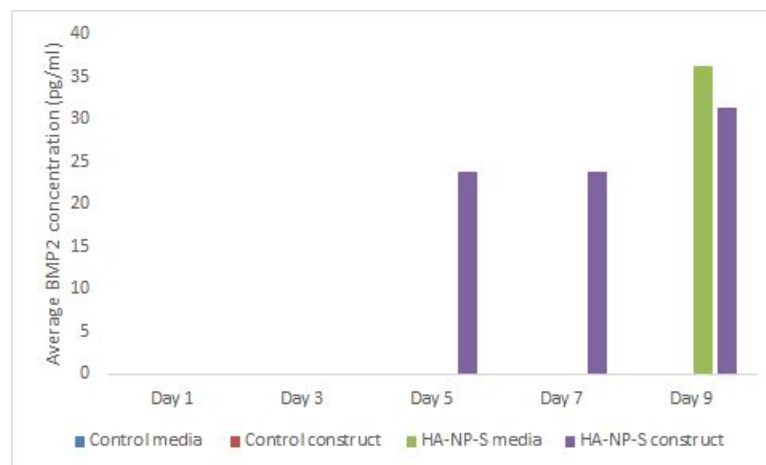
(b) Samples tested for BMP2 protein using the ELISA assay

Figure 6.6: Samples with or without HA-NP-S biomaterial were tested for BMP2 protein levels within the collagen tissue model construct, and the surrounding culture media using an ELISA assay. a) an example of the standard graph of BMP2 concentration against readings on the plate reader, b) amount of BMP2 detected from samples over 9 days in culture.

Initial studies have found that no BMP2 was detected in either the media or constructs of control samples only containing MG63 cells (figure 6.6b). Importantly, a steady amount of BMP2 was detected from within the HA-NP-S containing constructs, and culture media from days 5 and 9 respectively. Since simvastatin and BMP2 were known to have a very short half-lives (2 hours; (Aarthy et al., 2014)), the presence of the protein suggests the BMP2 was produced as the simvastatin was being slowly being released by the HA-NP.

However further repeats of the experiment did not yield consistent results, with some BMP2 protein detected from samples containing HA-NP-S, or control samples with MG63 cells only (figure 6.7).
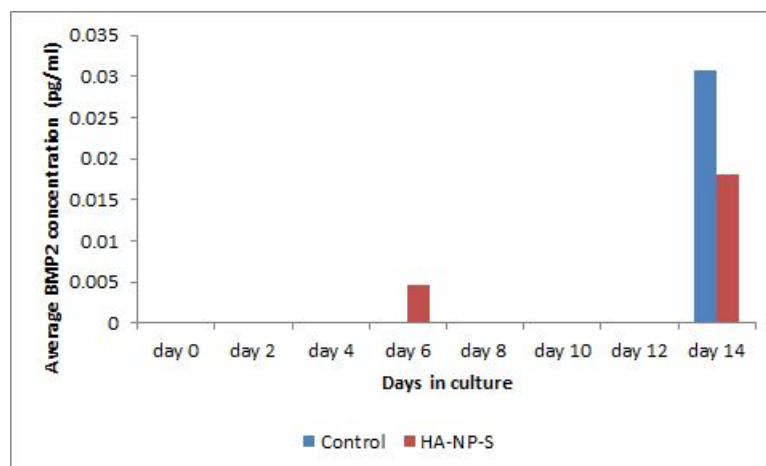
Figure 6.7: ELISA assay results for the BMP2 protein over 14 days in culture. This set of experiment was a repeat of that seen in figure 6.6. Results were however, not reproducible, with an extremely low amount of BMP2 protein detected from the culture media of both control and HA-NP-S containing samples.

6.4 Discussion

The efficiency of HA-NP entrapment within the hydrogel after plastic compression varied between 10.1 and 16.6%, with on average 13.5 ± 1.5 % HA-NP remaining within the collagen construct after plastic compression. This was a few percentage less than the average observed by Tan (2015) (19% HA-NP retention).

Attempts to improve the low retention rates of HA-NP in this study included changes to the collagen hydrogel fibrillogenesis conditions (i.e. pH (via CO_2), temperature), and therefore the collagen matrix architecture, to create hydrogels with an increased capacity to physically increase blockage to fluid and small particle (i.e. HA-NP) outflow. Both the lowered gelation temperature, and changes in environmental CO_2 levels did not results in changes to the hydrogel HA-NP trapping efficiency.

The incorporation of large mobile macromolecules (i.e. molecules that do not bind to the collagen matrix) was previously found (in chapter 5) to increase the filtration effect on fluids attempting to leave the hydrogel through the FLS. Although the incorporation of PEG 400kDa was hypothesised to increased HA-NP entrapment within the hydrogel, this was not found to be the case, as samples with, or without, PEG resulted in a similar HA-NP retention of 14.4 ± 7.6 % and 16.7 ± 13.3% respectively (p=0.448). However, note that the variation (standard deviation) within the results in PEG containing samples was high, which suggests that the incorporation of PEG may be efficient in increasing retention of HA-NP in at least some samples. However, why this result did not extent to all samples was unclear. Perhaps, the sensitivity of the hydrogel to gelling conditions, affected the matrix architecture in some samples, altering the extent of interfibrillar 'pore' blockage by the PEG 400kDa, allowing HA-NP escape in some cases.

The increase in initial collagen density from 2mg.ml^{-1} to 6mg.ml^{-1} improved HA-NP retention. This effect was likely due to an increased blockage at the FLS by tightly packing fibrils, and resulted in limited fluid and molecule outflow rates. In this case, HA-NP retention increased from 13.5% to 33.5% with the increase in collagen density of the hydrogel. Other factors (other than collagen density of the solution) may also contribute to this increased NP retention. For example, here the 6mg.ml^{-1} collagen solution was made up of atelocollagen (instead of tropocollagen used in the 2mg.ml^{-1}). The difference between both types of collagen molecules lie in the presence (or absence) of a short protein segment (telopeptide) on both terminals of the collagen molecule. Collagens without this telopeptide will aggregate less readily with adjacent collagen molecules (Brennan and Davison, 1981), meaning more collagen will be mobile, and available to clog the FLS at the time of compression - potentially enhancing HA-NP retention. The hydrogels made from 6mg.ml^{-1} also had an increased overall thickness, suggesting that a proportion of the HA-NP may be retained 'passively' through the increase in overall volume, and not solely through physical entrapment between the interfibrillar space. A combination of the above factors has likely contributed to the increased HA-NP retention observed in samples containing increased collagen density.

Interventions with a positive effect on HA-NP retention also included the alteration of the HA-NP biomaterial size, where HA-NP with a diameter of 680 nm or ∼200-250 nm were retained at a rate of 41.6% and 35.4% respectively (p=0.005); showing that significantly more large HA-NP material was retained. The changes in NP size was brought about by incorporating a drug (simvastatin) cargo, or by chemical rearrangement and compaction of the HA-NP particles at pH12.

The effect of particle size and mobility within the collagen hydrogel has previously been discussed in chapter 5, where it was concluded that small

molecules below a critical size, measured according to the amount of space between collagen fibrils within the matrix, were freely mobile (until it reached the FLS). Larger particles however may become trapped in between the collagen fibrils, and remain within the hydrogel; as demonstrated by (Hadjipanayi et al., 2011a).

All HA-NP biomaterials were within the range of 200-680nm, which was at least 10 times larger in size than the macromolecule hydrodynamic radius discussed in chapter 5, meaning in theory, most HA-NP should remain trapped within the collagen matrix during plastic compression. However contrary to this expectation, most HA-NP were lost to fluid flow during plastic compression.

Potential reasons for this discrepancy include erroneous estimation of interfibrillar pore size, or nanoparticle size. The collagen matrix pore size have previously been estimated to be $\sim$30nm through imaging (visual estimation); additionally, macromolecules at this size range affected plastic compression rates, and so at least some blockage of the interfibrillar 'pores' was achieved using macromolecule measuring $\sim$25nm (hydrodynamic radius). HA-NP size, on the other hand, was measured using either dynamic light scattering or visually through the scanning electron microscope, both being reliable methods to size nanoparticles. Therefore other reasons are more likely to be behind the low retention rates of the nanoparticles, and may lie in the nanoparticle surface charge and surface chemistry (Vllasaliu and Singh, 2014); although further tests will be necessary to determine HA-NP surface charge and surface chemistry characteristics.

Another paradox observed in this study, which may be attributed to the HA-NP chemistry was the improved trapping efficiency of the compacted (pH12 treated; $\sim$200-250nm diameter) HA-NP-S compared to 'empty' HA-NP carriers (486nm diameter).

Nevertheless, HA-NP was highly mobile within the hydrogel model, and

escaped the construct with the fluid flow. The implication of this high mobility identified using this model suggest a high potential for the biomaterial to travel through the systemic system when implanted *in vivo*. The systemic effects of nanoparticles will therefore be especially important, and require further study to determine safety and biomaterial fate of the biomaterial over time *in vivo*. Especially when the HA material can be taken up by binding to cell-surface receptors, such as CD44 (Xian Xu, 2012). Other responses *in vivo* to HA also included the mediation of inflammatory responses (i.e. inhibit macrophage migration and aggregation (Laurent and Fraser, 1992)), to name a few.

The concentration of HA-NP-S within the hydrogel was 0.1mg.ml^{-1}, with 9% (w/w) of the particle composed of the simvastatin drug cargo; therefore:

$$\text{Concentration of simvastatin within the hydrogel} = \frac{0.1}{100} \text{ x } 9$$

$$= 0.009$$

$$= \mathbf{0.009} mg.ml^{-1}$$

This concentration of simvastatin in comparison with other systems for simvastatin delivery was comparitively low. For example, a study also using HA material (hydrogel) to delivery simvastatin found that 1mg (rather than 0.1mg) simvastatin resulted in osteogenesis *in vivo* when bone defects were studied using x-ray radiography (Bae et al., 2011). However, the release rates of the simvastatin should also be taken into consideration as about 30% of the drug carried with in the hydrogel was released as an initial burst leaving less drug for subsequent sustained release in culture. However, targeted delivery systems, in theory, should require less drugs-dose for the required therapeutic effect, therefore an initial concentration of 0.009mg.ml^{-1} was a good starting point for screening effects of drug-doses. *In vitro* tissue models can eventually be used

to look at dosing of drug for optimum BMP-2 production and eventual bone production.

The main hypothesis this model was set out to test was the delivery of simvastatin, via HA-NP-S particles, to induce a sustained level of BMP2 protein production. BMP2 protein was detected from HA-NP-S containing constructs in initial ELISA studies. The first sign of BMP2 production was observed at day 5, at an average concentration of 24pg.ml^{-1} (figure 6.6). This level of BMP2 within the construct was maintained until the end of the experiment at day 9. By this time, BMP2 was also detected from the surrounding culture media at a concentration of 36 pg.ml^{-1}. It was important to note that BMP2 was only detected in samples containing HA-NP-S particles; and not control hydrogels.

Results suggest that BMP2 protein detected at day 5 was triggered by the release of the simvastatin drug cargo from the HA-NP-S within the construct. MG63 cells were then stimulated to produce BMP2, which diffuses out of the construct (into the culture media) with time. The fact that a BMP2 was continuously detected within the construct between days 5 and 9 suggests that the simvastatin was released gradually over time from their HA-NP carrier, because simvastatin has a half-life of $\sim$2 hours (Aarthy et al., 2014).

However, subsequent repeats of the experiment were not able to reproduce results; for example BMP2 was detected within the HA-NP-S constructs at day 6 and 14, but only at extremely small quantities, suggesting the BMP2 detected may be background 'noise' from the ELISA assay.

Nevertheless, the differences between experiments meant that the results of growth factor production in response to the delivery of drug was inconclusive; and the hypothesis cannot be proven at this stage. It was not possible to rule out batch variances of the HA-NP-S material as the cause of the variable results. However other possibilities for the lack of BMP2 production in subsequent experiments include variation in cell activity, variation in simvastatin

availability (i.e. amount of simvastatin delivered within the HA-NP, or released by the nanoparticle over time); or the interaction between the BMP2 and collagen proteins which may render it unavailable to the sandwich-ELISA assay. This model may also be over simplified (environment may need more bone-like features i.e. hydroxyapatite, increased stiffness, topography, etc.), and so did not efficiently stimulate MG63 cell production of BMP2.

A review of the delivery methods of simvastatin and BMP2 protein can be found by Aarthy et al. (2014) and Anderson and Shive (1997). Durg delivery using fitc-containing silk NP (further trapped within a silk based hydrogel) had demonstrated a similar constant release of drugs over several days (at earlier time points) (Numata et al., 2012) (Numata and Kaplan, 2010). Although degradation of the hydrogel led to an initial burst release of the trapped material within the first hour, the NP was then released gradually, and constantly, over 5 days. In the study involving HA-NP here, a burst release of the delivery drugs was not likely (although not conclusive),as no initial BMP2 was detected from either the hydrogel and surrounding culture media.

In vivo, the action of statins appear to promote osteogenesis (osteoblast differentiation), inhibit osteoblast apoptosis and suppress osteoclastgenesis via molecules such as farnesyl pyrophosphate (FPP), which affects expression of BMP2 and Runx2 downstream (Ruan et al., 2012).

Further studies will be necessary to test whether this model was able to elicit a response representative of the *in vivo* environment, when simvastatin was administered locally. The development of a 'non-invasive/non-end-point' imaging method to track nanoparticle distribution *in vitro* will be beneficial for studying drug delivery and their localised therapeutic effects (Ricketts et al., 2014).

Chapter 7

Results: *In vitro* tissue model for biomaterial fate

7.1 Introduction

Biomaterials implanted into the body are usually remodeled (natural materials) or replaced by cell-produced ECM (synthetic biomaterials) over time. As discussed in section 1.3.3, synthetic biomaterials are commonly used as implant materials due to the ease of manipulation of the construct mechanical properties and physical features. However, since these implant materials are not natural to the human body, the effect of the biomaterial or its degradation products at the implant site may not be completely clear, and may influence the eventual implant success; particularly when the effect of the biomaterial on cells resident at the implant site is not always fully understood.

The role of an implanted biomaterial can range from a supporting scaffold for cell culture, to the delivery of drugs or other bioactive molecules. The rate of material degradation therefore affects the functional aspects of the material (i.e. material integrity, release rates of the bioactive molecules). This makes the understanding of material degradation rate a main target (especially in the

long-term) in biomaterial testing.

The ability to define and control biomaterial degradation rate is especially important, when the success of the tissue replacement depend on closely matched biomaterial degradation and cell-produced ECM deposition rates within the construct. 2D *in vitro* assays are commonly used to assess biomaterial degradation rates, but as previously discussed (see section 1.3.2), they may not always reflect *in vivo* conditions. Animal models on the other hand often only provide the partial picture of material degradation, owing to the lack of material (and surrounding tissue) accessibility during the culture period. An accessible model tissue is therefore required for real-time biomaterial assays within a physiological tissue-like environment.

Here, a dense ECM-like structure (plastically compressed collagen hydrogel) is formed with encased cells and biomaterials; used to assess the material in an *in vitro* tissue-like model. Cell involvement in the fate/destination of the biomaterial over time will also be studied. A fluorescent PLGA biomaterial (further discussed below) is used in conjunction within the compressed hydrogel model to track biomaterial degradation rates, and biomaterial fate with culture.

7.1.1   Degradation of biomaterials

Degradation of biomaterials can be defined as the "molecular change due to chemical chain scission within a polymer chain" (Yildirimer and Seifalian, 2014).

One of the current challenges is to precisely measure and control biomaterial degradation within a tissue environment. Cells within the scaffold need to remain physically supported to encourage cell-matrix interactions leading to the biosynthesis of the 'new' ECM (ideally with associated ECM components and tissue response in the correct sequence i.e. collagen synthesis, inflam-

mation, angiogenesis and innervation). It is also essential to evaluate each component/degradation product of the biomaterial to ensure safety on cells and tissues.

Degradation rates of biomaterials can be affected by external conditions such as temperature, pH and fluid dynamics around the biomaterial; but also the intrinsic properties of the material, such as the surface area of the construct exposed to degradation (directly influenced by construct dimensions, pore size, porosity and overall design). Additionally, the chemistry of the biomaterial (i.e. hydrophilicity/hydrophobicity, mode of degradation (erosion, enzymatic, hydrolysis, etc.) also have a major role in determining material degradation rates. Therefore, biomaterial degradation rates can vary from hours (e.g. hyaluronic acid (Laurent and Fraser, 1992)) to years (e.g. silk (Cao and Wang, 2009)).

Many biomaterials are designed with multi-functionality to support both tissue structure, and to deliver cells and biologically active molecules (such as drugs, growth factors, cytokines, genes) within a biodegradable matrix. The ability to modulate the release kinetics of these bioactive factors is important for the tissue to adapt to their new environment and gain function over time (Chen et al., 2011).

Changes to implanted biomaterials and surrounding tissue with time may include:

- Degradation of material

- ECM production and remodeling of existing tissue matrix by resident cells

- Changes to material physical properties (i.e. dimensions, porosity)

- Fate/destination of degraded products (i.e. uptake by cells, resorption or remain in surrounding tissue)

In the current tissue model of material degradation, a simple reductionist

matrix made of collagen (type-I) with physiological density and interstitial cells, is used to study biomaterial degradation rates.

7.1.2   Biomaterial tested in current model: what is PLGA?

Poly(lactic-co-glycolic acid) (PLGA) is a type of thermoplastic aliphatic poly(ester) that has been approved for drug delivery use by the FDA. The material is a polymer of poly(lactic acid) (PLA) and poly(glycolic acid) (PGA) as seen schematically in figure 7.1 below. They have good biocompatibility, material strength and can be made into any shape or size; ranging from nanoparticles to 3D constructs capable of bridging large tissue gaps. The range of PLGA manufacturing techniques (using different types of solvents) also means that drugs, proteins or cells with very different properties can be incorporated into the material (reviewed by (Jain, 2000)).
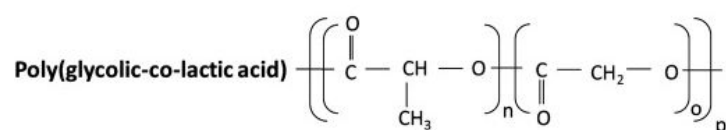
Figure 7.1: Chemical formula of the PLGA polymer adapted from (Yildirimer and Seifalian, 2014). The polymer chain can involve different proportions of poly(lactic acid) and poly(glycolic acid).

PLGA degradation

Degradation of PLGA occurs via hydrolysis by cleaving ester linkages in the polymer backbone. Whether enzymatic degradation is involved in PLGA degradation (due to the differences *in vivo* and *in vitro* degradation rates (Lu et al., 2000)) is controversial.

In the review by Jain (2000), the three phases of PLGA degradation was summarised as:

1. Random chain cleavage, where the molecular weight of polymers decreased with no overall loss of mass

2. Further cleavage of polymer with rapid loss of mass as soluble oligomeric and monomeric products are formed (i.e. degradation products small enough to be mobile)

3. Soluble monomers are formed from the smaller fragments until polymer is completely solubilised

Once degradation begins, more water soluble carboxylic end groups will be exposed, further catalysing biodegradation (Schliecker et al., 2003) (Oh et al., 2006). As hydrogen ions dissociate from these end groups, the pH in the surrounding solution/tissue drops, and further catalyses the degradation of PLGA. The end products of the degradation process are lactic and glycolic acids which are eventually metabolised, *in vivo*, into carbon dioxide and water.

Since PLGA degrades (at least primarily) by hydrolysis, water permeability of the construct (i.e. its porosity, size/shape, surface-to-volume ratio) will affect the rate of PLGA degradation. Large constructs $>300\mu$m were found to have heterogenous degradation rates where the core of the construct will degrade at a higher rate compared to the surface (Anderson and Shive, 1997). However, small particles under 300μm degrades at a homogeneous rate throughout the particle.

Additionally, PLGA has a glass transition temperature (Tg) above body temperature, and so has a glassy appearance and high mechanical strength at physiological conditions. This Tg, and their polymer degradation rates is highly dependent, and predictable, based on the composition of the polymer (i.e. proportion of lactic and glycolic acids; among other factors discussed below). Generally, increases in PGA content will decrease the crystallinity of the PLGA polymer. Crystallinity can affect the material strength, swelling properties and

degradation rates; with a highly crystallised polymer degrading over a longer period of time. Additionally, glycolic acid is more hydrophilic than lactic acid, and so a PLGA construct with high amounts of PGA which will absorb more water, and encourage its diffusion through the scaffold (Xu et al., 2013); resulting in a material with increased degradation rates. The exception is a polymer made of a ratio of 50:50 PLA and PGA, which has the highest degradation rates.

Fluorescent PLGA

Fluorescent poly(lactic-co-glycolic acid)(PLGA) tagged with rhodamine B isothiocyanate was provided by Ms K.Barnsley of Keele University, UK. The material consisted of equal proportions of lactic and glycolic acid which are known to have high degradation rates. The fluorescent rhodamine is evenly and covalently bound to the PLGA, so degradation products can be traced by measuring fluorescence within the construct or in the surrounding ECM-like structure or culture media.

The ability to track the biomaterial is fundamental in assessing its long term consequence in a tissue-like environment. The aim of this study is to test and track biomaterials as they degrade within an *in vitro* 3D tissue model. The model tissue is based on the rapid fabrication of cellular compressed hydrogels, which can be formed around a biomaterial. Fluorescent PLGA μ-particles (50-150μm diameter) were tested in this system.

Since PLGA materials are known to undergo hydrolysis and form smaller mobile units, it is hypothesised that with time, these degradation products will diffuse away from their implant site, and can be found in the tissue construct and culture media. Additionally, the reports of cell uptake of PLGA nanoparticles (Cartiera et al., 2009) led to the hypothesis that smaller degraded PLGA will be taken up by resident cells with culture.

7.2 Methods

Methods listed below are specific to this study. Further methods common to studies throughout the thesis are listed in Chapter 2.

7.2.1 Preparing fluorescent PLGA materials for use

The rhodamine B isothiocyanate-tagged PLGA were supplied in two formats, namely μ-particles (50-150 μm) and 2mm porous discs (pore size 100-200μm). All PLGA material were stored at $4°c$ in a desiccator and wrapped in foil to prevent the hydrolysis of the material and blanching of the fluorescence during storage.

Rhodamine-tagged PLGA was sterilised by treatment with isopropanol for 15 minutes and subsequently washed in sterile PBS three times. PLGA in its μ-particle form were recovered by centrifugation at 12000rpm for 2 minutes after isopropanol treatment and each of the 3 washes. Finally the PLGA particles were suspended in PBS at a concentration of 1mg.ml^{-1}. The suspension was sonicated for 10 minutes to obtain a homogenous suspension.

7.2.2 Detection of rhodamine-tagged PLGA

Fluorescence of rhodamine-tagged PLGA were measured from the PBS (in 2D assays) or the culture media surrounding the 3D model. Unless otherwise specified, samples were measured in 24-well plates at room temperature with excitation and emission wavelengths set at 530nm and 590nm respectively (Infinite M200Pro microplate reader, Tecan).

7.2.3 PLGA degradation rate in PBS (2D system)

PLGA samples used within the model were first tested in 2D to ensure the degradation products can be detected in the surrounding media, and to test the material degradation rates in solution. 2mm rhodamine-tagged PLGA discs were weighed and submerged in in 4ml PBS for incubation at 37°c. The amount of fluorescence (degradation products) was measured from the PBS over 34 days (at 0 and 1 hours; 1, 7, 8, 12, 21 and 34 days). For the measurements, PBS samples were was transferred into a cuvette, and measured on a fluorescence spectrometer (LS 50B; Perkin-Elmer) at 530nm excitation and 590nm emission wavelengths. The same PBS solution was returned to the respective PLGA sample for continuous incubation. Therefore, fluorescence detected from the PBS was cumulative for each sample.

7.2.4 Trapping efficiency of PLGA μ-particles within the hydrogel

The ability of the collagen hydrogel to retain PLGA μ-particles after compression was measured by comparing the amount of fluorescence (from the PLGA material) in gels, pre- and post-compression.

Hydrogels for this study were produced by adding 10% (v/v) 1mg.ml^{-1} PLGA μ-particle solution to ice-cold neutralised collagen solution, consisting of 80% (v/v) type-I acid-soluble collagen and 10% (v/v) 10xMEM (neutralised using 5M and 1M NaOH). 1ml of this PLGA collagen solution was transferred to each well of a 24-well plate, and incubated at 37°c, 5% CO_2 for 30 minutes for hydrogels to set. Gels either remained uncompressed, or were fully compressed as described in section 2.4. All gels (both compressed and non-compressed) were subjected to collagenase-I digestion (0.2% solution in PBS; Gibco, USA) for 20-30 minutes at 37°c (on a shaker) until the gels were fully digested. Sam-

ples were then measured for fluorescence as described in section 7.2.2.

7.2.5 PLGA μ-particle degradation rates in 3D (with or without cells)

Compressed collagen hydrogels were formed around the PLGA biomaterial, and incubated for up to 21 days to study biomaterial degradation over time.

The main variable in this test was the incorporation of cells (human dermal fibroblasts (HDF)), to see if their presence will affect the kinetics of PLGA degradation and release from their implant site. A two-layered compressed collagen hydrogel model was used to place cells and fluorescent PLGA μ-particles in separate, but adjacent, layers (figure 7.2). In the first layer, 1ml collagen hydrogel containing either no cells, or 500,000 HDFs were set within each well of a 24-well plate (produced as described in 2.2). Once the hydrogel has gelled after 30 minutes of incubation (37℃, 5% CO2), a second layer containing 10% 1mg.ml^{-1} sterile PLGA μ-particles (added to the neutralised collagen solution instead of cells) was gelled above the first layer. After another 30 minutes of incubation, both super-hydrated layers were compressed together using upward flow plastic compression, until compression was complete (please see section 2.4 for detailed method). 1.5ml DMEM (supplemented with 10% fetal calf serum and 1% penicillin steptomycin) was added to each well to prevent the dehydration of the compressed gel. All resultant compressed gels were detached from the base of the well (i.e. so that it is free-floating), and were incubated at 37℃, 5% CO_2 for up to 21 days. At days 0, 3, 7, 11, 14 and 21, the media surrounding the construct was collected and frozen at -20℃ for subsequent fluorescence detection.
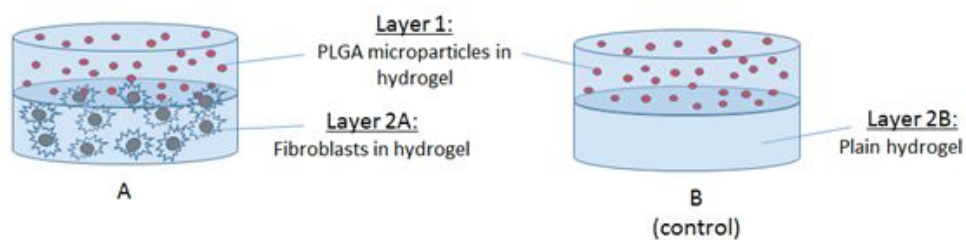
Figure 7.2: Schematic representation of the 2-layered model used in biomaterial testing. PLGA microparticles were set in collagen hydrogels containing fibroblasts (A) or a plain hydrogel (B; as a control). Layers 1 and 2 were compressed together to ensure good contract between both layers.

7.2.6 Histological analysis of model

Samples were fixed, histologically processed and embedded in paraffin wax for sectioning. 8 μm sections were collected and viewed under a Olympus (BH2-RFCA) microscope with a corresponding filter to detect red rhodamine fluorescence within the construct. Images were captured in black and white on a digital camera (C4742-95, Hamamatsu) attached to the microscope. ImageJ was used to superimpose colour, onto the black-and-white images captured on the camera. Samples were fixed, histologically processed and embedded in paraffin wax for sectioning. 8 μm sections were collected and viewed under a Olympus (BH2-RFCA) microscope with a corresponding filter to detect red rhodamine fluorescence within the construct. Images were captured in black and white on a digital camera (C4742-95, Hamamatsu) attached to the mi-croscope. ImageJ was used to superimpose colour, onto the black-and-white images captured on the camera. Samples were fixed, histologically processed and embedded in paraffin wax for sectioning. 8 μm sections were collected and viewed under a Olympus (BH2-RFCA) microscope with a corresponding filter to detect red rhodamine fluorescence within the construct. Images were captured in black and white on a digital camera (C4742-95, Hamamatsu) at-tached to the microscope. ImageJ was used to superimpose colour, onto the black-and-white images captured on the camera.

7.2.7 Cell uptake of PLGA degradation products in the 3D environment

In order to study the effects of biomaterial degradation products on surrounding tissues, it is necessary to establish the fate/destination of these molecules. It was clear some PLGA degradation product was released into the surrounding matrix and culture media due to the fluorescence detected spectrophotometri-

cally, and visually (from histological samples).

Cell uptake of fluorescent material with prolonged culture was tested in a 3D, plastically compressed hydrogel, environment.

Collagen solutions were prepared similarly to methods described in 2.2, with slight alterations in volumes of solutes were used to account for the incorporation of both cells and PLGA μ-particles. Briefly, 75% type-I acid soluble collagen and 10% 10xMEM were neutralised with 5M and 1M NaOH. Once neutralised, 5% DMEM suspending 500,000 HDF/well and 10% PLGA μ-particles were added to the collagen solution. 1ml/well of the suspension was placed in a 24-well plate and gelled at 37℃, 5% CO2 for 30 minutes. Gels were compressed and incubated with 1ml DMEM.

Cells were recovered at days 0 and 10. The hydrogels were digested with 0.2% type-I collagenase (Gibco, USA; in PBS) at 37℃ and with constant agitation for 30 minutes. Cells from the samples were then recovered by centrifugation (2000rpm, 5 minutes) and supernatant were discarded. The recovered cells were then washed twice by re-suspension in PBS. Finally the HDF were re-suspended in 1ml PBS and transferred to a 24-well plate for 24 hours until cells were attached onto a flat surface for imaging. Fluorescence from PLGA was measured as described above.

Control gels containing only HDF (and no PLGA) were set up in parallel to the above samples.

7.2.8 Statistics

Statistical significance was determined by an independent sample t-test for data on PLGA trapping efficiency within the hydrogel. For all other experiments, one-way ANOVA (LSD post-hoc) was used. Confidence intervals were set at $p \leq 0.05$.

7.3   Results

7.3.1   PLGA degradation in PBS (2D)

Sample size of the 2mm PLGA discs averaged between 1.7 - 3.4 mg. Since the samples varied in mass, the results were reported in fluorescence (a.u.) per mg of sample material. Also, to account for burst release (if any) of the fluorescently tagged particles, all results were subtracted from the average baseline of 0.093 ± 0.013 a.u., detected at 0 hours (i.e. as soon as the PLGA was added to the PBS). Almost no fluorescent material was detected in the PBS at 0 and 1 hour after submerging the samples in PBS, suggesting the fluorescent rhodamine molecules were bound covalently to the PLGA material.

Some fluorescence was detected in the PBS by 24 hours in culture (figure 7.3). Significant cumulative increases in the fluorescent material was detected by day 21 of incubation (p=0.038). Degradation of the material continued until the end of the study period at day 34. By the end of the experiment, samples were visibly swollen and disintegrated in solution.

The degradation rates appear to be influenced by the physical size of the sample, as samples with a high surface area-to-volume ratio (sample 2) degraded at an increased rate compared to other samples - which progressed at an exponentially increasing rate (figure 7.4).
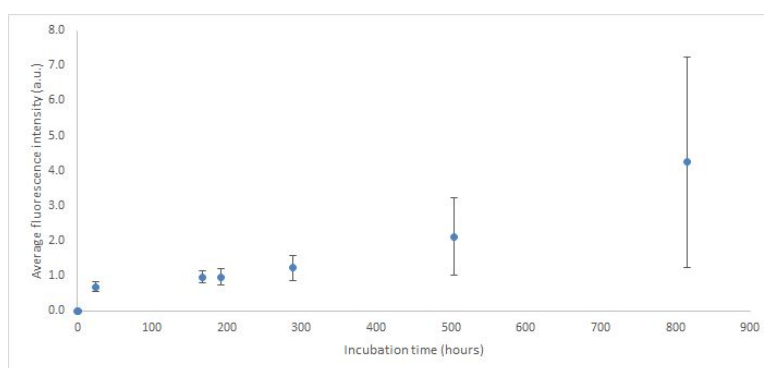
Figure 7.3: PLGA degradation rates in PBS (2D assay) over 34 days. PLGA degradation was determined by the fluorescent intensity of rhodamine tagged degradation products of PLGA material, found in the PBS solution, over time.
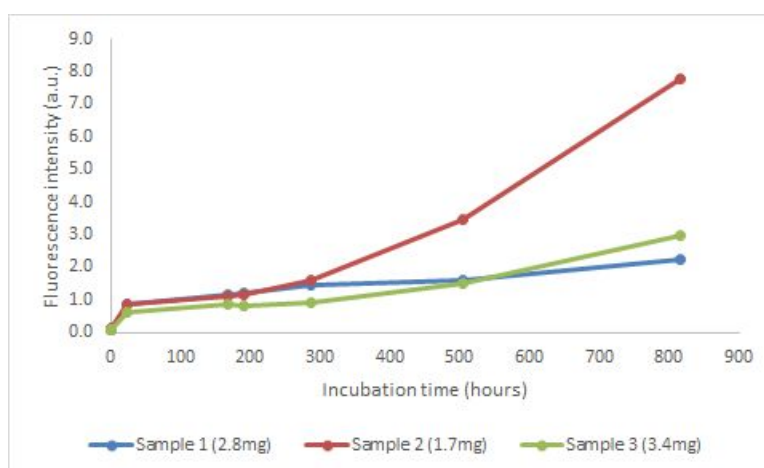
Figure 7.4: Fluorescence readings from individual PLGA 2mm disc samples submerged in PBS over 34 days with respective sample mass.

7.3.2 Trapping efficiency of PLGA μ-particles within hydrogels

Next stages in developing the material degradation model involved the incorporation of the biomaterial (in μ-particle form) within the compressed collagen hydrogel to form *in vitro* tissue-like models for the assay of material degradation rates and material fate.

The trapping efficiency of PLGA micro-particles within the collagen hydrogel was measured by comparing the amount of fluorescent PLGA particles within (otherwise identical) hydrogels, before and after plastic compression. Gels (both compressed and non-compressed) were digested in collagenase-I to re-suspend the μ-particles in solution prior to spectrometric measurement of the solution. The amount of fluorescent signal detected from uncompressed and compressed gels were almost identical, at 2814 $\pm$ 300.1 and 2848 $\pm$ 86.6 respectively (p=0.860). This suggests that most, if not all, of the fluorescent micro-particles have been retained within the hydrogel after plastic compression.

7.3.3 The effect of cells on material release from tissue models

Since μ-particles were retained within the compressed hydrogel after plastic compression, the next step was to track and quantify the amount of PLGA degradation products released from the 3D tissue model over time.

The cumulative amount of fluorescence detected in the media (subtracted from the baseline media-only readings) from cellular and acellular gels over 21 days have been plotted in figure 7.5.

Fluorescence was detected in the culture media surrounding both cellular (p

≤ 0.001) and acellular (p=0.004) matrices from day 7 of culture. However, the cumulative level of fluorescence detected from cellular gels was approximately 2.5 times more than that of the acellular gel, at 23166.5 a.u. and 8601.5 a.u (p ≤ 0.001) respectively. At all time points, except day 21 (p=0.244), a significant difference between cellular and acellular samples was observed.

The cumulative results show that fluorescent material was continuously released into the surrounding media in both sample types between days 7 and 21. However, the rate of release was highest between days 7 and 14 (at 2856.8 a.u. and 5883.1 a.u. per day respectively for acellular and cellular samples), which subsequently lowered to 1120.3 a.u. and 1628.5 a.u. per day respectively beyond 14 days in culture.
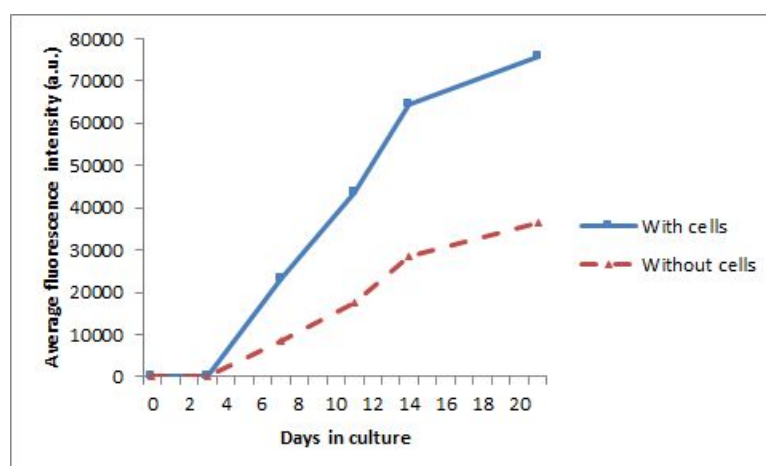
Figure 7.5: Cumulative average release of fluorescent material into the media surrounding the PLGA containing compressed hydrogel over 21 days. The amount of fluorescence detected from the media in cellular and a cellular constructs were compared to study cell influence over biomaterial degradation product release kinetics.

7.3.4 Histological analysis of two-layered model

Histological images of the cellular and acellular model at days 0 and 14 of culture also support the difference in material release rates from cellular and acellular gels (figure 7.5). Note the loosened construct structure of the cellular hydrogel layer in cellular samples at 14 days.

Both acellular and cellular samples at day 0 (figure 7.6) show the concentrated red fluorescence of μ-particles within one of the auto-fluorescing collagen layers. By day 14, the fluorescence from these μ-particles had diffused into the surrounding collagen construct in both acellular and cellular samples. This was most pronounced an visible in *cellular* samples (figure 7.6). Vacuoles (with a fluorescent outline) which appears to be the remnants of the PLGA μ-particle were observed in the biomaterial containing layer of the cellular bi-layer construct. Within the adjacent cellular layer, pockets of highly fluorescent clusters, which coincides with the shape and size of the interstitial cells (HDFs), suggests that cells may be able to take-up the degradation products of PLGA. These pockets of intensely fluorescent particles, away from the micro-particles, were not observed within the acellular samples.
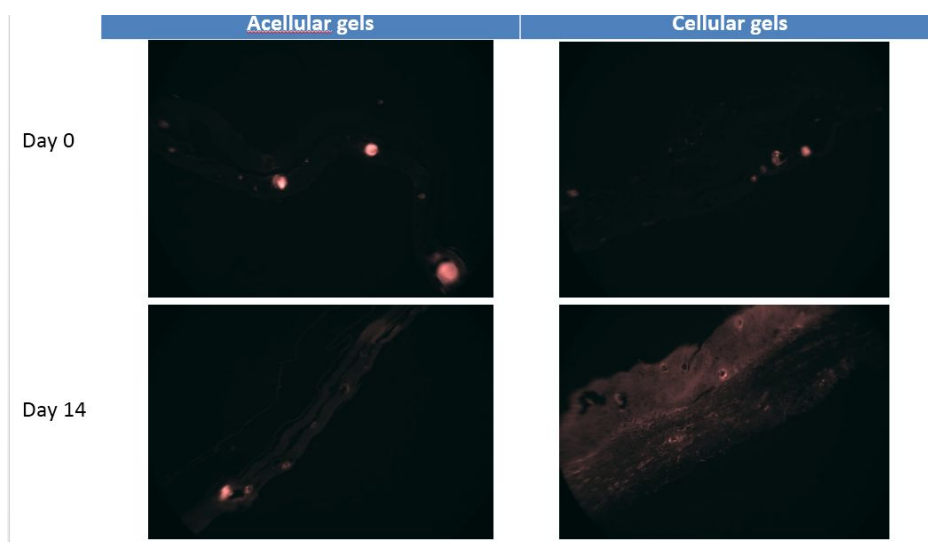
Figure 7.6: Histological sections of the bi-layer model, where cellular or acellular gels were compressed with a separate hydrogel containing PLGA microparticles. Samples cultured for 0 and 14 days were compared.

Cell uptake of PLGA degradation products

To test whether cells take-up PLGA degradation products, cellular compressed hydrogels (with or without PLGA) were incubated for 10 days, and subsequently digested to extract cells. Cells were recovered, washed and seeded on tissue culture plastic to enable visualisation on the microscope. Due to the faint fluorescence from the degraded PLGA material, it was not possible to visualise the particles using the camera during fluorescence imaging. The material could however, be observed in white light (as dark coloured dots; which were not present in samples without PLGA).

Particles were clearly visible within the cells in samples cultured with PLGA after 10 days (figure 7.7a). As expected, cells not cultured with PLGA material did not exhibit the clusters of material (figure 7.7b).
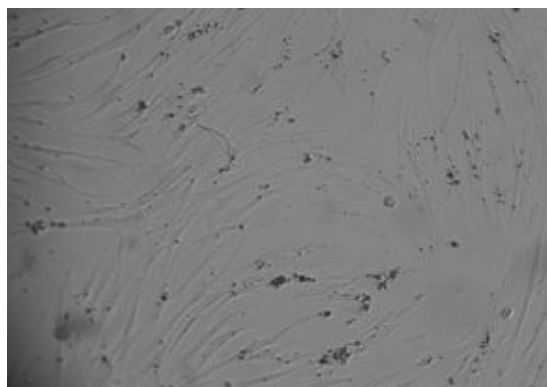
(a) Cells incubated with PLGA
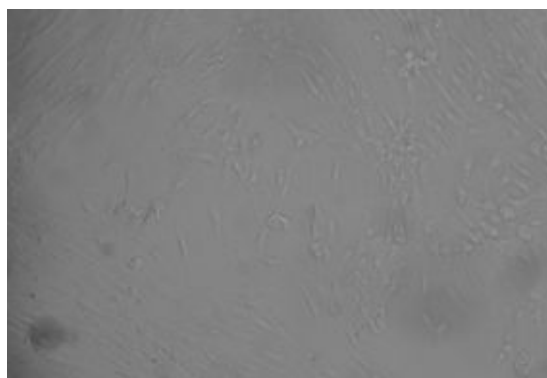
(b) Cells incubated without PLGA

Figure 7.7: Human dermal fibroblasts extracted from collagen gel model after 10 days in culture a) with or b) without PLGA, were subsequently seeded on tissue culture plastic for imaging.

7.4 Discussion

The ability to predict and detect the rate of material degradation within a tissue-like environment can have implications on the design and use of degradable biomaterials (Artzi et al., 2011). This was achieved *in vitro* within an optically permeable (plastically compressed) collagen matrix with the help of fluorescently-tagged PLGA material.

Degradation rates of rhodamine loaded PLGA material made of a 50:50 polymer of PLA:PGA was high as expected, with evidence of this degradation observed within 24 hours in the 2D model, and 7 days in 3D. This continued for the 34 and 21 days in 2D and 3D cultures respectively.

In the literature, the half-life of 50:50 PLGA scaffolds have been quoted as ~15 days (Anderson and Shive, 1997), or ~2 weeks and ~3 weeks *in vivo* and *in vitro* respectively (Lu et al., 2000). The degradation rates of the PLGA used in this experiment appear to fit into this time frame. However the release rates of degraded fluorescent material in the 2D and 3D model occurred with different patterns. PLGA material in the 2D model was released steadily into the PBS between 1 and 21 days in culture, with further increases in degradation rates at later time points between 21 and 34 days. This degradation pattern was more clearly observed from individual samples (figure 7.4), where rate of fluorescent material deposition into the PBS increased exponentially at later stages of incubation. This was not completely unexpected, since the accumulation of PLGA degradation products in the PBS can decrease local pH levels, which then further encourages hydrolysis of the material (Yildirimer and Seifalian, 2014). The fact that the same solution was used to incubate the PLGA samples during the experiment may explain the late-stage increase in degradation rates through pH changes, observed in the 2D model. Also as hydrolysis progressed within the sample, it was natural for the PLGA material

to have an increased exposure of carboxylic end groups, further increasing degradation rates (Schliecker et al., 2003) (Oh et al., 2006). Note also that by the end of the 34 days in culture, the samples were swollen (and mostly dissolved), meaning the surface area available for hydrolysis increased with time.

Release of fluorescent degradation products in the 3D model, however, was not observed until later in time (at day 7). PLGA μ-particle in the 3D sample were surrounded by a dense matrix which may explain the delayed release of the fluorescent particles into the surrounding culture media. The compressed collagen matrix was known to retain large particles (in relation to the "pore-size", or interfibrillar space between collagen fibrils) (Hadjipanayi et al., 2011a), so it was perhaps not surprising that the fluorescent particles were not detected immediately in the surrounding culture media. Since PLGA degradation began with the random cleavage of ester linkages within the material; loss of mass only occurs at later stages as smaller, soluble monomeric/oligomeric products were formed (Jain, 2000). So, further degradation of PLGA into smaller mobile particles was likely necessary before the degradation products can diffuse out of the hydrogel.

The difference in degradation rate could also potentially be due to the differences in size and shape of PLGA used in the 2D (2mm discs) and 3D models (μ-particles); more specifically, a larger surface area-to-volume ratio was likely to lead to an increased rate of PLGA degradation i.e. increase in surface exposed to surrounding fluid, and therefore hydrolysis.

One notable finding from the model was that a significantly higher amount of fluorescent PLGA particles was released into the surrounding culture medium from the cellular model (figure 7.5). If PLGA exclusively degraded by hydrolysis (and not by enzymatic activity as some report suggested (Lu et al., 2000)), the difference between the cellular and acellular models in the release profile of flu-

orescent degradation products will have been mediate by cell-induced changes to the extracellular matrix (i.e. remodeling); especially when fibroblasts were known to be capable at this task. Another sign that remodeling had taken place in the cellular construct was found in the histological studies, where the collagen matrix was transformed into a 'lacy' structure, with an increase in overall hydrogel thickness observed by 14 days (as seen in figure 7.6 and figure 7.8).
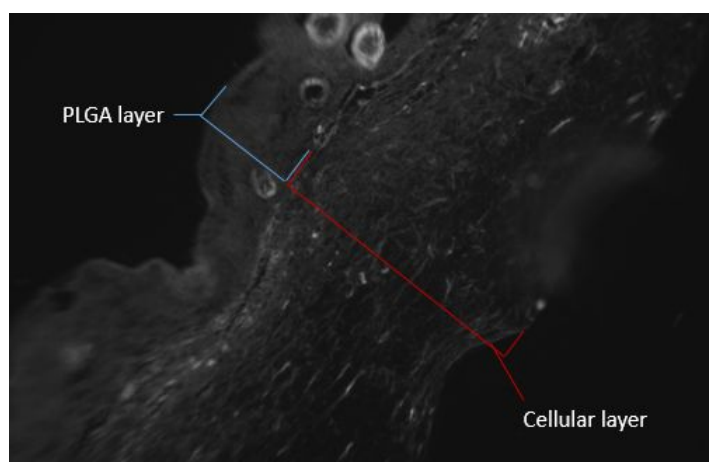
Figure 7.8: Cross section of the bi-layered 3D model at 14 days in culture. Layers either contained PLGA microparticles or cells (HDFs). Note that the thickness of the cellular layer was approximately 2.5 times that of their adjacent acellular (PLGA) layer.

In terms of the total amount of PLGA μ-particle within each hydrogel sample, a brief calculation showed that 0.1mg of the PLGA material was in each 1ml hydrogel (i.e. 10% volume of the hydrogel was made up of 1mg.ml^{-1} PLGA μ-particles). The overall mass of the samples used in the 3D assay was therefore much lower than those of the 2D assay (i.e. a smaller initial depot of 0.1mg, instead of $\sim$2mg of the material). Histological sections also revealed partially empty vacuoles in the PLGA layer (especially prominent in the cellular samples) by day 14 in culture (figure 7.6). Since the PLGA μ-particles had a size of $\sim$50-150μm, the degradation rates was expected to be uniform throughout the μ-particle (Anderson and Shive, 1997). However, the vacuoles with a brightly

fluorescent edge suggest degradation may have occurred starting from within the μ-particle.

Both the immobility of the large degradation products, and the small initial depot of fluorescent PLGA, may explain the pattern of degradation product released within the 3D model (i.e. delay in PLGA detection from the surrounding media and subsequent decrease in fluorescence detected beyond 14 days in the 3D samples (i.e. used up PLGA material)). There was a possibility that the μ-particles (considering their small size and high surface-to-volume ratio) were mostly degraded by the later stages of the culture period, before the degradation products had a chance to diffuse out of the hydrogel with subsequent culture. If indeed this was the case, it would be interesting to see if the incorporation of a bioreactor to induce fluid flow surrounding the construct will create a constant diffusion gradient for the PLGA degradation products, and improve the estimation of biodegradation rates compared to *in vivo* conditions.

Another variable studied was the fate of the degraded product. Cell uptake of the degraded particles was evident from images of cells isolated from the 3D constructs after incubation with PLGA material. In their nanoparticle form, PLGA have been shown to be taken up by endocytosis into endosomes, golgi apparatus and sometime the endoplasmic reticulum (in epithelial (2D) cell-lines (Cartiera et al., 2009)); but the destination of the NP, and the rate/extent of the uptake was dependent on the cell type. In the 3D model, involvement of cells was likely two folds. Cells firstly remodeled the matrix to encourage the dissipation of degradation products from the biomaterial implant site; and also (in the case of PLGA) internalised small degradation products.

The mode of PLGA uptake were previously studied in cell types such as epithelial cells (Cartiera et al., 2009) and macrophages (Tabata and Ikada, 1988). Cell-uptake of PLGA particles via phagocytosis was found to be size-sensitive, where particles over 10 μm (in macrophages) were not internalised

until further hydrolysed. When internalised, the phagocytosed microsphere degraded within the cell over time; and this degradation rate was controlled by the chemical composition of the PLGA material (i.e. the fast-degrading 50:50 PLGA was found to be completely degraded within the macrophage by 7 days) (Tabata and Ikada, 1988) (Tabata and Ikada, 1989) (Tabata et al., 2000).

Here, cell uptake of the degraded PLGA was also likely by phagocytosis as fibroblasts are phagocytic cells (Lee et al., 1996). However, the distribution of the PLGA particles within cells was not uniform (figure 7.7), with clusters of the material found in some cells. This may be because of the spatial arrangement of the cells and PLGA material in 3D, such that some cells will be in closer proximity to the PLGA material, and so experience a higher concentration of degradation material for their uptake. Alternatively, this difference in PLGA up-take between cells may be due to natural variances in cell activity.

Other considerations of PLGA degradation include the effect of decreased local pH levels on resident cells; especially when PLGA material have also been reported to cause the formation of local aseptic sinuses and can result in osteolytic changes and intermittent joint swelling when implanted (Athanasiou et al., 1996). Razaq et al. (2003) found that slight acidic conditions (at pH6.4) reduced cell matrix turnover and production of some essential proteins. Other studies have shown a similar effect of acidic extracellular pH on fibroblast growth, and gene expression of related proteins (Bumke et al., 2003). Acidic pH may even cause cell death, as observed in tumor-derived cells by 96 hours in pH6-7.5, and even sooner at pH5.5 (Lan et al., 2007). However, further studies into the difference between 2D and 3D will be needed to see if acidic conditions affect cells to the same extent in 3D, as the ECM may provides some shielding from acidic conditions or potentially harmful degradation products (Dobaczewski et al., 2010).

Potential systemic effects of mobile degradation products has also been a

source of concern in material development. Although systemic effects have been traditionally tested *in vivo* (i.e. toxicity of PLGA particle build-up in livers and kidneys). *In vitro* 3D models can potentially be used to study the effect of the biomaterial on individual cell types isolated from the target tissue (in separate models). For example, in the case of a full skin model of biomaterial degradation, 3D models containing HDFs (i.e. the present model), keratinocytes, macrophages, adipocites, etc. can be carried out in parallel (and co-culture systems) for a fully comprehensive study of the biomaterial in a target tissue. Although this will not completely replace the need for *in vivo* assays for material degradation, this will allow for improved accessibility, and ability to test individual cell types for a more comprehensive understanding of cell-biomaterial interaction.

Chapter 8

General discussions and conclusions

For the development of tissue models, it is essential to identify key functional variables that can influence the target cell behaviour; and subsequently refine the model until it is representative of tissue/cell response in the natural tissue (Brown, 2012, p.38).

To justify the effort in producing *in vitro* tissues models, it is important to obtain usable data from the model, which correlates with, and can represent the natural responses of human tissues to an external stimuli. The model will also need to be simple enough to isolate test variables; and accessible to evaluate tissue response to biomaterials (or other stimulus).

For example, important questions during biomaterial development may include:

- Is the biomaterial toxic to cells (both within the biomaterial and the surrounding tissue)?

- Do cells migrate between the biomaterial and the surrounding tissue (and other cell-biomaterial interactions)?

- Do cells synthesise new ECM within the biomaterial, and/or remodel existing natural matrix material?

- How long does the biomaterial persist within a tissue-like environment with culture?

- What is the optimum cell seeding density (if any) within the biomaterial for improved material-tissue integration? (and for optimum ECM deposition rates)

3D *in vitro* biomaterial testing platforms (i.e. plastically compressed collagen gel) has the advantage of suspending biomaterials in a tissue-like matrix (with relevant cell-matrix and cell-cell interactions), and enables real-time assessment of the accessible construct. Although there are limitations to these testing platforms, such as the relative simplicity of the model, and lack information on systemic effects; they can be useful as pre-clinical tests of biomaterials, for toxicity and localised tissue effects, over time.

However, even with the range of *in vitro* and *in vivo* test systems available to test biomaterials, the precise effects of implant materials on human tissues are often only fully understood in retrospect. An example of this can be seen in the case of joint replacement implants where previously unexplained tissue inflammation surrounding joint tissue implants was only later understood (from recovered implants/tissues) to be caused by material erosion and wear particles (Cuckler, 2012) (Knight et al., 2011).

In vitro 3D model tissues (developed here and elsewhere) can be used to improve our understanding of cell responses to these eroded/degraded biomaterials by isolating and simplifying test variables, and to study their effect on local cells. Ultimately, this can help improve material safety, and understand the underlying causes of material success, or failure, over time.

In order for cells to behave physiologically in this reductionist ECM-like scaffold, it is important to identify and reproduce the key cell-directing feature(s) of the target tissue within this *in vitro* model. This is because it is increasingly recognised that tissue models of the future have at least some reliance on cell activity to achieve functional tissue recovery; which is influenced by cell perception of their surrounding matrix.

In most natural tissue environments, type-I collagen is the main structural protein of the ECM. Therefore the *in vitro* tissue model used here was based on type-I collagen hydrogels; which has for many decades been used to study cell-matrix interactions (Grinnell, 2003) (Grinnell et al., 2005). The collagen material was derived from xenogenic sources, but the protein, including cell recognition sites are highly conserved throughout evolution (Boot-Handford and Tuckwell, 2003) (Garrone, 1999), and so can be recognised by human cells.

The ability to incorporate cells and chemical factors into the tissue model (i.e. drugs, growth factors) improved the versatility of the model platform for the production of tissue specific models. Plastic compression was used to increase collagen hydrogel density cell/biomaterial containing construct to increase the physiological relevance of the hydrogel for local cells.

In this study, all gels were compressed using the upward flow method (for details please see chapter 1.5) within culture well-plates, and therefore have good reproducibility, and the potential to be up-scaled for high throughput tests.

The main aim/goal of this study is to create next generation 3D *in vitro* model systems, based on a type-I collagen hydrogels, with particular focus on increasing matrix mechanical properties; and to investigate the use of 3D compressed collagen hydrogel soft tissue models in the testing of biomaterials. This was done in two distinct sections, by:

1. Developing a hydrogel with increased mechanical stiffness, also capable

of encapsulating live cells from time-zero of construct fabrication

2. Testing biomaterials in soft tissue models to study their degradation rates or drug-delivery propensities

The overarching hypothesis throughout this study was that models made from plastically compressed hydrogels, with cells and other cell-behaviour directing tissue features, will be able to predict and monitor (at least better than standard 2D *in vitro* cell-monolayer models) biomaterial behaviour and cell responses to biomaterials/drugs.

Part 1:

One of the issues next generation collagen hydrogel modeling platforms should address is their lack of mechanical properties; such that instant, live cell populations can be introduced into a *stiff* scaffold.

In the first part of the study (chapters 3 and 4), a novel collagen hydrogel with increased mechanical properties - which can encapsulate live cells as it is formed - was developed and tested for its cell compatibility and mechanical properties. The key characteristic of this novel material is that it is both *stiffer* than existing plastically compressed collagen hydrogels, and *can encapsulate cells within the hydrogel from time-zero*. Most previous approaches will have had to sacrifice either hydrogel mechanical properties (Brown et al., 2005) or interstitial cells (Wong et al., 2013) during construct fabrication.

This was achieved by using *pre-crosslinked* type-I collagen (polymeric collagen) as a starting material for hydrogel production. **A critical finding during material development was that although polymeric collagen spontaneously aggregated in solution at physiological pH, this can be delayed by blending acid-soluble collagen monomers into the polymeric collagen solution**; possibly by steric hinderance.

This delay allowed sufficient time for cell incorporation at physiological pH, prior to fibrillogensis. The resultant compressed polymeric collagen blend hydrogel had a 3-fold increase in material stiffness (compared to traditional plastically compressed collagen hydrogels).

There was, however, a problem associated with this compressed blend collagen hydrogel. A proportion of cells was damaged (extent dependent on the proportion of polymeric collagen within the hydrogel) during the plastic compression process. This result can be explained by the increased compression rates seen in polymeric collagen hydrogels, where a higher proportion of polymeric collagen corresponded to an increase in compression rates. High compression rates meant that fluid flow rates within the hydrogel (and so fluid shear stress on cells) was high, leading to cell damage. The increased in fluid flow rates in polymeric collagen containing samples was thought to be due to the reduced proportion of acid-soluble collagen, and so reduced mobile collagen monomers/oligomers which can contribute to the filtration effect at the FLS during plastic compression. This theory was supported by the finding that incorporation of mobile macromolecules into the hydrogel (i.e. to replace said monomers/oligomers, added to the collagen solution prior to fibrillogenesis) resulted in a reduced fluid flow rate within the hydrogel. The hydrodynamic size and concentration of the macromolecules were found to affect their ability in controlling compression rates. Optimum reduction in compression rates, and protection from cell damage was achieved by incorporation of 10mg.ml^{-1} poly(ethylene glycol) 400kDa into the hydrogel.

The methods for the production of this blended cellular hydrogel is summarised in the standard operating procedure (SOP) that can be found at the end of this chapter.

All-in-all, it was possible to create cellular hydrogels with increased mechanical properties using pre-crosslinked polymeric collagen as a starting ma-

terial as hypothesised; however there were slight deviations from the hypothesis in that although cells were encapsulated within the hydrogel, some cell damage was sustained in the subsequent plastic compression process (extent of damage depended on proportion of polymeric collagen within the hydrogel). This cell damage can be prevented by reducing compression rates by incorporating large, mobile macromolecules, into the hydrogel.

However, batch variation was high in these blend constructs, and since polymeric collagen blend hydrogels were too variable for use as a model tissue (where reproducibility between each sample is important), well-established plastically compressed hydrogels, made from acid-soluble tropocollagen, was used instead of the blend gels for studies in biomaterial degradation and drug-delivery.

Part 2:

The second part involved testing biomaterials (developed by other groups) within the tissue model to study their effect on local cells/matrix with culture.

Fast-degrading, fluorescently tagged, PLGA material was used to study biomaterial degradation in a tissue-like environment, and the subsequent destination of the degraded material. The hypothesis under test was that the PLGA material will diffuse away from their implant site, into the surrounding construct and culture medium; and that cells in the surrounding matrix will engulf small, partially degraded PLGA materials. This was investigated by incubating PLGA within the tissue model for the study of cell influence on the release rate of the fluorescent degradation products into the surrounding culture media. The results suggest that these degraded products traveled at a higher rate from the model tissue when cells were present within the tissue model, as cells were thought to 'loosen' the construct structure by remodeling the collagen matrix.

On a different note, imaging studies found evidence of cell-uptake of the

PLGA biomaterial. This was expected due to the known use of PLGA as a nanoparticle carrier which relies on cell-uptake for its function (Cartiera et al., 2009). Both results combine to support the hypothesis that PLGA degraded, and that its degradation products were mobile within the tissue model; ultimately detected in the surrounding culture media, and within cells.

For the modelling of drug delivery in tissues using HA-NP as a carrier, the first step was to increase nanoparticle retention within the model tissue following plastic compression. It was hypothesised that HA-NP retention can be improved by alterations to the compression process or the hydrogel. Also, that HA-NP-S can stimulate BMP-2 protein production in MG63 cells, where the 'single-dose' of simvastatin will be gradually released into the cell environment to stimulate a constant level of BMP-2 production. Results here found that the low HA-NP retention efficiency was improved by increasing collagen density within the hydrogel, and by introducing a filter layer between the hydrogel and plunger during plastic compression. This was thought to be potentially due to increase in the filtration effect at the FLS for fluids leaving the hydrogel during plastic compression.

Growth factor production (BMP-2) in response to the simvastatin drug cargo, however, was not reproducible between experiments, meaning no conclusions can be drawn at this stage, apart from the fact that growth factors can be detected using ELISA assays when the protein was present within the model.

Finally, note also that the efficiency of biomaterial encapsulation within the plastically compressed collagen hydrogel varied depending on biomaterial size; where the μ-particular PLGA had almost complete biomaterial retention, whilst the smaller nanoparticle HA-NP had a retention of between 10.1 ± 1.7 and 16.6 ± 1.2 % (again depending on size). This size dependence for retention of particles within the hydrogel was also previously demonstrated and discussed by Hadjipanayi et al. (2011a).

Enabling the recovery of lost tissue function was one of the main motivators in regenerative medicine. Although tissue engineering is not the only way to achieve this; i.e. with bionic prosthesis a successful alternative in recovering gross limb functions (with promises to recover some complicated biological senses such as sight (Lewis et al., 2015) and tactile senses (Saal and Bensmaia, 2015) in the future); true tissue regeneration with the capability to control/remodel/regulate tissue function over time, will be ideal in the long run (i.e. no need for maintenance or immunosuppression). However, the current extent of tissue function restoration using TE implants is only partial (or with caveats) at best, and genuine tissue regeneration complete with a vasculature, nervous system, function and seamless integration with the existing tissue (as seen in some amphibians (Brown, 2012)), is still a goal for the future. 3D *in vitro* tissue models, such as those developed here will be important to further our understanding of cell processes, and biomaterial interaction with the surrounding tissue over time.

8.1 Conclusions

The aim of this study was to develop next-generation 3D soft tissue models for the *in vitro* testing of biomaterials. Plastically compressed collagen hydrogels have been used here as a model tissue to study biomaterial degradation rates, their fate within a tissue-like environment and the delivery of drug-carrying nanoparticles.

The first part of the study demonstrated that it was possible to generate a cellular hydrogel with increased mechanical properties (at time-zero) using pre-crosslinked collagen extracted from natural sources. Although these hydrogels were less stable, and can collapse quickly during compression, it was found that the presence of mobile macromolecules (i.e. PEG) prevented cell damage

by reducing compression rates, and fluid shear stress on cells.

The second part of the study tested biomaterials in soft tissue models made from the conventional (acid-soluble collagen derived) compressed gels. It was found that the extent of PLGA degradation product diffusion from the tissue-like model depended on the presence of local cells which can remodel the matrix. These cells were also able to take-up degradation products.

The delivery of drugs using HA-NP particles into the tissue model was found to be improved by increased collagen density within the hydrogel, and the incorporation of a fine filter layer between the hydrogel and plunger. The simvastatin drug cargo stimulated the production of a low amount of BMP2 protein. However the overall effectiveness of the drug carrier, and indeed the tissue model, require further study.

8.2 Further work

The findings of this study have furthered understanding of hydrogel plastic compression processes. The ability to control the physical characterisics of the construct was key to direct cell behaviour within the model. One of the main purposes of the tissue model is to improve the efficiency and reliability of *in vitro* biomaterial testing; and in doing so, reduce reliance on *in vivo* models (which can be complex, variable and have limited accessibility).

Further increasing the reproducibility of polymeric collagen containing constructs will be necessary before the can potentially be used as a biomaterial testing platform. As shown in the findings of this study, pre-crosslinked type-I collagen extracted from natural tissue sources can be used in hydrogels to increased their mechanical properties, without resorting to cytotoxic chemical crosslinking treatment. Further studies will need to look at of the composition/impurities in the initial collagen source which can potentially affect the ag-

gregation of collagen, and cause the variation between batches observed in the current study.

With regards to the study of implantable biomaterials, models have studied both the degradation, and drug-delivery potentials, of biomaterials. For future studies, particularly for degradation models, the incorporation of microfluidics (i.e. bioreactors) into the model during *in vitro* culture will likely affect release rates of biomaterial (or their degradation products) from the hydrogel. Other potential tests include assays to monitor cell and tissue response to the degraded product. For example, the PLGA material have been known to cause the production of fibrous capsules around the implant material. A model tissue may improve the understanding of underlying cell mechanisms, and rate of fibrosis in response to different concentrations and formulation of the biomaterial (e.g. change in hydrogel opacity with changes to the matrix density over time).

Furthermore, since cell uptake of the degradation products have been evident, it will be important to test for its effect on cell activity in the long run.

Since plastically compressed constructs can be built into more complex models, through layering and co-culturing with different cell types, it is possible to test for complex cell-cell interactions which was not currently possible in 2D cell models, or *in vivo*. Further tests may include temporal changes in protein/growth factor production in response to drugs or biomaterials within a complex model.

However, ultimately the results gained from the *in vitro* 3D models will need to be correlated with *in vivo* data, to establish the effectiveness of the current model in predicting natural cell responses to biomaterial (or other external stimuli). The results from *in vivo* assays will be able to feedback into the model for further refinement (with chemical/physical cues), in order to encourage resident cells to behave in a physiological manner.

8.3 Standard operating procedure (SOP) - Polymeric collagen containing hydrogels as tissue models

Standard operating procedure (SOP) for the production of a tissue model based on compressed polymeric collagen blended hydrogels for biomaterial testing.

8.3.1 Purpose

To describe the procedure for producing hydrogels with a blend of polymeric and monomeric collagens, to create cell-compatible hydrogels with pre-existing collagen cross-links (traditionally only obtainable by cytotoxic cross-linking methods).

8.3.2 Supplies

For the polymeric collagen solution:

A stock solution of polymeric collagen, diluted to 2mg.ml^{-1} in 0.5M acetic acid(or to match concentration of monomeric collagen used) (procedure further described in section 3.2.1), and will require:

- Tendon granules (i.e. potential sources are calf tendon and other young/growing tendons)

- EDTA

- 0.5M acetic acid

- Magnetic stirrer

- Beaker

- Distilled water

- Chloroform

Other materials:

- Acid soluble collagen

- 10X minimum essential media (MEM) (containing phenol red)

- Sodium hydroxide (NaOH; 1M and 5M) (in 1ml syringes with fine needles)

- Cell culture media

- 400kDa polyethylene glycol (PEG) ($20mg.ml^{-1}$ in distilled water)

- Ice

- Plastic compression kit (with sterile well sized absorbent plungers and tweezers

- Flat-based container (i.e. 100ml and 500ml beakers)

- 24-well plate

- Sterile pipettes

- Test biomaterials
  Note. Biomaterials can be in nano- or micro-particle form, or larger discs (up to a diameter of 1cm (to ensure a comfortable fit in 24 well plates) and a depth of $\sim$2mm (to ensure a good level of plastic compression of the surrounding hydrogel)

The proportion of each reagent within the hydrogel solution:

Proportion of reagent in solution (%)	Reagent
80	Blended collagen solution (upto 50% polymeric collagen)
10	10xMEM
5	400kDa PEG solution
5	Cell culture media (with or without cells)
-	Sodium hydroxide

Table 8.1: The proportion of each reagent used to produce blended collagen hydrogels. The amount of sodium hydroxide required to neutralise the collagen solution (i.e. until a colour change is observed in the solution) varies between batches, and so is not specified here.

8.3.3   Scope

This procedure applies to cellular and acellular hydrogel soft tissue models made from a blend of polymeric and monomeric collagens.

8.3.4   Procedure

Note. All procedure must be prepared in a sterile environment, on ice, unless otherwise stated.

1. Chill a flat-based container on ice

2. Pipette equal volumes of polymeric collagen (2mg.ml^{-1}; in 0.5M acetic

acid) and acid-soluble (monomeric) collagen (2mg.ml^{-1}) (for a 1:1 ratio blend) into the chilled container, with a sterile magnetic stirrer

3. Seal container and transfer onto a stirrer, at 4°C, for at least 3 hours - until the solution is visually homogeneous

   Note. It is recommended that the proportion of polymeric collagen within the solution to not exceed 50% for stability of the hydrogel

4. Add required volume of blended collagen (from step 3), 10xMEM and PEG solutions (for proportions of each reagent, see table 8.1) into a separate chilled wide-based container

5. Gently swirl to mix the solution, and neutralise using 5M and 1M NaOH (dropwise) until the point is reached where a colour change from yellow to fushia pink is observed (due to the phenol red indicator contained within the 10xMEM solution)

   Note. Take care to avoid excess NaOH incorporation, as this will prevent proper gellation of the hydrogel

6. Add cell culture media (with or without cells) to the neutralised collagen solution, and swirl to mix

7. Pipette 1ml of the solution into each well of a 24-well plate whilst taking care to minimise air bubbles within the solution

   Note. Each well of a 24 well plate can take up to 2ml of the neutralised collagen solution (for a thicker hydrogel)

8. Seal and transfer to a 37°C, 5% CO_2, incubator for 30 minutes

9. (Optional. Place biomaterial onto the surface of the hydrogel (produced in step 8), and repeat steps 7 and 8, to 'sandwich' the biomaterial between two layers of collagen hydrogel)

10. Compress the hydrogel layer(s) with a sterilised absorbent plunger until fully compressed (typically $\sim 20 - 40$ minutes for gels containing PEG solutions - depending on the thickness of the hydrogel and the proportion of polymeric collagen within the blend)

11. Immediately add 1ml of cell culture media (pre-warmed) to each well to prevent the dehydration of the compressed hydrogels

12. Detach hydrogels from the base of the wells using sterilsed tweezers

13. Seal and incubate at 37℃ and 5% CO_2 for required length of time

Incorporation of biomaterials into the model can be carried out at step 4, 6 or 8, depending on the chemical and physical structure of the biomaterial, and on the required distribution of biomaterial within the model.

• Nano- and micro-particles can be incorporated into the hydrogel directly as the hydrogel is formed. This can be done by adding the biomaterial suspension to the collagen solution before (step 4) or after (step 6; providing the biomaterial is suspended in a solution of neutral pH) neutralisation of the collagen solution

• Larger 3D biomaterials can be incorporated into the model by "sandwiching" the material between two layers of collagen hydrogel (step 9) which are then compressed together

Note. Some nanoparticles or small microparticles can be lost during plastic compression, and this loss will need to be taken into account - the extent of particle loss will depend on biomaterial size and the extent of blockage at the fluid leaving surface of the collagen matrix (see section 5.1.1 for further information).

8.3.5 Troubleshooting

Problem	Possible cause	Cause solution
Polymeric collagen aggregates into visible clumps during neutralisation	Insufficient blending together of polymeric and monomeric collagen solutions. Polymeric collagen did not 'dissolve' sufficiently into acetic acid - possibly a problem with the tendon source with excessive cross-linking of the tendon collagen matrix.	Discard the partially neutralised solution. Stir the collagen blend for longer period of time prior to neutralisation. Source tendons from younger and/or growing tissues.
A hydrogel does not form after 30 minutes at 37℃	Solution not at a neutral pH (possibly too much NaOH added during neutralisation).	Discard and start again. Use 1M NaOH for better control of neutralisation, as soon as hints of pink/orange (from the pH indicator) is observed in the collagen solution.

Table 8.2: Common problems and solutions encountered during the production of blended, polymeric collagen containing hydrogels.

Note: Commercial compression kits (RAFT 3D Cell Culture System; in 24-well plate or 96-well plate formats) are available from TAP Biosystems. Other-

wise refer to section 2.4 and figure 1.3 of this thesis for details on the compression process.

Bibliography

S. Aarthy, B. Vedha Hari, and D. Ramya Devi. Current trends in simvastatin therapy for enhanced efficiency. *International Journal of Pharma and Bio Sciences*, 5(3):279–288, 2014.

E. A. Abou Neel, U. Cheema, J. C. Knowles, R. A. Brown, and S. N. Nazhat. Use of multiple unconfined compression for control of collagen gel scaffold density and mechanical properties. *Soft Matter*, 2(11):986, 2006.

J. Abraham, N. Kumar, and A. Ezra. Collagen. In *Biodegradable Polymers in Clinical Use and Clinical Development*. John Wiley & Sons, USA, 2011.

T. Alekseeva, H. Jawad, M. Purser, and R. Brown. New Improved Technique of Plastic Compression of Collagen Using Upward Fluid Flow. *IFMBE Proceedings*, 30:5–8, 2011.

T. Alekseeva, E. A. Abou Neel, J. C. Knowles, and R. A. Brown. Development of Conical Soluble Phosphate Glass Fibers for Directional Tissue Growth. *Journal of Biomaterials Applications*, 26(6):733–744, Feb. 2012a.

T. Alekseeva, E. Hadjipanayi, E. A. Neel, and R. A. Brown. Engineering stable topography in dense bio-mimetic 3d collagen scaffolds. *Eur. Cells Mater.*, 23:28–40, 2012b.

N. Anandagoda, D. G. Ezra, U. Cheema, M. Bailly, and R. A. Brown. Hyaluronan hydration generates three-dimensional meso-scale structure in engi-

neered collagen tissues. *Journal of The Royal Society Interface*, 9(75):2680–2687, Oct. 2012.

M. Ananta, R. A. Brown, and V. Mudera. A Rapid Fabricated Living Dermal Equivalent for Skin Tissue Engineering: An *In Vivo* Evaluation in an Acute Wound Model. *Tissue Engineering Part A*, 18(3-4):353–361, Feb. 2012.

J. Anderson and M. Shive. Biodegradation and biocompatibility of PLA and PLGA microspheres. *Adv. Drug Deliv. Rev.*, 28(1):5–24, Oct. 1997.

P. Angele, J. Abke, R. Kujat, H. Faltermeier, D. Schumann, M. Nerlich, B. Kinner, C. Englert, Z. Ruszczak, R. Mehrl, and R. Mueller. Influence of different collagen species on physico-chemical properties of crosslinked collagen matrices. *Biomaterials*, 25(14):2831–2841, June 2004.

A. G. Ardakani, U. Cheema, R. A. Brown, and R. J. Shipley. Quantifying the correlation between spatially defined oxygen gradients and cell fate in an engineered three-dimensional culture model. *Journal of the Royal Society, Interface / the Royal Society*, 11(98):20140501, Sept. 2014.

J. K. Armstrong, R. B. Wenby, H. J. Meiselman, and T. C. Fisher. The Hydrodynamic Radii of Macromolecules and Their Effect on Red Blood Cell Aggregation. *Biophys J*, 87(6):4259–4270, Dec. 2004.

N. Artzi, N. Oliva, C. Puron, S. Shitreet, S. Artzi, A. bon Ramos, A. Groothuis, G. Sahagian, and E. R. Edelman. In vivo and in vitro tracking of erosion in biodegradable materials using non-invasive fluorescence imaging. *Nat Mater*, 10(9):704–709, Sept. 2011.

K. A. Athanasiou, G. G. Niederauer, and C. M. Agrawal. Sterilization, toxicity, biocompatibility and clinical applications of polylactic acid/ polyglycolic acid copolymers. *Biomaterials*, 17(2):93–102, Jan. 1996.

M. S. Bae, D. H. Yang, J. B. Lee, D. N. Heo, Y.-D. Kwon, I. C. Youn, K. Choi, J. H. Hong, G. T. Kim, Y. S. Choi, E. H. Hwang, and I. K. Kwon. Photo-cured hyaluronic acid-based hydrogels containing simvastatin as a bone tissue regeneration scaffold. *Biomaterials*, 32(32):8161–8171, Nov. 2011.

A. J. Bailey. The stabilization of the intermolecular crosslinks of collagen with ageing. *Gerontologia*, 15(2):65–76, 1969.

A. J. Bailey and C. M. Peach. Isolation and structural identification of a labile intermolecular crosslink in collagen. *Biochem. Biophys. Res. Commun.*, 33 (5):812–819, Dec. 1968.

J. B. L. Bard and J. A. Chapman. Polymorphism in Collagen Fibrils precipitated at Low pH. *Nature*, 219(5160):1279–1280, Sept. 1968.

E. Bellas, M. Seiberg, J. Garlick, and D. L. Kaplan. In vitro 3d full-thickness skin-equivalent tissue model using silk and collagen biomaterials. *Macromol Biosci*, 12(12):1627–1636, Dec. 2012.

R. A. Berg and D. J. Prockop. The thermal transition of a non-hydroxylated form of collagen. Evidence for a role for hydroxyproline in stabilizing the triple-helix of collagen. *Biochem. Biophys. Res. Commun.*, 52(1):115–120, May 1973.

M. Bitar, R. A. Brown, V. Salih, A. G. Kidane, J. C. Knowles, and S. N. Nazhat. Effect of cell density on osteoblastic differentiation and matrix degradation of biomimetic dense collagen scaffolds. *Biomacromolecules*, 9(1):129–35, Jan. 2008.

R. P. Boot-Handford and D. S. Tuckwell. Fibrillar collagen: the key to vertebrate evolution? A tale of molecular incest. *Bioessays*, 25(2):142–151, Feb. 2003.

M. Brennan and P. F. Davison. Influence of the telopeptides on type I collagen fibrillogenesis. *Biopolymers*, 20(10):2195 − 2202, 1981.

B. Brodsky, G. Thiagarajan, B. Madhan, and K. Kar. Triple-helical peptides: An approach to collagen conformation, stability, and self-association. *Biopolymers*, 89(5):345–353, May 2008.

R. A. Brown. *Extreme Tissue Engineering: Concepts and Strategies for Tissue Fabrication*. Wiley, Dec. 2012. ISBN 978-0-470-97447-6.

R. A. Brown. In the beginning there were soft collagen-cell gels: towards better 3d connective tissue models? *Experimental cell research*, 319(16):2460–9, Oct. 2013a.

R. A. Brown. Direct collagen-material engineering for tissue fabrication. *Tissue engineering. Part A*, 19(13-14):1495–8, July 2013b.

R. A. Brown and P. D. Byers. Swelling of cartilage and expansion of the collagen network. *Calcif. Tissue Int.*, 45(4):260–261, Oct. 1989.

R. A. Brown, M. Wiseman, C.-B. Chuo, U. Cheema, and S. N. Nazhat. Ultrarapid Engineering of Biomimetic Materials and Tissues: Fabrication of Nano- and Microstructures by Plastic Compression. *Advanced Functional Materials*, 15(11):1762–1770, Nov. 2005.

M. A. Bumke, D. Neri, and G. Elia. Modulation of gene expression by extracellular pH variations in human fibroblasts: a transcriptomic and proteomic study. *Proteomics*, 3(5):675–688, May 2003.

E. G. Canty and K. E. Kadler. Procollagen trafficking, processing and fibrillogenesis. *Journal of Cell Science*, 118(7):1341–1353, Apr. 2005.

Y. Cao and B. Wang. Biodegradation of silk biomaterials. *Int J Mol Sci*, 10(4): 1514–1524, Apr. 2009.

M. S. Cartiera, K. M. Johnson, V. Rajendran, M. J. Caplan, and W. M. Saltz-man. The uptake and intracellular fate of PLGA nanoparticles in epithelial cells. *Biomaterials*, 30(14):2790–2798, May 2009.

B. P. Chan and K.-F. So. Photochemical crosslinking improves the physico-chemical properties of collagen scaffolds. *Journal of Biomedical Materials Research Part A*, 75A(3):689–701, Dec. 2005.

P. L. Chandran, D. C. Paik, and J. W. Holmes. Structural mechanism for al-teration of collagen gel mechanics by glutaraldehyde crosslinking. *Connect. Tissue Res.*, 53(4):285–297, 2012.

U. Cheema, C.-B. Chuo, P. Sarathchandra, S. Nazhat, and R. Brown. Engi-neering Functional Collagen Scaffolds: Cyclical Loading Increases Material Strength and Fibril Aggregation. *Advanced Functional Materials*, 17(14): 2426–2431, Sept. 2007a.

U. Cheema, S. N. Nazhat, B. Alp, F. Foroughi, N. Anandagoda, V. Mudera, and R. A. Brown. Fabricating tissues: Analysis of farming versus engineering strategies. *Biotechnol. Bioprocess Eng.*, 12(1):9–14, Feb. 2007b.

U. Cheema, R. A. Brown, B. Alp, and A. J. MacRobert. Spatially defined oxygen gradients and vascular endothelial growth factor expression in an engineered 3d cell model. *Cellular and Molecular Life Sciences*, 65(1):177–186, Jan. 2008.

U. Cheema, T. Alekseeva, E. A. Abou-Neel, and R. A. Brown. Switching off angiogenic signalling: creating channelled constructs for adequate oxygen delivery in tissue engineered constructs. *European cells & materials*, 20: 274–80; discussion 280–1, 2010.

U. Cheema, M. Ananta, and V. Muder. Collagen: Applications of a Natural Polymer in Regenerative Medicine. In D. Eberli, editor, *Regenerative Medicine and Tissue Engineering - Cells and Biomaterials*. InTech, Aug. 2011. ISBN 978-953-307-663-8.

C. Chen, A. Constantinou, and M. Deonarain. Modulating antibody pharmacokinetics using hydrophilic polymers. *Expert Opin Drug Deliv*, 8(9):1221–1236, Sept. 2011.

D. L. Christiansen, E. K. Huang, and F. H. Silver. Assembly of type I collagen: fusion of fibril subunits and the influence of fibril diameter on mechanical properties. *Matrix Biol.*, 19(5):409–420, Sept. 2000.

J. M. Collins, K. Ramamoorthy, A. Da Silveira, P. Patston, and J. J. Mao. Expression of matrix metalloproteinase genes in the rat intramembranous bone during postnatal growth and upon mechanical stresses. *J Biomech*, 38(3): 485–492, Mar. 2005.

W. D. Comper and A. Veis. The mechanism of nucleation for in vitro collagen fibril formation. *Biopolymers*, 16(10):2113–2131, Oct. 1977.

T. Courtney, M. Sacks, J. Stankus, J. Guan, and W. Wagner. Design and analysis of tissue engineering scaffolds that mimic soft tissue mechanical anisotropy. *Biomaterials*, Mar. 2006.

J. M. Cuckler. If hip implant retrievals could speak, what would they tell us? *J Bone Joint Surg Br*, 94(11 Suppl A):11–13, Nov. 2012.

E. Cukierman, R. Pankov, D. R. Stevens, and K. M. Yamada. Taking cell-matrix adhesions to the third dimension. *Science*, 294(5547):1708–1712, Nov. 2001.

K. S. Cunningham and A. I. Gotlieb. The role of shear stress in the pathogenesis of atherosclerosis. *Lab. Invest.*, 85(1):9–23, Jan. 2005.

S. L. M. Dahl, R. B. Rucker, and L. E. Niklason. Effects of copper and cross-linking on the extracellular matrix of tissue-engineered arteries. *Cell Transplant*, 14(10):861–868, 2005.

D. Deng, W. Liu, U. Cheema, V. Mudera, E. Hadjipanayi, and R. A. Brown. Less is more: new biomimetic approach to control spatial and temporal cell loading for tissue engineering. *Journal of biomedical materials research. Part A*, 102(11):4108–17, Nov. 2014.

J.-Y. Dewavrin, N. Hamzavi, V. P. W. Shim, and M. Raghunath. Tuning the architecture of three-dimensional collagen hydrogels by physiological macromolecular crowding. *Acta Biomater*, 10(10):4351–4359, Oct. 2014.

D. E. Discher, P. Janmey, and Y.-L. Wang. Tissue cells feel and respond to the stiffness of their substrate. *Science*, 310(5751):1139–1143, Nov. 2005.

M. Dobaczewski, C. Gonzalez-Quesada, and N. G. Frangogiannis. The extracellular matrix as a modulator of the inflammatory and reparative response following myocardial infarction. *J. Mol. Cell. Cardiol.*, 48(3):504–511, Mar. 2010.

K. J. Doege and J. H. Fessler. Folding of carboxyl domain and assembly of procollagen I. *J. Biol. Chem.*, 261(19):8924–8935, May 1986.

A. D. Doyle, F. W. Wang, K. Matsumoto, and K. M. Yamada. One-dimensional topography underlies three-dimensional fibrillar cell migration. *J. Cell Biol.*, 184(4):481–490, Feb. 2009.

A. D. Doyle, R. J. Petrie, M. L. Kutys, and K. M. Yamada. Dimensions in cell migration. *Curr. Opin. Cell Biol.*, 25(5):642–649, Oct. 2013.

M. P. Drake, P. F. Davison, S. Bump, and F. O. Schmitt. Action of Proteolytic Enzymes on Tropocollagen and Insoluble Collagen*. *Biochemistry*, 5(1):301–312, 1966.

E. East, D. B. de Oliveira, J. P. Golding, and J. B. Phillips. Alignment of Astrocytes Increases Neuronal Growth in Three-Dimensional Collagen Gels and Is Maintained Following Plastic Compression to Form a Spinal Cord Repair Conduit. *Tissue Eng Part A*, 16(10):3173–3184, Oct. 2010.

T. Elsdale and J. Bard. Collagen substrata for studies on cell behavior. *J. Cell Biol.*, 54(3):626–637, Sept. 1972.

A. J. Engler, M. A. Griffin, S. Sen, C. G. Bnnemann, H. L. Sweeney, and D. E. Discher. Myotubes differentiate optimally on substrates with tissue-like stiffness. *J Cell Biol*, 166(6):877–887, Sept. 2004.

F. Ennever, T. Noonan, and H. Rosenkranz. The predictivity of animal bioassays and short-term genotoxicity tests for carcinogenicity and noncarcinogenicity to humans. *Mutagenesis*, 2(2):73–78, 1987.

C. H. Evans and B. J. Drouven. The promotion of collagen polymerization by lanthanide and calcium ions. *Biochem J*, 213(3):751–758, Sept. 1983.

F. Foroughi, D. Aibibu, C. Aulin, J. Hilborn, and R. A. Brown. Bulk collagen incorporation rates into knitted stiff fibre polymer in tissue-engineered scaffolds: the rate-limiting step. *Journal of tissue engineering and regenerative medicine*, 2(8):507–14, Dec. 2008.

M. X. Fu, K. J. Knecht, S. R. Thorpe, and J. W. Baynes. Role of oxygen in cross-linking and chemical modification of collagen by glucose. *Diabetes*, 41 Suppl 2:42–48, Oct. 1992.

M. X. Fu, K. J. Wells-Knecht, J. A. Blackledge, T. J. Lyons, S. R. Thorpe, and J. W. Baynes. Glycation, glycoxidation, and cross-linking of collagen by glucose. Kinetics, mechanisms, and inhibition of late stages of the Maillard reaction. *Diabetes*, 43(5):676–683, May 1994.

I. R. Garrett and G. R. Mundy. The role of statins as potential targets for bone formation. *Arthritis Res*, 4(4):237–240, 2002.

R. Garrone. Collagen, a common thread in extracellular matrix evolution - Springer. *Proc. Indian Acad. Sci. (Chem. Sci.)*, 111(1):51–56, 1999.

M. Georgiou, S. C. J. Bunting, H. A. Davies, A. J. Loughlin, J. P. Golding, and J. B. Phillips. Engineered neural tissue for peripheral nerve repair. *Biomaterials*, 34(30):7335–7343, Oct. 2013.

J. R. Glossop and S. H. Cartmell. Effect of fluid flow-induced shear stress on human mesenchymal stem cells: differential gene expression of IL1b and MAP3k8 in MAPK signaling. *Gene Expr. Patterns*, 9(5):381–388, June 2009.

M. K. Gordon and R. A. Hahn. Collagens. *Cell Tissue Res*, 339(1):247–257, Jan. 2010.

F. Grinnell. Fibroblast biology in three-dimensional collagen matrices. *Trends Cell Biol.*, 13(5):264–269, May 2003.

F. Grinnell, L. Brocha, C. Iucu, S. Rhee, and H. Jiang. Nested collagen matrices: A new model to study migration of human fibroblast populations in three dimensions. *Experimental Cell Research*, Oct. 2005.

B. M. Gumbiner. Cell adhesion: the molecular basis of tissue architecture and morphogenesis. *Cell*, 84(3):345–357, Feb. 1996.

K. H. Gustavson. The function of hydroxyproline in collanges. *Nature*, 175 (4445):70–74, Jan. 1955.

M. F. Hadi, E. A. Sander, J. W. Ruberti, and V. H. Barocas. Simulated remodeling of loaded collagen networks via strain-dependent enzymatic degradation and constant-rate fiber growth. *Mech Mater*, 44:72–82, Jan. 2012.

E. Hadjipanayi, R. A. Brown, and V. Mudera. Interface integration of layered collagen scaffolds with defined matrix stiffness: implications for sheet-based tissue engineering. *Journal of Tissue Engineering and Regenerative Medicine*, 3(3):230–241, Mar. 2009a.

E. Hadjipanayi, V. Mudera, and R. A. Brown. Close dependence of fibroblast proliferation on collagen scaffold matrix stiffness. *Journal of Tissue Engineering and Regenerative Medicine*, 3(2):77–84, Feb. 2009b.

E. Hadjipanayi, V. Mudera, and R. A. Brown. Guiding cell migration in 3d: A collagen matrix with graded directional stiffness. *Cell Motility and the Cytoskeleton*, 66(3):121–128, Mar. 2009c.

E. Hadjipanayi, R. Brown, V. Mudera, D. Deng, W. Liu, and U. Cheema. Controlling physiological angiogenesis by hypoxia-induced signaling. *Journal of Controlled Release*, 146(3):309–317, Sept. 2010.

E. Hadjipanayi, M. Ananta, M. Binkowski, I. Streeter, Z. Lu, Z. F. Cui, R. A. Brown, and V. Mudera. Mechanisms of structure generation during plastic compression of nanofibrillar collagen hydrogel scaffolds: towards engineering of collagen. *Journal of Tissue Engineering and Regenerative Medicine*, 5(7):505–519, July 2011a.

E. Hadjipanayi, U. Cheema, V. Mudera, D. Deng, W. Liu, and R. A. Brown. First implantable device for hypoxia-mediated angiogenic induction. *Journal of controlled release : official journal of the Controlled Release Society*, 153 (3):217–24, Aug. 2011b.

J. R. Harris and A. Reiber. Influence of saline and pH on collagen type I fibrillogenesis in vitro: fibril polymorphism and colloidal gold labelling. *Micron*, 38(5):513–521, 2007.

A. J. Hodge and F. O. Schmitt. The charge profile of the tropocollagen macromolecule and the packing arrangement in native-type collagen fibrils. *Proc. Natl. Acad. Sci. U.S.A.*, 46(2):186–197, Feb. 1960.

D. J. Hulmes, A. Miller, D. A. Parry, K. A. Piez, and J. Woodhead-Galloway. Analysis of the primary structure of collagen for the origins of molecular packing. *J. Mol. Biol.*, 79(1):137–148, Sept. 1973.

R. O. Hynes. Integrins: bidirectional, allosteric signaling machines. *Cell*, 110 (6):673–687, Sept. 2002.

R. O. Hynes. The Extracellular Matrix: Not Just Pretty Fibrils. *Science*, 326 (5957):1216–1219, 2009.

S. Ibusuki, G. J. Halbesma, M. A. Randolph, R. W. Redmond, I. E. Kochevar, and T. J. Gill. Photochemically cross-linked collagen gels as three-dimensional scaffolds for tissue engineering. *Tissue Eng.*, 13(8):1995–2001, Aug. 2007.

D. S. Jackson and J. P. Bentley. On the significance of the extractable collagens. *The Journal of biophysical and biochemical cytology*, 7(1):37–42, 1960.

R. A. Jain. The manufacturing techniques of various drug loaded biodegradable poly(lactide-co-glycolide) (PLGA) devices. *Biomaterials*, 21(23):2475–2490, Dec. 2000.

H. Jiang and F. Grinnell. Cell-matrix entanglement and mechanical anchorage

of fibroblasts in three-dimensional collagen matrices. *Mol. Biol. Cell*, 16(11): 5070–5076, Nov. 2005.

S. Jimenez, M. Harsch, and J. Rosenbloom. Hydroxyproline stabilizes the triple helix of chick tendon collagen. *Biochem. Biophys. Res. Commun.*, 52 (1):106–114, May 1973.

K. E. Kadler, Y. Hojima, and D. J. Prockop. Assembly of collagen fibrils de novo by cleavage of the type I pC-collagen with procollagen C-proteinase. Assay of critical concentration demonstrates that collagen self-assembly is a classical example of an entropy-driven process. *J. Biol. Chem.*, 262(32): 15696–15701, Nov. 1987.

A. H. Kang and J. Gross. Relationship between the Intra and Intermolecular Cross-links of Collagen. *Proceedings of the National Academy of Sciences*, 67(3):1307–1314, 1970.

K. Kar, P. Amin, M. A. Bryan, A. V. Persikov, A. Mohs, Y.-H. Wang, and B. Brodsky. Self-association of collagen triple helic peptides into higher order structures. *J. Biol. Chem.*, 281(44):33283–33290, Nov. 2006.

D. Karamichos, R. A. Brown, and V. Mudera. Collagen stiffness regulates cellular contraction and matrix remodeling gene expression. *Journal of biomedical materials research. Part A*, 83(3):887–94, Dec. 2007.

D. Karamichos, J. Skinner, R. Brown, and V. Mudera. Matrix stiffness and serum concentration effects matrix remodelling and ECM regulatory genes of human bone marrow stem cells. *Journal of Tissue Engineering and Regenerative Medicine*, 2(2-3):97–105, Mar. 2008.

H. Kayhanian, S. Jones, J. Phillips, M. Lewis, R. Brown, and V. Mudera. Host muscle cell infiltration in cell-seeded plastic compressed collagen constructs.

Journal of tissue engineering and regenerative medicine, 3(1):72–5, Jan. 2009.

J. G. Kerns, K. Buckley, J. Churchwell, A. W. Parker, P. Matousek, and A. E. Goodship. Is the Collagen Primed for Mineralization in Specific Regions of the Turkey Tendon? An Investigation of the ProteinMineral Interface Using Raman Spectroscopy. *Anal. Chem.*, 88(3):1559–1563, Feb. 2016.

J. Khoshnoodi, J.-P. Cartailler, K. Alvares, A. Veis, and B. G. Hudson. Molecular recognition in the assembly of collagens: terminal noncollagenous domains are key recognition modules in the formation of triple helical protomers. *J. Biol. Chem.*, 281(50):38117–38121, Dec. 2006.

Y. Kim, Y.-S. Lee, J.-H. Hahn, J. Choe, H. J. Kwon, J. Y. Ro, and D. Jeoung. Hyaluronic acid targets CD44 and inhibits FcepsilonRI signaling involving PKCdelta, Rac1, ROS, and MAPK to exert anti-allergic effect. *Mol. Immunol.*, 45(9):2537–2547, May 2008.

M. Kisiel, A. S. Klar, M. Ventura, J. Buijs, M.-K. Mafina, S. M. Cool, and J. Hilborn. Complexation and Sequestration of BMP-2 from an ECM Mimetic Hyaluronan Gel for Improved Bone Formation. *PLoS One*, 8(10), Oct. 2013.

S. R. Knight, R. Aujla, and S. P. Biswas. Total Hip Arthroplasty - over 100 years of operative history. *Orthop Rev (Pavia)*, 3(2):e16, Sept. 2011.

R. R. Kohn, A. Cerami, and V. M. Monnier. Collagen aging in vitro by nonenzymatic glycosylation and browning. *Diabetes*, 33(1):57–59, Jan. 1984.

J. C. Kuo. Mechanotransduction at focal adhesions: integrating cytoskeletal mechanics in migrating cells. *J. Cell. Mol. Med.*, 17(6):704–712, June 2013.

A. Kureshi, U. Cheema, T. Alekseeva, A. Cambrey, and R. Brown. Alignment hierarchies: engineering architecture from the nanometre to the micrometre

scale. *Journal of The Royal Society Interface*, 7(Suppl␣6):S707–S716, Dec. 2010.

A. Lan, D. Lagadic-Gossmann, C. Lemaire, C. Brenner, and G. Jan. Acidic extracellular pH shifts colorectal cancer cell death from apoptosis to necrosis upon exposure to propionate and acetate, major end-products of the human probiotic propionibacteria. *Apoptosis*, 12(3):573–591, Mar. 2007.

R. Langer and J. P. Vacanti. Tissue engineering. *Science*, 260(5110):920–926, May 1993.

R. R. Lareu, K. H. Subramhanya, Y. Peng, P. Benny, C. Chen, Z. Wang, R. Rajagopalan, and M. Raghunath. Collagen matrix deposition is dramatically enhanced in vitro when crowded with charged macromolecules: The biological relevance of the excluded volume effect. *FEBS Letters*, 581(14):2709–2714, June 2007.

T. C. Laurent and J. R. Fraser. Hyaluronan. *FASEB J.*, 6(7):2397–2404, Apr. 1992.

W. Lee, J. Sodek, and C. A. McCulloch. Role of integrins in regulation of collagen phagocytosis by human fibroblasts. *J. Cell. Physiol.*, 168(3):695–704, Sept. 1996.

K. R. Legate and R. Fssler. Mechanisms that regulate adaptor binding to beta-integrin cytoplasmic tails. *J. Cell. Sci.*, 122(Pt 2):187–198, Jan. 2009.

S. J. Leibovich and J. B. Weiss. Electron Microscope Studies of Effects of Endopeptidase and Exopeptidase Digestion on Tropocollagen. *Biochimica Et Biophysica Acta*, 214(3):445–454, 1970.

P. M. Lewis, H. M. Ackland, A. J. Lowery, and J. V. Rosenfeld. Restoration

of vision in blind individuals using bionic devices: a review with a focus on cortical visual prostheses. *Brain Res.*, 1595:51–73, Jan. 2015.

Y. Li and E. P. Douglas. Effects of various salts on structural polymorphism of reconstituted type I collagen fibrils. *Colloids Surf B Biointerfaces*, 112: 42–50, Dec. 2013.

Y. Li, S.-K. Chen, L. Li, L. Qin, X.-L. Wang, and Y.-X. Lai. Bone defect animal models for testing efficacy of bone substitute biomaterials. *Journal of Orthopaedic Translation*, 3(3):95–104, July 2015.

Y.-M. Lim, S. Yao, S. L. Gras, C. McSweeney, T. Lockett, M. A. Augustin, and P. R. Gooley. Hydrodynamic radii of solubilized high amylose native and modified starches by pulsed field gradient NMR diffusion measurements. *Food Hydrocolloids*, 40:16–21, Oct. 2014.

D. C. Liu, Y. K. Lin, and M. T. Chen. Optimum Condition of Extracting Collagen from Chicken Feet and its Characteristics. *Asian-Australasian Journal of Animal Sciences*, 14(11):1638–1644, Nov. 2001.

L. Lu, S. J. Peter, M. D. Lyman, H. L. Lai, S. M. Leite, J. A. Tamada, S. Uyama, J. P. Vacanti, R. Langer, and A. G. Mikos. In vitro and in vivo degradation of porous poly(DL-lactic-co-glycolic acid) foams. *Biomaterials*, 21(18):1837–1845, Sept. 2000.

J. F. Mano, G. A. Silva, H. S. Azevedo, P. B. Malafaya, R. A. Sousa, S. S. Silva, L. F. Boesel, J. M. Oliveira, T. C. Santos, A. P. Marques, N. M. Neves, and R. L. Reis. Natural origin biodegradable systems in tissue engineering and regenerative medicine: present status and some moving trends. *J R Soc Interface*, 4(17):999–1030, Dec. 2007.

M. Marenzana, N. Wilson-Jones, V. Mudera, and R. A. Brown. The origins

and regulation of tissue tension: Identification of collagen tension-fixation process in vitro. *Experimental Cell Research*, 312(4):423–433, Feb. 2006.

M. Marenzana, D. J. Kelly, P. J. Prendergast, and R. A. Brown. A collagen-based interface construct for the assessment of cell-dependent mechanical integration of tissue surfaces. *Cell and tissue research*, 327(2):293–300, Feb. 2007.

F. J. Maritz, M. M. Conradie, P. A. Hulley, R. Gopal, and S. Hough. Effect of Statins on Bone Mineral Density and Bone Histomorphometry in Rodents. *Arterioscler Thromb Vasc Biol*, 21(10):1636–1641, Jan. 2001.

B. N. Mason, J. P. Califano, and C. A. Reinhart-King. Matrix Stiffness: A Regulator of Cellular Behavior and Tissue Formation. In S. K. Bhatia, editor, *Engineering Biomaterials for Regenerative Medicine*, pages 19–37. Springer New York, 2012. ISBN 978-1-4614-1079-9 978-1-4614-1080-5. NOOPDOI: 10.1007/978-1-4614-1080-5_2.

M. B. Mathews. The interaction of collagen and acid mucopolysaccarides. A model for connective tissue. *Biochem J*, 96(3):710–716, Sept. 1965.

J. A. Matthews, G. E. Wnek, D. G. Simpson, and G. L. Bowlin. Electrospinning of collagen nanofibers. *Biomacromolecules*, 3(2):232–238, Apr. 2002.

S. McCue, S. Noria, and B. L. Langille. Shear-induced reorganization of endothelial cell cytoskeleton and adhesion complexes. *Trends Cardiovasc. Med.*, 14(4):143–151, May 2004.

P. McGonigle and B. Ruggeri. Animal models of human disease: challenges in enabling translation. *Biochem. Pharmacol.*, 87(1):162–171, Jan. 2014.

M. Mekhail, K. K. H. Wong, D. T. Padavan, Y. Wu, D. B. O'Gorman, and W. Wan.

Genipin-Cross-linked Electrospun Collagen Fibers. *Journal of Biomaterials Science, Polymer Edition*, 22(17):2241–2259, Jan. 2011.

A. S. Meshel, Q. Wei, R. S. Adelstein, and M. P. Sheetz. Basic mechanism of three-dimensional collagen fibre transport by fibroblasts. *Nat. Cell Biol.*, 7 (2):157–164, Feb. 2005.

D. K. Mishra, J. H. Sakamoto, M. J. Thrall, B. N. Baird, S. H. Blackmon, M. Ferrari, J. M. Kurie, and M. P. Kim. Human Lung Cancer Cells Grown in an Ex Vivo 3d Lung Model Produce Matrix Metalloproteinases Not Produced in 2d Culture. *PLoS One*, 7(9), Sept. 2012.

T. Miyahara, A. Murai, T. Tanaka, S. Shiozawa, and M. Kameyama. Age-related differences in human skin collagen: solubility in solvent, susceptibility to pepsin digestion, and the spectrum of the solubilized polymeric collagen molecules. *Journal of gerontology*, 37(6):651–655, 1982.

A. Montagnani, S. Gonnelli, C. Cepollaro, S. Pacini, M. S. Campagna, M. B. Franci, B. Lucani, and C. Gennari. Effect of simvastatin treatment on bone mineral density and bone turnover in hypercholesterolemic postmenopausal women: a 1-year longitudinal study. *Bone*, 32(4):427–433, Apr. 2003.

L. Moroni and J. Elisseeff. Biomaterials engineered for integration. *Materials Today*, 11(5):44–51, 2008.

V. Mudera, M. Morgan, U. Cheema, S. Nazhat, and R. Brown. Ultra-rapid engineered collagen constructs tested in anin vivo nursery site. *Journal of Tissue Engineering and Regenerative Medicine*, 1(3):192–198, May 2007.

G. Mundy, R. Garrett, S. Harris, J. Chan, D. Chen, G. Rossini, B. Boyce, M. Zhao, and G. Gutierrez. Stimulation of bone formation in vitro and in rodents by statins. *Science*, 286(5446):1946–1949, Dec. 1999.

L. Muthusubramaniam, L. Peng, T. Zaitseva, M. Paukshto, G. R. Martin, and T. A. Desai. Collagen fibril diameter and alignment promote the quiescent keratocyte phenotype. *J Biomed Mater Res A*, 100(3):613–621, Mar. 2012.

K.-H. Nam, A. S. T. Smith, S. Lone, S. Kwon, and D.-H. Kim. Biomimetic 3d Tissue Models for Advanced High-Throughput Drug Screening. *J Lab Autom*, 20(3):201–215, June 2015.

C. P. Ng and M. A. Swartz. Fibroblast alignment under interstitial fluid flow using a novel 3-D tissue culture model. *Am. J. Physiol. Heart Circ. Physiol.*, 284(5):H1771–1777, May 2003.

K. Numata and D. L. Kaplan. Silk-based delivery systems of bioactive molecules. *Adv. Drug Deliv. Rev.*, 62(15):1497–1508, Dec. 2010.

K. Numata, S. Yamazaki, and N. Naga. Biocompatible and biodegradable dual-drug release system based on silk hydrogel containing silk nanoparticles. *Biomacromolecules*, 13(5):1383–1389, May 2012.

A. Nyga, U. Cheema, and M. Loizidou. 3d tumour models: novel in vitro approaches to cancer studies. *J Cell Commun Signal*, 5(3):239–248, Aug. 2011.

S. H. Oh, S. G. Kang, and J. H. Lee. Degradation behavior of hydrophilized PLGA scaffolds prepared by melt-molding particulate-leaching method: comparison with control hydrophobic one. *J Mater Sci Mater Med*, 17(2): 131–137, Feb. 2006.

L. H. Olde Damink, P. J. Dijkstra, M. J. van Luyn, P. B. van Wachem, P. Nieuwenhuis, and J. Feijen. Cross-linking of dermal sheep collagen using a water-soluble carbodiimide. *Biomaterials*, 17(8):765–773, Apr. 1996.

L. E. R. O'Leary, J. A. Fallas, E. L. Bakota, M. K. Kang, and J. D. Hartgerink. Multi-hierarchical self-assembly of a collagen mimetic peptide from triple helix to nanofibre and hydrogel. *Nat Chem*, 3(10):821–828, Oct. 2011.

D. A. Ossipov, X. Yang, O. Varghese, S. Kootala, and J. Hilborn. Modular approach to functional hyaluronic acid hydrogels using orthogonal chemical reactions. *Chem. Commun.*, 46(44):8368–8370, Nov. 2010.

J. E. Paderi, R. Sistiabudi, A. Ivanisevic, and A. Panitch. Collagen-binding peptidoglycans: a biomimetic approach to modulate collagen fibrillogenesis for tissue engineering applications. *Tissue Eng Part A*, 15(10):2991–2999, Oct. 2009.

A. V. Persikov, J. A. Ramshaw, A. Kirkpatrick, and B. Brodsky. Amino acid propensities for the collagen triple-helix. *Biochemistry*, 39(48):14960–14967, Dec. 2000.

A. V. Persikov, J. A. M. Ramshaw, A. Kirkpatrick, and B. Brodsky. Electrostatic interactions involving lysine make major contributions to collagen triple-helix stability. *Biochemistry*, 44(5):1414–1422, Feb. 2005.

R. Puxkandl, I. Zizak, O. Paris, J. Keckes, W. Tesch, S. Bernstorff, P. Purslow, and P. Fratzl. Viscoelastic properties of collagen: synchrotron radiation investigations and structural model. *Philos. Trans. R. Soc. Lond., B, Biol. Sci.*, 357(1418):191–197, Feb. 2002.

R. Rago, J. Mitchen, and G. Wilding. DNA fluorometric assay in 96-well tissue culture plates using Hoechst 33258 after cell lysis by freezing in distilled water. *Anal. Biochem.*, 191(1):31–34, Nov. 1990.

G. N. Ramachandran and G. Kartha. Structure of collagen. *Nature*, 174(4423): 269–270, Aug. 1954.

G. N. Ramachandran and G. Kartha. Structure of collagen. *Nature*, 176(4482): 593–595, Sept. 1955.

G. N. Ramachandran, M. Bansal, and R. S. Bhatnagar. A hypothesis on the role of hydroxyproline in stabilizing collagen structure. *Biochim. Biophys. Acta*, 322(1):166–171, Sept. 1973.

L. Ramage. Integrins and extracellular matrix in mechanotransduction. *Cell Health and Cytoskeleton*, page 1, Dec. 2011.

S. Ramesh, K. Rajagopal, D. Vaikkath, P. D. Nair, and V. Madhuri. Enhanced encapsulation of chondrocytes within a chitosan/hyaluronic acid hydrogel: a new technique. *Biotechnol. Lett.*, 36(5):1107–1111, May 2014.

J. Rao and W. R. Otto. Fluorimetric DNA assay for cell growth estimation. *Anal. Biochem.*, 207(1):186–192, Nov. 1992.

S. Razaq, R. J. Wilkins, and J. P. G. Urban. The effect of extracellular pH on matrix turnover by cells of the bovine nucleus pulposus. *Eur Spine J*, 12(4): 341–349, Aug. 2003.

H. Rich, M. Odlyha, U. Cheema, V. Mudera, and L. Bozec. Effects of photo-chemical riboflavin-mediated crosslinks on the physical properties of collagen constructs and fibrils. *J Mater Sci Mater Med*, 25(1):11–21, 2014.

K. P. M. Ricketts, U. Cheema, A. Nyga, A. Castoldi, C. Guazzoni, T. Magdeldin, M. Emberton, A. P. Gibson, G. J. Royle, and M. Loizidou. A 3d in vitro cancer model as a platform for nanoparticle uptake and imaging investigations. *Small*, 10(19):3954–3961, Oct. 2014.

S. P. Robins and A. J. Bailey. Relative stabilities of the intermediate reducible crosslinks present in collagen fibres. *FEBS letters*, 33(2):167–171, 1973.

F. Ruan, Q. Zheng, and J. Wang. Mechanisms of bone anabolism regulated by statins. *Biosci Rep*, 32(6):511–519, Dec. 2012.

A. Rubin, M. P. Drake, P. F. Davison, D. Pfahl, P. Speakman, and F. O. Schmitt. Effects of Pepsin Treatment on the Interaction Properties of Tropocollagen Macromolecules. *Biochemistry*, 4(2):181–190, 1965.

H. P. Saal and S. J. Bensmaia. Biomimetic approaches to bionic touch through a peripheral nerve interface. *Neuropsychologia*, 79(Pt B):344–353, Dec. 2015.

G. B. Sajithlal, P. Chithra, and G. Chandrakasan. Advanced glycation end products induce crosslinking of collagen in vitro. *Biochim. Biophys. Acta*, 1407(3):215–224, Sept. 1998.

L. Sando, S. Danon, A. G. Brownlee, R. J. McCulloch, J. A. M. Ramshaw, C. M. Elvin, and J. A. Werkmeister. Photochemically crosslinked matrices of gelatin and fibrinogen promote rapid cell proliferation. *J Tissue Eng Regen Med*, 5(5):337–346, May 2011.

G. Schliecker, C. Schmidt, S. Fuchs, R. Wombacher, and T. Kissel. Hydrolytic degradation of poly(lactide-co-glycolide) films: effect of oligomers on degradation rate and crystallinity. *International Journal of Pharmaceutics*, 266(12): 39–49, Nov. 2003.

J. D. Schofield, I. L. Freeman, and D. S. Jackson. The isolation, and amino acid and carbohydrate composition, of polymeric collagens prepared from various human tissues. *Biochem J*, 124(3):467–473, Sept. 1971.

V. Serpooshan, N. Muja, B. Marelli, and S. N. Nazhat. Fibroblast contractility and growth in plastic compressed collagen gel scaffolds with microstructures

correlated with hydraulic permeability. *J Biomed Mater Res A*, 96(4):609–20, 2011.

J. G. Snedeker and A. Gautieri. The role of collagen crosslinks in ageing and diabetes - the good, the bad, and the ugly. *Muscles Ligaments Tendons J*, 4 (3):303–308, July 2014.

J. M. Snowden and D. A. Swann. The formation and thermal stability of in vitro assembled fibrils from acid-soluble and pepsin-treated collagens. *Biochim. Biophys. Acta*, 580(2):372–381, Oct. 1979.

J. M. Snowden and D. A. Swann. Effects of glycosaminoglycans and pro-teoglycan on the in vitro assembly and thermal stability of collagen fibrils. *Biopolymers*, 19(4):767–780, Apr. 1980.

H. Spichtin and F. Verzar. Calcium as stabilizing factor of the collagen macro-molecule. *Experientia*, 25(1):9–11, Jan. 1969.

F. S. Steven. The Nishihara Technique for the Solubilization of Collagen. Appli-cation to the Preparation of Soluble Collagens from Normal and Rheumatoid Connective Tissue. *Annals of the rheumatic diseases*, 23:300–1, July 1964.

F. S. Steven. The effect of chelating agents on collagen interfibrillar matrix interactions in connective tissue. *Biochimica et biophysica acta*, 140(3):522–8, Aug. 1967.

F. S. Steven and H. Thomas. Preparation of insoluble collagen from human cartilage. *The Biochemical journal*, 135(1):245–7, Sept. 1973.

F. S. Steven, D. S. Jackson, J. D. Schofield, and J. B. Bard. Polymeric colla-gen isolated from the human intestinal submucosa. *Gut*, 10(6):484–7, June 1969.

A. T. Stratmann, D. Fecher, G. Wangorsch, C. Gttlich, T. Walles, H. Walles, T. Dandekar, G. Dandekar, and S. L. Nietzer. Establishment of a human 3d lung cancer model based on a biological tissue matrix combined with a Boolean in silico model. *Mol Oncol*, 8(2):351–365, Mar. 2014.

I. Streeter and N. H. de Leeuw. A molecular dynamics study of the interprotein interactions in collagen fibrils. *Soft Matter*, 7(7):3373–3382, Apr. 2011.

E. Suzuki and R. D. B. Fraser. Role of hydroxyproline in the stabilization of the collagen molecule via water molecules. *International Journal of Biological Macromolecules*, 2(1):54–56, 1980.

Y. Tabata and Y. Ikada. Macrophage phagocytosis of biodegradable microspheres composed of L-lactic acid/glycolic acid homo- and copolymers. *J. Biomed. Mater. Res.*, 22(10):837–858, Oct. 1988.

Y. Tabata and Y. Ikada. Protein precoating of polylactide microspheres containing a lipophilic immunopotentiator for enhancement of macrophage phagocytosis and activation. *Pharm. Res.*, 6(4):296–301, Apr. 1989.

Y. Tabata, M. Miyao, M. Ozeki, and Y. Ikada. Controlled release of vascular endothelial growth factor by use of collagen hydrogels. *J Biomater Sci Polym Ed*, 11(9):915–930, 2000.

N. S. Tan. *Engineering a Tissue Mimic for Predictive Nanoparticle Assessment*. Doctoral Thesis, University College London, London, UK, 2015.

N. S. Tan, T. Alekseeva, and R. A. Brown. Roofed grooves: Rapid layer engineering of perfusion channels in collagen tissue models. *Journal of Biomaterials Applications*, 29(4):605–616, Oct. 2014.

J. A. J. van der Rijt, K. O. van der Werf, M. L. Bennink, P. J. Dijkstra, and

J. Feijen. Micromechanical testing of individual collagen fibrils. *Macromol Biosci*, 6(9):697–702, Sept. 2006.

V. van Duinen, S. J. Trietsch, J. Joore, P. Vulto, and T. Hankemeier. Microfluidic 3d cell culture: from tools to tissue models. *Curr. Opin. Biotechnol.*, 35: 118–126, Dec. 2015.

O. P. Varghese, W. Sun, J. Hilborn, and D. A. Ossipov. In Situ Cross-Linkable High Molecular Weight HyaluronanBisphosphonate Conjugate for Localized Delivery and Cell-Specific Targeting: A Hydrogel Linked Prodrug Approach. *J. Am. Chem. Soc.*, 131(25):8781–8783, July 2009.

D. Vllasaliu and I. Singh. particle characterisation in drug delivery. *European Pharmaceutical Review*, 19(4):37–40, 2014.

R. S. Walton, D. D. Brand, and J. T. Czernuszka. Influence of telopeptides, fibrils and crosslinking on physicochemical properties of type I collagen films. *J Mater Sci Mater Med*, 21(2):451–461, Feb. 2010.

D. J. White, S. Puranen, M. S. Johnson, and J. Heino. The collagen receptor subfamily of the integrins. *Int. J. Biochem. Cell Biol.*, 36(8):1405–1410, Aug. 2004.

C. F. Whittington, E. Brandner, K. Y. Teo, B. Han, E. Nauman, and S. L. Voytik-Harbin. Oligomers modulate interfibril branching and mass transport properties of collagen matrices. *Microsc. Microanal.*, 19(5):1323–1333, Oct. 2013.

B. R. Williams, R. A. Gelman, D. C. Poppke, and K. A. Piez. Collagen fibril formation. Optimal in vitro conditions and preliminary kinetic results. *J. Biol. Chem.*, 253(18):6578–6585, Sept. 1978.

J. P. Wong, D. Baptista, and R. A. Brown. Pre-crosslinked polymeric collagen in 3-D models of mechanically stiff tissues: Blended collagen polymer hy-

drogels for rapid layer fabrication. *Acta biomaterialia*, 10(12):5005–11, Dec. 2014.

J. P. F. Wong, A. J. MacRobert, U. Cheema, and R. A. Brown. Mechanical anisotropy in compressed collagen produced by localised photodynamic cross-linking. *Journal of the Mechanical Behavior of Biomedical Materials*, 18:132–139, Feb. 2013.

G. C. Wood and M. K. Keech. The formation of fibrils from collagen solutions 1. The effect of experimental conditions: kinetic and electron-microscope studies. *Biochem J*, 75(3):588–598, June 1960.

C. C. Wu, S. J. Ding, Y. H. Wang, M.-J. Tang, and H.-C. Chang. Mechanical properties of collagen gels derived from rats of different ages. *Journal of Biomaterials Science, Polymer Edition*, 16(10):1261–1275, Jan. 2005.

A. K. J. Xian Xu. Hyaluronic Acid-Based Hydrogels: From a Natural Polysaccharide to Complex Networks. *Soft matter*, 8(12):3280–3294, 2012.

J. Xing, L. Yang, and Y. Li. Effect of anions on type I collagen fibrillogenesis in aqueous solution. In *2011 International Symposium on Water Resource and Environmental Protection (ISWREP)*, volume 4, pages 2975–2978, May 2011.

Q. Xu, S. E. Chin, C.-H. Wang, and D. W. Pack. Mechanism of drug release from double-walled PDLLA(PLGA) microspheres. *Biomaterials*, 34 (15):3902–3911, May 2013.

M. Yamauchi, R. E. London, C. Guenat, F. Hashimoto, and G. L. Mechanic. Structure and formation of a stable histidine-based trifunctional cross-link in skin collagen. *J. Biol. Chem.*, 262(24):11428–11434, Aug. 1987.

L. Yang, C. F. Fiti, K. O. van der Werf, M. L. Bennink, P. J. Dijkstra, and J. Feijen. Mechanical properties of single electrospun collagen type I fibers. *Biomaterials*, 29(8):955–962, Mar. 2008.

X. Yang, S. Kootala, J. Hilborn, and D. A. Ossipov. Preparation of hyaluronic acid nanoparticlesvia hydrophobic association assisted chemical crosslinkingan orthogonal modular approach. *Soft Matter*, 7(16):7517–7525, Aug. 2011.

L. Yildirimer and A. M. Seifalian. Three-dimensional biomaterial degradation - Material choice, design and extrinsic factor considerations. *Biotechnol. Adv.*, 32(5):984–999, Oct. 2014.

A. Zemel, F. Rehfeldt, A. E. X. Brown, D. E. Discher, and S. A. Safran. Optimal matrix rigidity for stress fiber polarization in stem cells. *Nat Phys*, 6(6):468–473, June 2010.

Y. Zhang and Z. Xu. Atomic radii of noble gas elements in condensed phases. *Americal Mineralogist*, 80:670–75, 1995.

List of Conference Abstracts

1. JPF Wong, AJ MacRobert, U Cheema and RA Brown. Engineering anisotropy in mechanical properties by orientated collagen cross-linking. European Cells and Materials Vol. 23. Suppl.4, 2012 (page 80) Abstract Tissue and Cell Engineering Society (TCES) meeting. Liverpool, UK, 2012

2. JPF Wong, DF Baptista and RA Brown. Fabrication of cellular pre-crosslinked collagen based hydrogel. European Cells and Materials Vol. 26. Suppl.7, 2013 (page 88) Abstract Tissue and Cell Engineering Society (TCES) meeting. Cardiff, UK, 2013

3. JPF Wong, DF Baptista and RA Brown. Engineering pre-crosslinked polymeric collagen based constructs. Tissue Engineering and Regenerative Medicine International Society (TERMIS) meeting, Istanbul, Turkey, 2013

4. JPF Wong and RA Brown. Control of collagen hydrogel compression for cell rescue. European Cells and Materials Vol. 28. Suppl.4, 2014 (page 19) Abstract Tissue and Cell Engineering Society (TCES) meeting. Newcastle, UK, 2014

5. JPF Wong and RA Brown. Rescue of interstitial cells in novel stiff collagen hydrogels during plastic compression. Tissue Engineering and

Regenerative Medicine International Society (TERMIS) meeting, Genoa, Italy, 2014

List of Publications

1. JP Wong, D Baptista and RA Brown, Pre-crosslinked polymeric collagen in 3-D models of mechanically stiff tissues: blended collagen polymer hydrogels for rapid layer fabrication. Acta Biomater. 2014, 10(12):5005-11.

2. JP Wong, AJ MacRobert, U Cheema and RA Brown, Mechanical anisotropy in compressed collagen produced by localised photodynamic cross-linking. J Mech Behav Biomed Mater. 2013, 18:132-9.